General Disclaimer

One or more of the Following Statements may affect this Document

- This document has been reproduced from the best copy furnished by the organizational source. It is being released in the interest of making available as much information as possible.

- This document may contain data, which exceeds the sheet parameters. It was furnished in this condition by the organizational source and is the best copy available.

- This document may contain tone-on-tone or color graphs, charts and/or pictures, which have been reproduced in black and white.

- This document is paginated as submitted by the original source.

- Portions of this document are not fully legible due to the historical nature of some of the material. However, it is the best reproduction available from the original submission.

NASA CR-72462

ANALYTICAL & EXPERIMENTAL INVESTIGATION OF SIDELOBE SUPPRESSION TECHNIQUES FOR REFLECTOR TYPE SPACECRAFT ANTENNA

by

F.J. GOEBELS JR, R. MEIER AND R.K. THOMAS

prepared for

NATIONAL AERONAUTICS AND SPACE ADMINISTRATION

CONTRACT NAS 3—9717

GENERAL ELECTRIC
MISSILE AND SPACE DIVISION
Valley Forge Space Technology Center
P.O. Box 8555 • Philadelphia, Penna. 19101

NASA CR-72462

FINAL TECHNICAL REPORT

ANALYTICAL & EXPERIMENTAL INVESTIGATION OF SIDELOBE SUPPRESSION TECHNIQUES FOR REFLECTOR TYPE SPACECRAFT ANTENNA

BY

F.J. GOEBELS JR., R. MEIER AND R.K. THOMAS

PREPARED FOR

NATIONAL AERONAUTICS AND SPACE ADMINISTRATION

1 SEPTEMBER 1968

CONTRACT NO. NAS 3-9717

TECHNICAL MANAGEMENT

NASA LEWIS RESEARCH CENTER

CLEVELAND, OHIO

GENERAL ELECTRIC

SPACE SYSTEMS ORGANIZATION

Valley Forge Space Center

P. O. Box 8555 • Philadelphia, Penna. 19101

Analytical And Experimental Investigation
of Sidelobe Suppression Techniques
for Reflector Type Spacecraft Antenna

by

F.J. Goebels, Jr., R. Meier, R.K. Thomas

ABSTRACT

Several near axis sidelobe suppression techniques for circularly-polarized, reflector-type antennas were identified, investigated, tested and evaluated. Heavy taper, blockage compensation and active zone suppression techniques were simultaneously applied to a 13-wavelength diameter paraboloid. This achieved -40 db sidelobes for linear polarization. A demonstration of sidelobe suppression for circular polarization was precluded by a helical primary feed problem. Only 3.3 percent of the total rf power radiated was supplied to the helical suppressor elements.

SUMMARY

The purpose of this study is to identify, characterize, test and evaluate near axis-sidelobe suppression techniques for circularly-polarized, reflector-type antennas. Three techniques--namely, heavy taper, blockage compensation and active-zone suppression -- were simultaneously demonstrated with a 13-wavelength-diameter paraboloid with -30 db sidelobes and shown to satisfy an asymmetric pattern goal requirement in one pattern-plane of the paraboloid. This result included achieving -40 db sidelobes for linear polarization. The helical suppressor elements required only 3.3 percent of the total rf power radiated. A helical primary feed problem precluded a demonstration of substantial sidelobe suppression for circular polarization.

The principal conclusions drawn from this study are that heavy taper, blockage compensation and active-zone suppression are useful sidelobe suppression techniques for paraboloid antennas. The blockage compensation technique offers a simple but effective method to correct for aperture blockage and to significantly suppress the sidelobe structure. Active-zone suppression is a more complex, larger, and heavier method. However, it is capable of suppressing more of the sidelobe structure.

TABLE OF CONTENTS

LIST OF ILLUSTRATIONS (Cont'd)

SECTION 1

INTRODUCTION

1.1 BACKGROUND

With the advent of space broadcast systems, the need has arisen to have the capability to selectively illuminate areas of the earth without introducing substantial signal strength in the surrounding regions. This need, when translated into the design of spacecraft antennas, means very low near axis sidelobe levels as shown in Figure 1.1-1. Such levels are

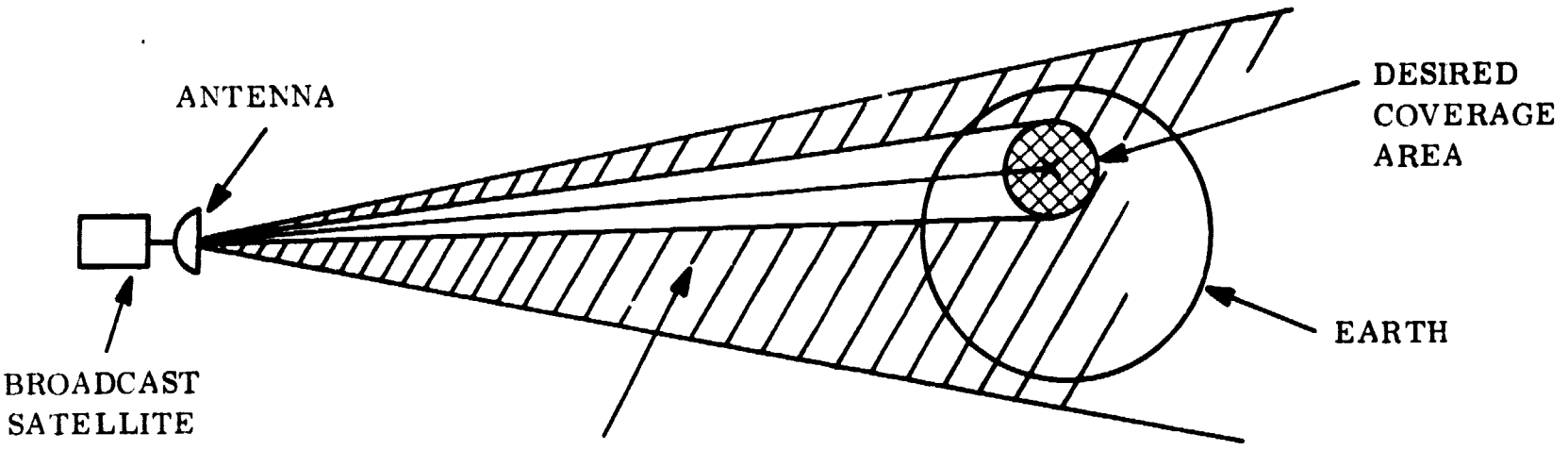

Figure 1.1-1. Coverage Area and Sidelobe Suppression Area

currently not characteristic of these antennas. Sidelobe levels as low as -40 db are being considered. In this study such low sidelobe designs have been examined for reflector-type antennas.

Meeting this requirement for relector-type antennas is a challenging task. Many factors must be accurately controlled or compensated for including the primary feed pattern and phase center, the reflector curvature, the back-lobe structure from the primary feed, the blockage effects of the primary feed and edge diffraction effects from the feed or reflector to name a few. These factors have been carefully examined and dealt with in this investigation. In addition, adequate range facilities and test equipment have been employed to permit the measurement of -40 db sidelobes.

1.2 SCOPE AND OBJECTIVE

The scope of this program was to identify and characterize sidelobe suppression techniques and to exploit their potential by analytical studies and experimental tests. The analytical studies defined four sidelobe suppression techniques that were investigated during the experimental phase of the program.

The objective of the experimentation was to demonstrate sidelobe suppression in one pattern plane of a paraboloid antenna by applying, individually or collectively, one of the following:

a. A heavy taper

b. A blockage compensation technique

c. An active zone suppression technique

d. A defocusing technique

The pattern goals for sidelobe suppression were designated and are shown in Figures 1.2-1 and 1.2-2. In Figure 1.2-1, symmetric suppression of near-in sidelobes on both sides of the main lobe is sought. Here, the most challenging suppression goal is -40db sidelobes from the main lobe null out to $\pm$ 15 degrees. In Figure 1.2-2 the reduction of the sidelobes to -40 db on only one side of the main lobe is sought. For the pattern goals, half-power beamwidths should lie between 2 and 6 degrees and the polarization should be circular.

1.3 RANGE FACILITY

A 46-meter test range was utilized for the pattern measurements. The range is located between two buildings 21.3 meters high (see Figure 1.3-1). Calculations for this range were performed at 8.0 GHz to determine the desirability of using a linearly polarized, 22 db gain horn as a source antenna to illuminate the test reflector. One calculation was concerned with the phase error present across the reflector aperture as introduced by

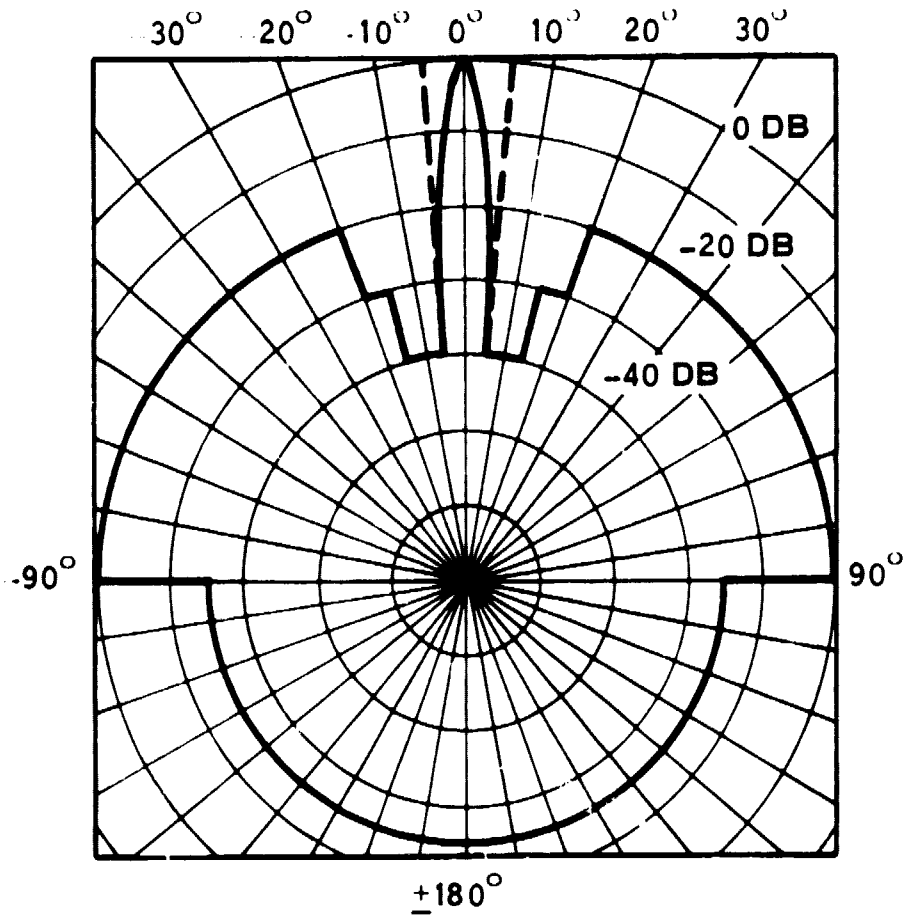

Figure 1.2-1. Sidelobe Suppression Goal for Symmetric Pattern

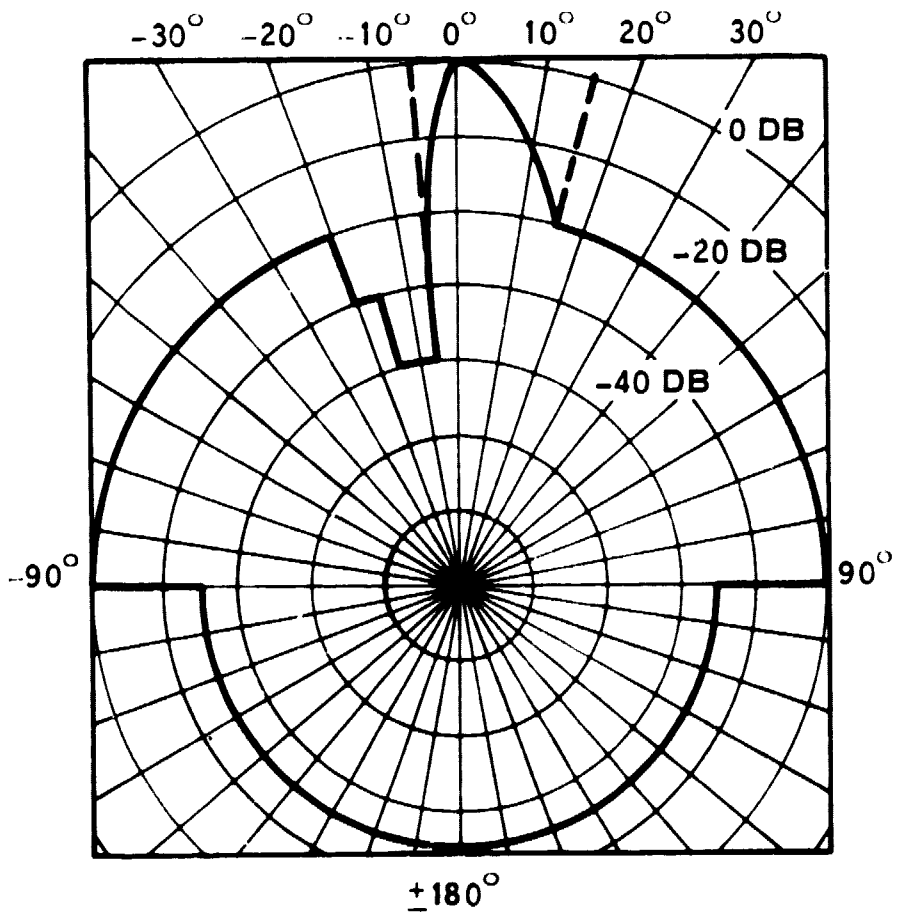

Figure 1.2-2. Sidelobe Suppression Goal for Asymmetric Pattern

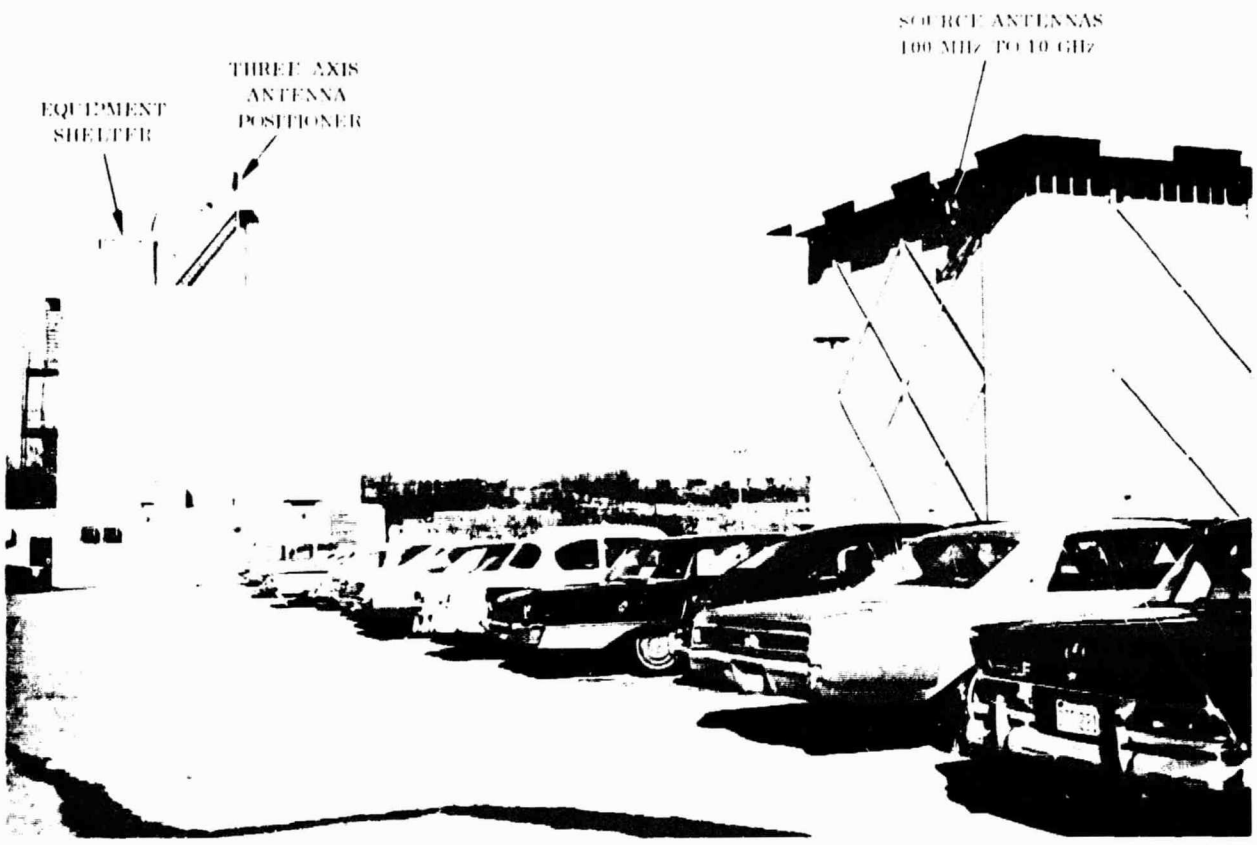

Figure 1.3-1. 46 Meter Antenna Test Range

a spherical phase front from the transmitting source. Here the maximum phase error, located at the edge of the reflector, was 6.3 degrees. This phase error is associated with a range distance equal to $7.2\ D^2/\lambda$ and alters the level of a -40 db sidelobe by less than 1 db. A second calculation dealt with the amplitude taper that exists across the reflector aperture because of the narrow beamwidth of the trasmit antenna. This calculation revealed that less than 0.006 db reduction in power from the illuminating wave existed at the edge of the reflector relative to its center. A third calculation related the variation in space attenuation loss of the illuminating wave to relatively small changes in reflector-range distance. These range changes would occur when the reflector is located at an extended radial distance from the axis of rotation of the pedestal and consequently would produce a change in range as the reflector rotates in aximuth. The change in space attenuation loss was found to be negligible for radial extensions of the reflector up to about 1.52 meters.

The pattern range was equipped with a Scientific Atlanta receiver, Series 1710, which provided square law operation over a 40 db dynamic range.

SECTION 2

ANALYTICAL INVESTIGATION

2.1 GENERAL SURVEY

This program commenced with a survey of pertinent literature in order to avoid any possible duplication of work. Numerous references were reviewed, but none were found to be of direct value insofar as this study is concerned. In these references, the sidelobe reduction was principally concerned with far-out lobes and the related control of stray currents on feed structures by means of absorbing material. In contrast, the objectives of this contract center about the control of aperture illumination, with the close inside lobes being of major importance. Reviews of the reports covered by the survey are given in Appendix A.

The well known standard references relating to pattern control by appropriate selection of the aperture illumination are included in this list. Since the illumination and its resulting pattern are Fourier mates, considerable mathematical technique may be brought to bear on this problem. It was hoped that some of the references sought might present novel means of implementing such techniques, but this was not the case.

It should be noted that, for the purposes of this study, the sidelobe structure after initially being made very small is allowed to increase somewhat beyond a certain point. This is in contrast with the conventional solution to the low sidelobe problem which is intended to hold all lobes below a given level. This permits the possible use of what might otherwise appear to be rather strange illumination functions.

2.2 MODIFICATION OF REFLECTOR ANTENNAS FOR SIDELOBE SUPPRESSION

In a reflector system the reflector shape, the feed pattern, or a combination of the two may be controlled in order to approximate a desired pattern. The possibilities afforded by feed pattern control are considered first.

2.2.1 PATTERN CONTROL - FEED MODIFICATION

A circularly polarized feed was required for this study. An end fire type was chosen to minimize sidelobes due to blockage. Appendix B supports the fact that capture area of such a feed, which is larger than its physical cross section, does not manifest itself in blockage but instead affects the axial ratio of the secondary pattern to a limited degree.

If the end fire structure is modulated in periodic fashion, the resulting traveling wave distribution is such that much higher gain may be realized than was formerly considered possible for such antennas. This has been conclusively domonstrated by Simon and Weill,(*) who report the construction and measurement of an 80 λ disc-on-rod element with a gain of 28 db. The structural modulation consisted of a simple periodic variation of the disc diameters.

By using a more complex variation, corresponding to additional spatial frequencies, the pattern shape may be varied. Since a desired shape may be specified by means of the transform relationship, this provides a conceptual means of approaching the objective. There are two practical objections to continuing along these lines, however, as follows:

a. Precise control implies very long elements. This is of course analogous to the waveform-spectrum relationship in circuit theory which requires large bandwidths for short rise times.

b. The reduction to practice of this technique is in itself a substantial research project beyond the scope of the present contract.

For these reasons it was decided to emphasize the utilization of reflector control as a more realistic means of proceeding.

2.2.2 REFLECTOR CONTROL

The analytical expression for the pattern of a reflector antenna may be expressed as

*J. C. Simon and G. Weill, "Un Nouveau Type D'Aerien a Rayonnement Longitudinal," Annales de Radioelectricite, July 1953, pp. 183-193

$$F(\theta, \phi) = \int_S \frac{E_F}{\rho} \left[\bar{n} \times (\bar{\rho}_1 \times \bar{e}_1) \right] e^{-jk(\rho - \bar{\rho} \cdot \bar{R}_1)} dS$$

where

θ, ϕ are the far field d tion angles

E_F is the feed amplitude pattern

$\bar{n}$ is the unit vector normal to reflector surface

ρ is the distance from focus to point on reflector

$\bar{\rho}_1$ is the unit vector for ρ, $\bar{\rho} = \bar{\rho}_1 \rho$

$\bar{e}_1$ is the unit polarization vector

$\bar{R}_1$ is the unit far field direction vector.

The general geometry of the configuration is shown in Figure 2.2-1.

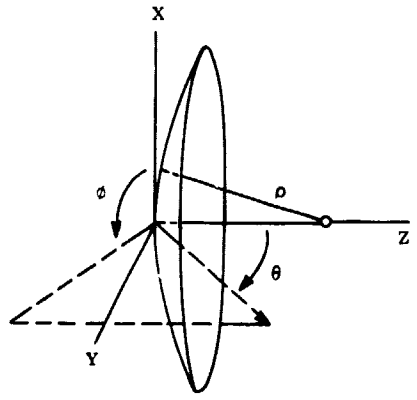

Figure 2.2-1. Configuration General Geometry

Various simplifications will be introduced in order to develop a model for analysis. In the first of these only E_θ or E_ϕ field components are considered, the others being negligible in the far field. The integral is replaced by a finite summation, and we may therefore determine n coefficients I_i using n equations as follows:

$$F(\theta_1, \phi_1) = I_1 e^{j\psi_1 (\theta_1, \phi_1)} \Delta S_1 + \text{--+} I_n e^{j\psi_n (\theta_1, \phi_1)} \Delta S_n$$

$$F(\theta_n, \phi_n) = I_1 e^{j\psi_1 (\theta_n, \phi_n)} \Delta S_1 + \text{--+} I_n e^{j\psi_n (\theta_n, \phi_n)} \Delta S_n$$

In the above, the I_i represent illuminations on different regions of the reflector as produced physically by the feed pattern E_F through the distance ρ. These regions will be taken to be circular annuli on a plane projection of the reflector. Thus we may fit the pattern at n points by means of n rings each having a prescribed amplitude value. The relationship of this model to the actual situation, in which the illuminated regions are on the curved surface of the reflector, is of course not exact. We are interested at this point in identifying a general approach, the detailed implementation of which is to be experimentally determined.

The number of rings was arbitrarily set at 20 for computational purposes. This introduced a major simplification. Instead of solving n equations to fit n pattern points, we adjust the ring amplitudes to suppress the first sidelobe only, which is equivalent to fitting the pattern at one point in addition to the main beam maximum. In order to do this, a computer was programmed to identify the contribution of each ring to each calculated pattern point. By this means we may readily determine the side-lobe components and alter the ring amplitudes in such a fashion that these are made to cancel. The solution is not unique; thus, there is a possibility of applying this procedure simultareously to the second side lobe, and so on. Figure 2.2-2 shows the results of equating the first sidelobe to zero, when using the nominal amplitude function $0.3 + 0.7 (1 - r^2)$ which represents a 10 db edge taper. It will be noted that the pattern with suppression is broader at the base than the altered one, and that the third lobe is larger than the original second lobe. This effect was achieved by reducing the amplitude of Rings 13, 14 and 15 by 20 db.

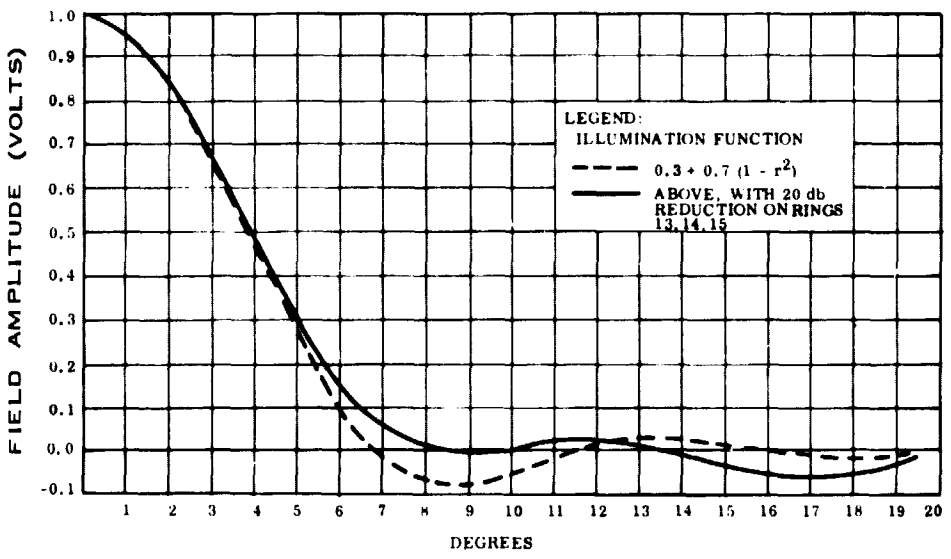

Figure 2.2-2. Pattern of 11.8 λ Aperture for Twenty Rings

Insofar as the accuracy of this analysis is concerned, the use of 20 rings implies that we consider the amplitude to be constant over 1/20 of the projected aperture diameter. The nominal amplitude function used in the calculation, corresponding to realistic situations, is

$$A = 0.3 + 0.7\,(1 - r^2)$$

Its variation with radius is

$$\frac{dA}{dr} = -1.4\,r\,, \quad \text{or} \quad \Delta A = \frac{-1.4r}{20}$$

The greatest variation is at the edge where $r = 1$

so that $\left|\Delta A_{MAX}\right| = 0.07$, compared to the assumption that it has a constant value of 0.3 at this point. The error in amplitude is about 1/4 db, which would require very careful control to realize in practice.

2.2.2.1 Absorber Rings

The physical realization of this condition might be approximated by using absorbing material on the three rings in question. This approach was rejected since the power in this zone is lost by such a technique.

2.2.2.2 Active Zone Compensation

This situation requires that some of the ring amplitudes be increased over their normal values, corresponding physically to the use of amplification in such regions. The additional power required to do this is used constructively, rather than being lost in order to satisfy the amplitude function.

For this case, the same amplitude function was used and the pattern was computed for the same 11.8 wavelength aperture. By examining the ring contributions it was found that the addition of Ring 25 (thus leaving Rings 21, 22, 23 and 24 vacant) with amplitude 0.247 would

suppress the first sidelobe. The details are given in Table 2.2-1. Column A is the pattern of the 20-ring aperture. Column B is the pattern of Ring 25. Column B is obtained by cancelling the first sidelobe of the aperture pattern at 8.5 degrees. That is, the ring contribution of 0.296 is made equal to 0.073 (the negative of the sidelobe value) by multiplying Column B by 0.247. The normalized sum of A and B' is shown as Column C, representing the adjusted pattern, and plotted in Figure 2.2-3. It is seen that the main beam has become narrower which is due to the fact that the antenna is effectively larger, now having a diameter increased by the factor 25/20. The corresponding efficiency calculation in Appendix C shows an aperture efficiency of 65 percent for this configuration.

Table 2.2-1. Pattern Computation - First Sidelobe Removed

	A	B	B'	A + B'	C
Degrees	Entire Aperture	Ring 25 Norm. to 1	Adjusted Amplitude		Normalized
0	1.000	1.000	0.247	1.247	1.000
0.5		0.960			
1.0	0.956	0.843	0.208	1.164	0.933
1.5	0.904	0.665	0.164	1.068	0.856
2.0	0.834	0.446	0.110	0.944	0.757
2.5	0.749	0.212	0.052	0.801	0.642
3.0	0.655	-0.011	-0.003	0.652	0.523
3.5	0.554	-0.197	-0.049	0.505	0.405
4.0	0.451	-0.328	-0.081	0.370	0.297
4.5	0.351	-0.395	-0.097	0.254	0.204
5.0	0.256	-0.394	-0.097	0.159	0.128
5.5	0.171	-0.334	-0.082	0.089	0.071
6.0	0.097	-0.227	-0.056	0.041	0.033
6.5	0.036	-0.095	-0.023	0.013	0.010
7.0	-0.011	0.043	0.011	0	0
7.5	-0.044	0.164	0.040	-0.004	-0.003
→ 8.0	-0.064	0.252	0.062	-0.002	-0.002
→ 8.5	-0.073	0.296	→ 0.073	0	0
9.0	-0.072	0.292	0.072	0	0
9.5	-0.063	0.244	0.060	-0.003	-0.002
10.0	-0.050	0.161	0.040	-0.010	-0.008
10.5	-0.034	0.057	0.014	-0.020	-0.016
11.0	-0.017	-0.050	-0.012	-0.029	-0.023
11.5	-0.001	-0.145	-0.036	-0.037	-0.030
12.0	0.012	-0.214	-0.053	-0.041	-0.033
	↑ Original pattern				↑ First sidelobe cancelled pattern

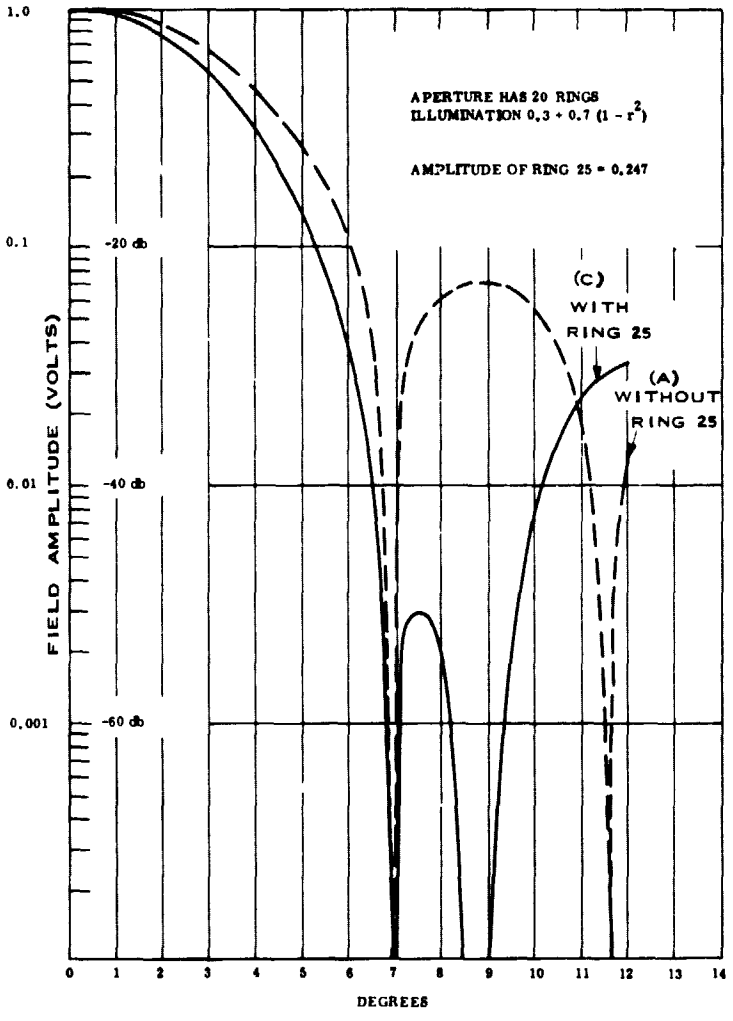

Figure 2.2-3. Computer Pattern of 11.8 λ Aperture for Plus Ring 25

2.3 SELECTION OF THE MOST PROMISING TECHNIQUES

An investigation was carried out to determine the extent to which conventional heavy tapering might prove advantageous, in theory at least, in comparison to the two techniques mentioned previously and summarized below:

a. Use of Absorber Rings. 11.8 wavelength diameter aperture with 10 db taper and 20 db absorber on Rings 13, 14, 15 (entire aperture consists of 20 rings). Efficiency, including 19% power lost in absorber, is 62 percent (0.77 x 0.81).

b. Active Zone Compensation. Same aperture without absorber, having an active compensation ring of radius 1.25 times the aperture radius. This provides a 6 percent (1/4 db) gain increase over the unmodified aperture, due to the fact that the antenna is effectively larger. Efficiency, including power gained in the active zone, is 65 percent.

The heavy taper analysis was based on design data from Figures 2.3-1 and 2.3-2. These

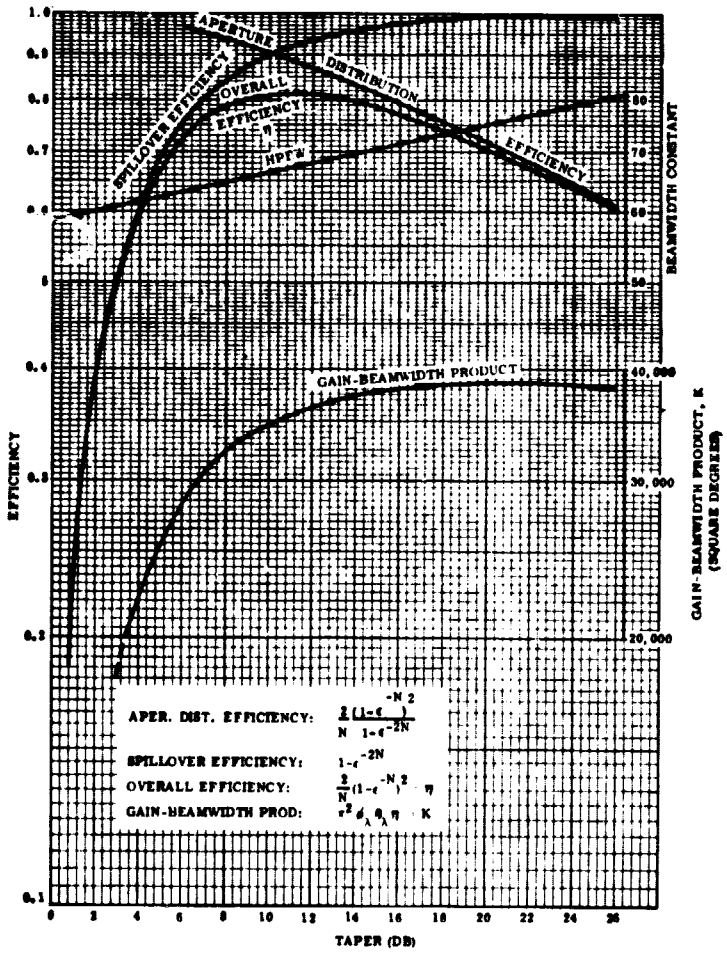

Figure 2.3-1.

Aperture Distribution Efficiency, Spillover Efficiency, Overall Efficiency, Half-Power Beamwidth Product for a Circular Aperture with Incomplete Gaussian Amplitude Distribution of Various Edge Taper

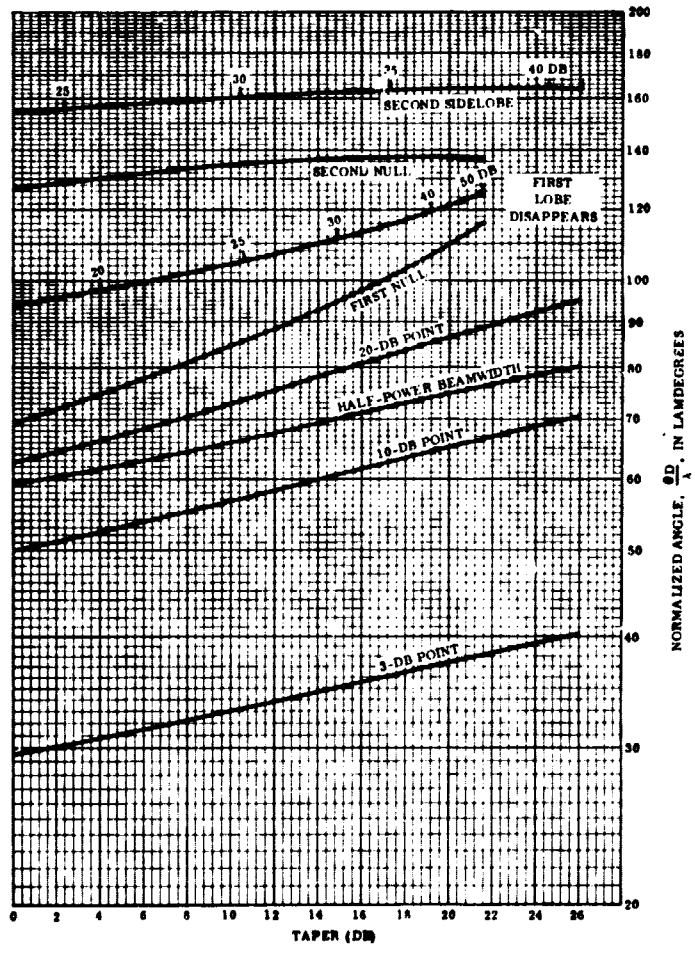

Figure 2.3-2.

First and Second Sidelobe Level and Position; First and Second Null; 3 db, 10 db, and 20 db Points for Circular Aperture with Incomplete Gaussian Amplitude Distribution of Various Edge Taper

show sidelobe levels, beamwidths, first nulls and efficiencies as a function of the incomplete or truncated Gaussian amplitude distribution. The results of this analysis are given in Figure 2.3-3 which shows that for the electrically large apertures (36 wavelengths) it is theoretically possible to achieve -40 db sidelobe levels by the use of a sufficiently heavy taper; 20 db in this case. This cannot be done for the smaller apertures (12 wavelengths) because the feed blockage is now proportionately excessive. This assumes the use of broadside type feeds.

As the taper is increased to decrease the side-lobes, the antenna diameter must be increased to maintain the first null in the same angular location. Under this condition the beamwidth will narrow and the gain will increase. Figure 2.3-4 shows these relationships. For a 20 db taper, the aperture diameter must increase by 26 percent. The beamwidth is 88 percent of the original value and the gain has increased by 1.46 db. This approach is attractive for the larger apertures since it is the simplest means of achieving the desired result.

It is concluded that the heavy taper approach is best for the larger apertures and that the active zone approach is best for the smaller ones when broadside type feeds are used. This is not necessarily the case when using end-fire feeds. As shown in Appendix B, the use of the latter will not produce blockage sidelobe problems in the same fashion as broadside feeds.

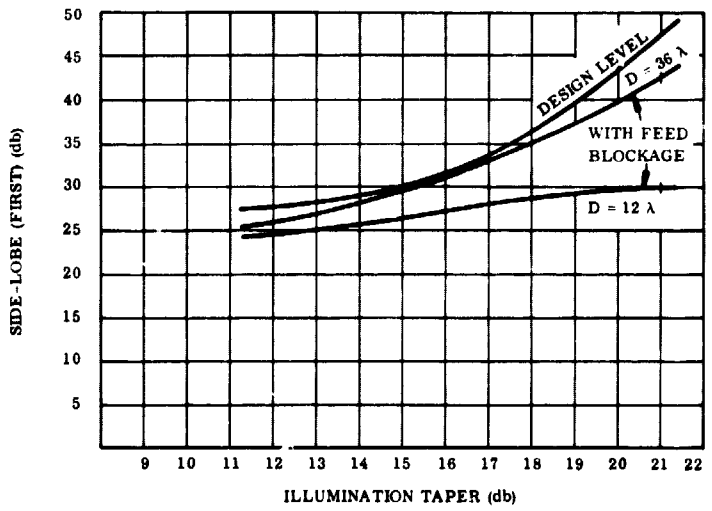

Figure 2.3-3.
Effect of Feed Blockage on Sidelobe Levels

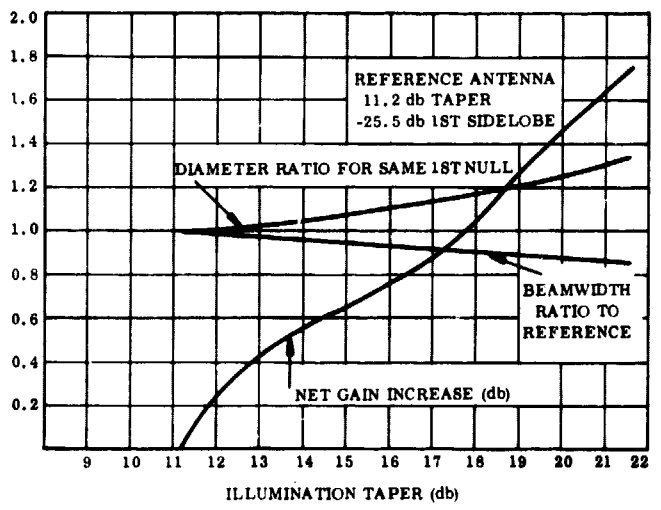

Figure 2.3-4.
Effect of Increasing Antenna Diameter to Keep First Null in Same Angular Location as for Reference

The data shown in Figures 2.3-3 and 2.3-4 apply to broadside feeds only. For endfire feeds, the blockage area does not vary and different conclusions would follow. Experimental evidence in this connection is not available from the test program since the model was used with linear, rather than circular, polarization in the interest of simplicity. In a circularly polarized system it is expected that heavy tapering would prove advantageous for apertures smaller than that allowed by Figure 2.3-3.

An alternative technique lies in using a single active element on the rear of the feed to cancel blockage sidelobes due to the presence of the feed. Another possible procedure is to defocus the feed and use the rear lobe of the feed pattern to correct the aperture blockage.

For the smaller aperture antenna that was investigated in this program, the four following techniques were selected to realize low sidelobes:

a. Heavy Taper

b. Blockage Compensation

c. Active Zone Suppression

d. Feed Defocussing

The last three techniques are depicted in Figure 2.3-5.

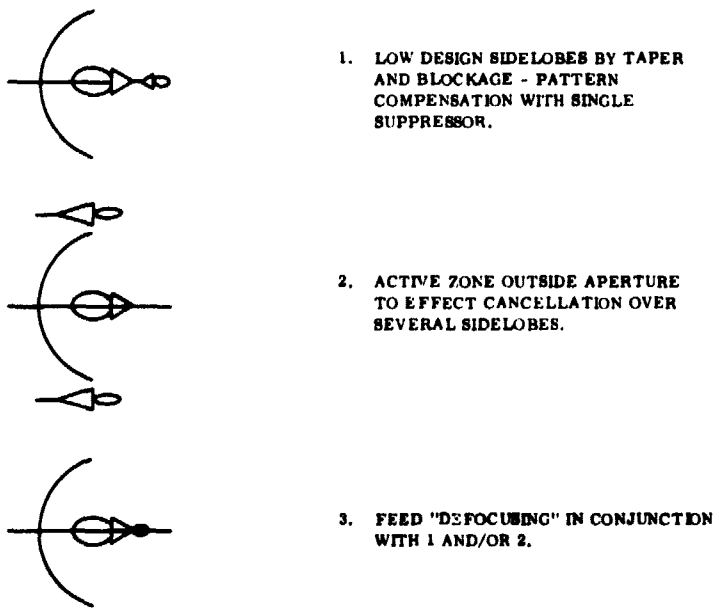

Figure 2.3-5. Three Sidelobe Suppression Techniques Refined by Analytical Study

2.4 DETAILED ANALYSIS

Sidelobe suppression analyses were performed on a 13 λ diameter paraboloid using the blockage compensation and active zone suppression techniques in conjunction with tapered paraboloid aperture distribtions. For the purpose of making the calculations, a frequency of 8.0 GHz was assumed. Helix radiators were considered as the elements to be employed as the primary feed; they were also considered in the implementation of the blockage compensation and active zone suppression techniques.

The calculations of paraboloid power patterns assumed no aperture blockage. This was done in order to assess the relative effectiveness of the blockage compensation technique and the active zone suppression technique in suppressing only paraboloid pattern sidelobes. In practice, of course, aperture blockage is present and produces a constant-amplitude, out-of-phase field in the vicinity of broadside. This field, when superimposed on the paraboloid pattern, raises sidelobe levels and fills-in nulls. However, it is anticipated that the application of blockage compensation will correct this blockage effect and reduce the problem to the suppression of the paraboloid sidelobes alone.

The pattern calculations were limited to the critical angular region $19.5^{o} \geq \theta \geq -19.5^{o}$ about the normal to the aperture, wherein substantial sidelobe suppression (i.e., -40 db for $15^{o} \geq \theta \geq -15^{o}$) was a design goal.

The paraboloid was assumed to have three aperture distributions:

$$A(r) = 0.3 + 0.7(1 - r^2) \qquad \text{(i.e., -22.8 db first sidelobes)}$$

$$A(r) = 0.1 + 0.9(1 - r^2) \qquad \text{(i.e., -24.4 db first sidelobes)} \qquad (2.4\text{-}1)$$

$$A(r) = 0.1 + 0.9(1 - r^2)^2 \qquad \text{(i.e., -36.5 db first sidelobes)},$$

where $1 \geq r \geq -1$ and $2r$ = diameter of the aperture.

The blockage compensation technique for sidelobe suppression involves the use of a single helix, possibly located on the reverse side of the helix primary feed, but always oriented along the axis of the paraboloid. The pattern assumed for this elemental radiator is given by Kraus[1] as,

$$E_{HELIX} = E_H \sin\left(\frac{\pi}{2M}\right) \frac{\cos\left[\pi S_\lambda M (1 - \cos\theta)\right] \cos\theta}{\sin\left\{\pi\left[S_\lambda (1 - \cos\theta) 2\frac{1}{2M}\right]\right\}}$$

where E_H is the amplitude of the field, M is the number of helix turns, and $S_\lambda = 0.22$ is the axial distance between helix turns.

The active zone suppression technique consists of two helix elements spaced many wavelengths apart. Its pattern is described analytically by

$$E_{ACTIVE\ ZONE} = E_I \sin\left(\frac{\pi}{2M}\right) \frac{\cos\left[\pi S_\lambda M (1 - \cos\theta)\right] \cos(\pi d/\lambda \sin\theta) \cos\theta}{\sin\left\{\pi\left[S_\lambda (1 - \cos\theta) + \frac{1}{2M}\right]\right\}} \qquad (2.3\text{-}3)$$

where E_I is the amplitude of the field and d/λ is the spacing in wavelengths between the two helices. This configuration will provide sidelobe suppression in one pattern plane of the paraboloid and, thus, can be termed a linear zone suppressor. (A circular zone suppressor, i.e., a ring of helices, would provide sidelobe suppression in all pattern planes of the paraboloid.) It achieves this by pairing its maxima in phase opposition with the sidelobe maxima of the paraboloid pattern.

Both sidelobe suppression techniques were separately applied to each paraboloid aperture distribution in Equations 2.4-1 through 2.4-3 and their effects noted in Figures 2.4-1 through 2.4-4. Where more than one sidelobe was present in the angular region $15^o \geq \theta \geq -15^o$, the criterion employed was to suppress all to minimum but equal field strength levels.

---

1. Kraus, Antennas, McGraw Hill Book Company Inc., New York, 1950, p. 202.

Figure 2.4-1 illustrates the degree of sidelobe suppression obtained for the aperture distribution $A(r) = 0.3 + 0.7(1 - r^2)$ using 6-turn helices. As shown, a single 6-turn helix fed in-phase with the main lobe of the paraboloid pattern, suppressed sidelobes from a mixiumum level of -22.8 to -26.0 db; the active zone suppressor of two 6-turn helices, spaced 14.37 λ apart and fed in-phase, reduced the first two sidelobes to a -34.0 db level. Blockage compensation suppression of sidelobes is limited because the suppressor field, while subtracting from the field of the first sidelobe, adds to the field of the second sidelobe. With the second technique, the proper phasing for multiple sidelobes reduction is present, but the helix element pattern is too broad in beam width to adequately match the amplitudes of the first two sidelobes of the paraboloid pattern. These sidelobes differ in peak amplitude by a factor of 2.4:1. In order to satisfy this amplitude envelope, a very narrow-beamwidth helix element pattern would be required. In Figure 2.4-2, the effect of using this element in both sidelobe suppression techniques is shown. For the first technique, sidelobe levels are reduced to -27.8 db, while for the second technique they became -37.7 db.

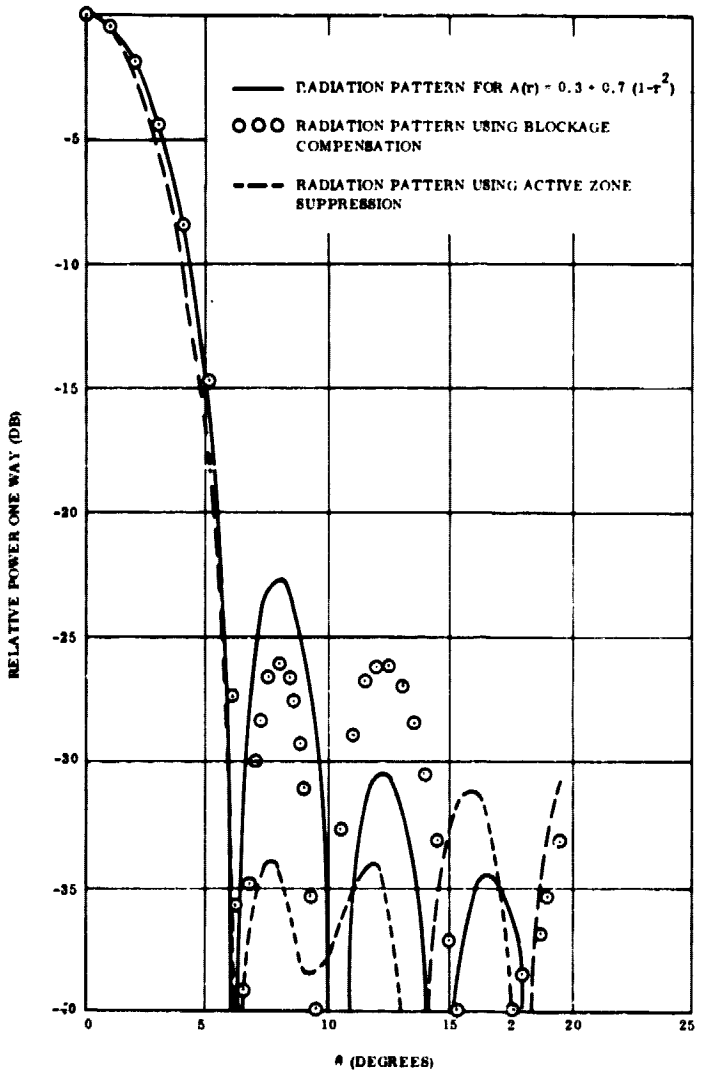

Figure 2.4-1.
Sidelobe Suppression for Aperture Distribution $A(r) = 0.3 + 0.7(1 - r^2)$ Using 6-turn Helix

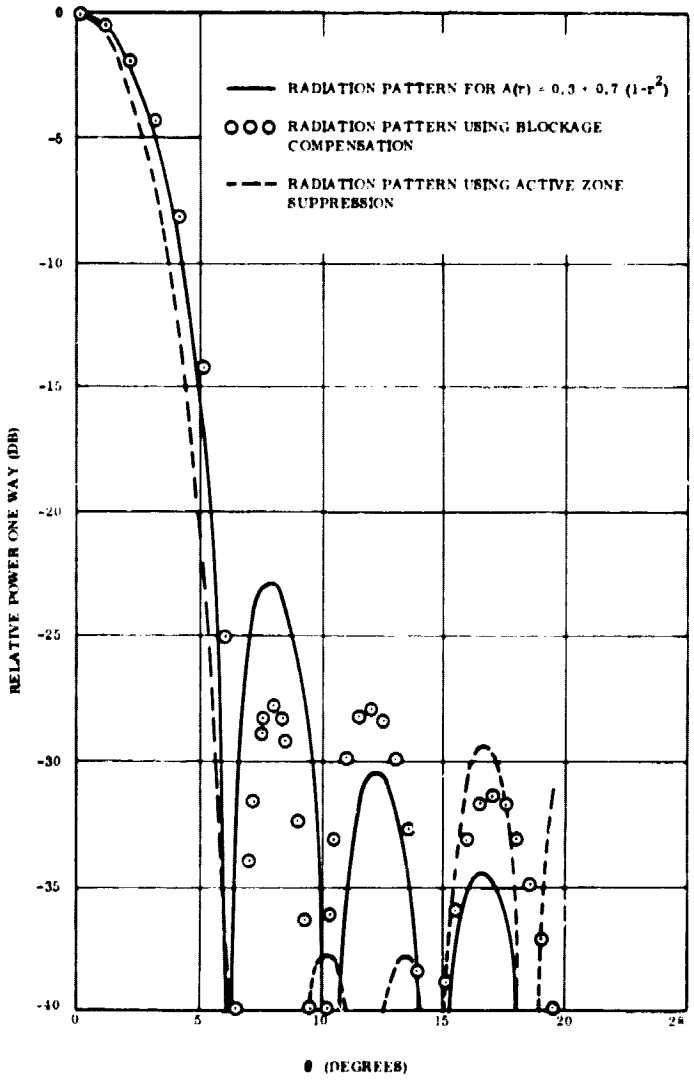

Figure 2.4-2.
Sidelobe Suppression for Aperture Distribution $A(r) = 0.3 + 0.7(1 - r^2)$ Using a Narrow Beamwidth Element

Introducing a greater amplitude taper across the aperture of the paraboloid has the effect of lowering the sidelobe levels in its radiation pattern. Furthermore, the lower the sidelobe level is, the easier it becomes to suppress these lobes to a desired level. In Figure 2.4-3, and especially Figure 2.4-4, this fact becomes quite evident. In Figure 2.4-3, -24.4 db sidelobes are suppressed to -28.2 db using the blockage compensator suppressor: they are also suppressed to -34.7 db using the active zone technique with an interelement spacing of 13.53 λ. In Figure 2.4-4, -36.5 db sidelobes were suppressed below -40 db by using either a single 6-turn helix or two 6-turn helices with an interspacing of 12.12 λ.

These calculations indicate the degree of sidelobe suppression attainable by using blockage compensation and active zone suppression and a heavy taper. Where more than one sidelobe appears above the desired -40 db level, the active zone suppression technique is more effective in reducing multiple sidelobes; whereas, if only one sidelobe is to be suppressed blockage compensation would suffice.

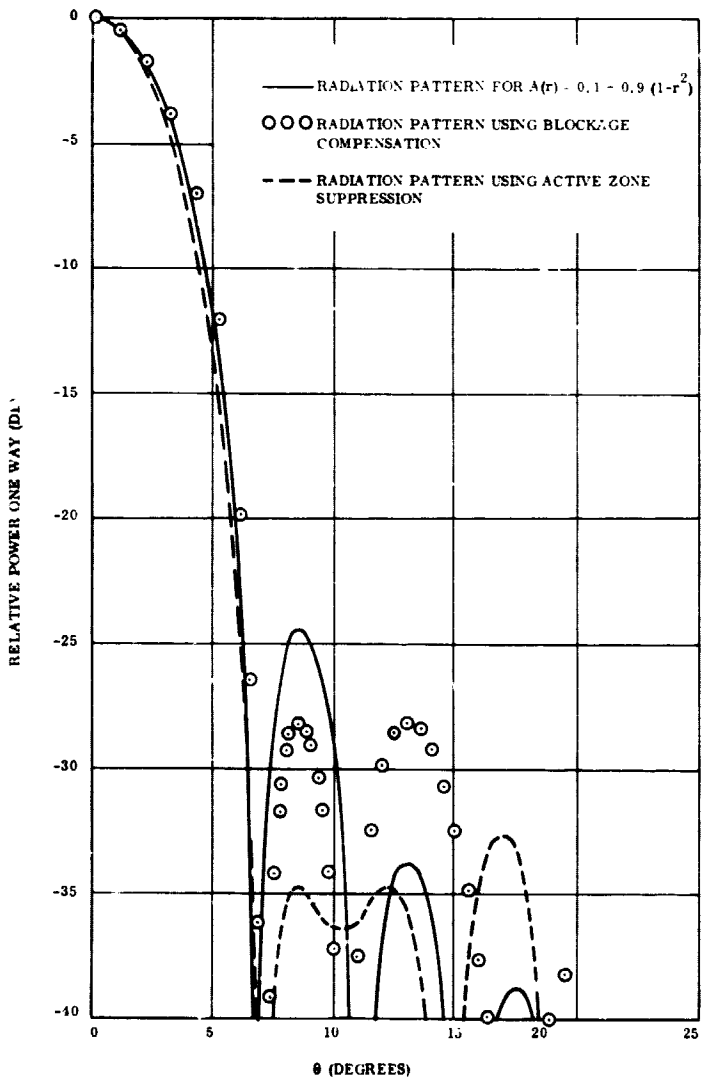

Figure 2.4-3.
Sidelobe Suppression for Aperture Distribution A (r) = 0.1 + 0.9 (1 - r^2) Using 6-Turn Helix

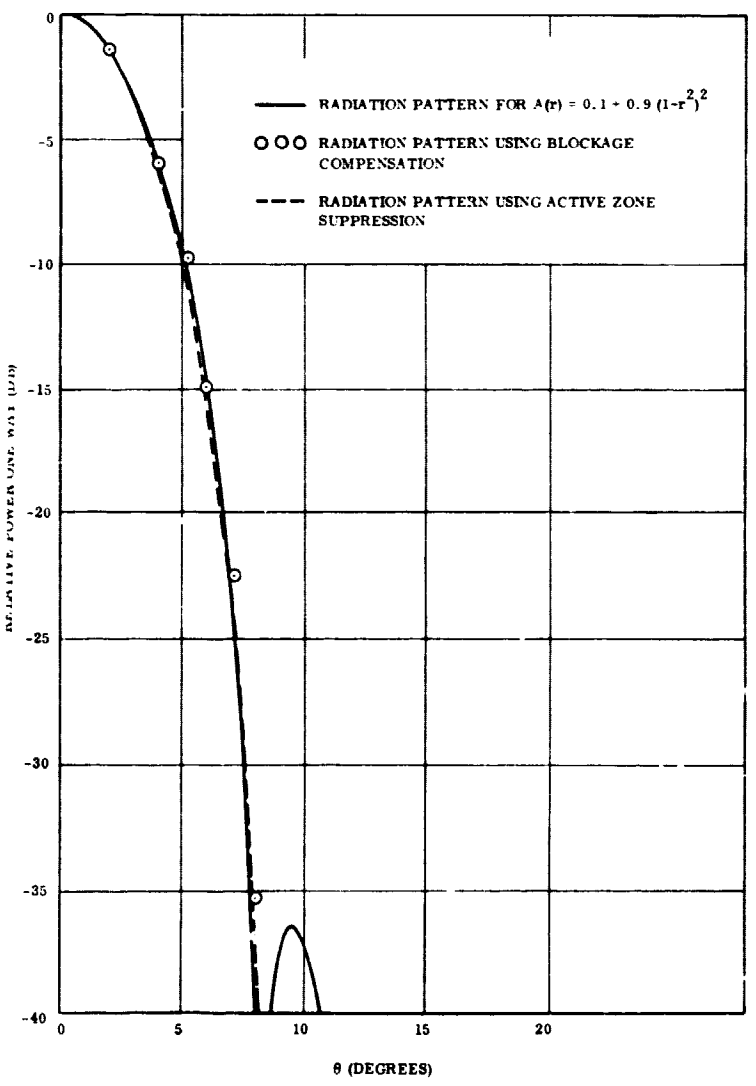

Figure 2.4-4.
Sidelobe Suppression for Aperture Distribution A (r) = 0.1 + 0.9 (1 - r^2)^2 Using 6-Turn Helix

SECTION 3

EXPERIMENTAL INVESTIGATION

The experimental phase of this program dealt with the design, fabrication and testing of the sidelobe suppression techniques as applied to a precision-cut paraboloid reflector.

3.1 OBJECTIVE

The objective of the experimentation was to demonstrate sidelobe suppression in one pattern plane of a paraboloid antenna by applying, individually or collectively:

a. A heavy taper

b. A blockage compensation technique

c. A linear zone suppression technique

d. A defocusing technique

The pattern goals for sidelobe suppression were designated and are shown in Figures 3.1-1 and 3.1-2. In Figure 3.1-1, symmetric suppression of near-in sidelobes on both sides of the main lobe is sought. Here, the most challenging suppression goal is -40 db sidelobes from the main lobe null out to ± 15 degrees. In Figure 3.1-2 the reduction of the sidelobes to -40 db on only one side of the main lobe is desired. For the pattern goals, half-power beamwidths should lie between 2 and 6 degrees and the polarization should be circular.

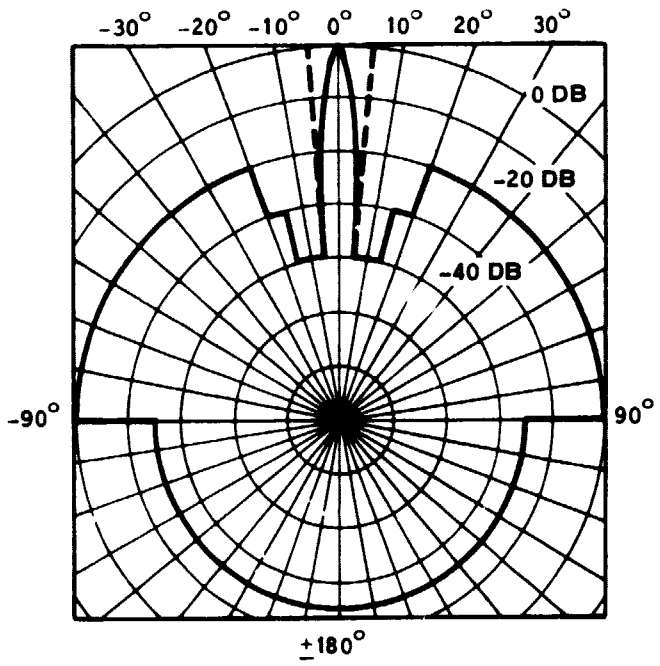

Figure 3.1-1. Sidelobe Suppression Goal for Symmetric Pattern

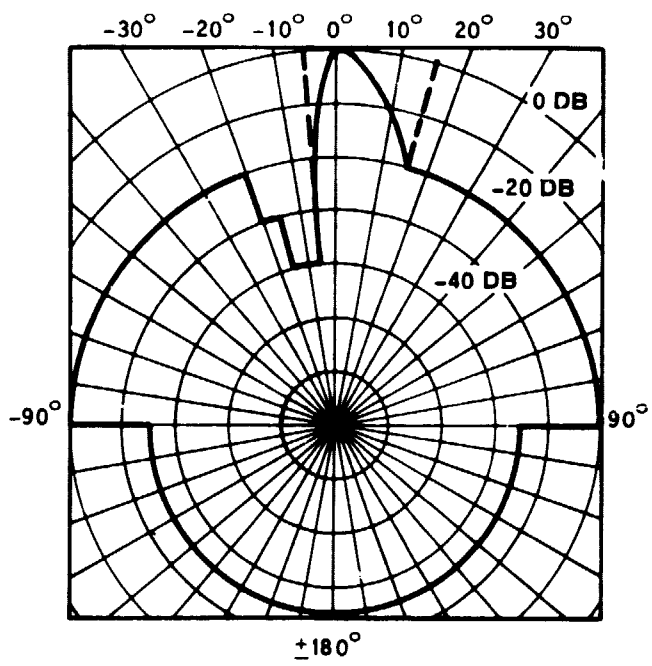

Figure 3.1-2. Sidelobe Suppression Goal for Asymmetric Pattern

3.2 IMPLEMENTATION

The frequency band chosen for experimentation was at X-band. A paraboloid with a diameter of 49 cm and a focal length of 19.6 cm (i.e., focal length/paraboloid diameter = 0.4) was accurately machined from hardened aluminum stock. Measurement of the paraboloid surface revealed an RMS surface tolerance of 0.002 cm, which is more than adequate to realize -40 db sidelobes. Photographs of the paraboloid and a support structure to attach it to the pedestal are shown in Figures 3.2-1 and 3.2-2 respectively.

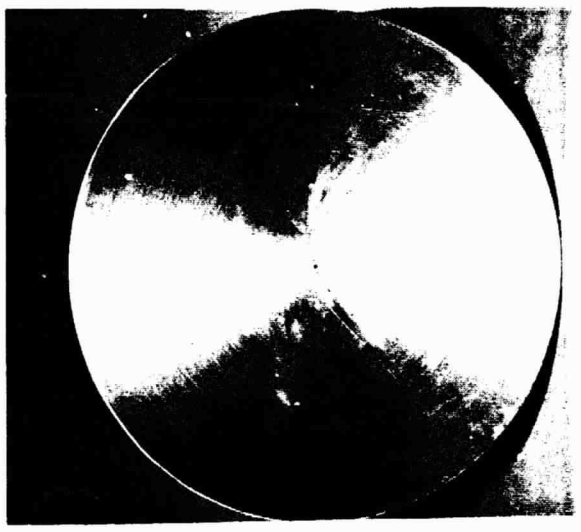

Figure 3.2-1. Front View of 49 cm Diameter Paraboloid

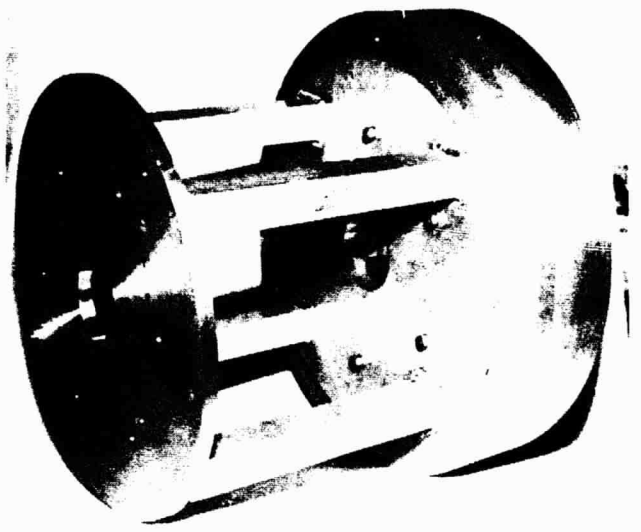

Figure 3.2-2. Aft View of Paraboloid Support Structure

A clockwise-wound helix was used as the feed for the paraboloid to meet the circular polarization requirement. The helix was chosen because (1) it could be axially supported, thereby removing the scattering effects from feed support struts; (2) it indicated a singular phase center*; (3) it exhibited small aperture blockage; and (4) it was simple and inexpensive to fabricate.

The blockage compensation technique employed a counter-clockwise wound helix whose preferred location would be on the back-side of the primary feed of the reflector.

Two, counter clockwise wound helices, spaced many wavelengths apart, were the antennas used in the active zone suppression technique. The defocusing technique required no additional hardware.

---

* Experimental results obtained by S. Sander of RCA and D.K. Cheng of Syracuse indicated a common phase center for the helix element. Their findings are given in a paper entitled, "Phase Center of Helical Beam Antennas," which appeared in the IRE National Convention Record, 1958.

An rf circuit was implemented which permitted independent amplitude and phase control of the above suppressor techniques and combined their signals with the paraboloid signal. Details on this circuit and the helix designs will be discussed in a later section of this report.

3.3 MEASUREMENTS OF HELIX FEEDS

Four-turn through 6-turn helices, in 1/2-turn increments, were designed and fabricated at X-band; associated reflector cups and reflector plates which ranged in diameter from 2.54 to 5.08 cm were also fabricated as shown in Figures 3.3-1 and 3.3-2.

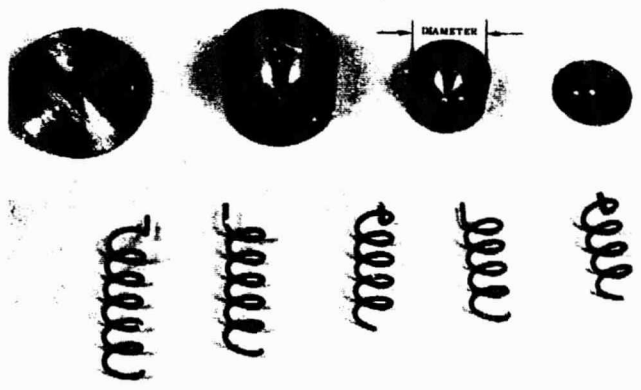

Figure 3.3-1. Disassembled Helix Feeds

Figure 3.3-2. Assembled Helix Feeds

Initial helix measurements were concerned with establishing the operating test frequency within X-band by observing the frequency at which most helix-reflector combinations exhibited minimum axial ratios. This frequency was determined to be 7.5 GHz.

Principal-plane helix patterns were taken using vertical and horizontal polarizations. From these data, three candidate feed configurations were chosen which best satisfied:

a. Symmetric illumination of the paraboloid over a conical angle of 128 degrees (this is the subtended angle of the paraboloid at its focal point)

b. A paraboloid edge illumination which was about -17 db below that at its center

These feed configurations were a 4-turn helix with a 3.19 cm diameter cup and a 5-turn and 6-turn helix with a 3.3 cm-diameter cup. Cups were shown to be preferred to reflector plates because they eliminated beam squint.

The patterns and axial ratios are shown for each in Figures 3.3-3 through 3.3-8. (The

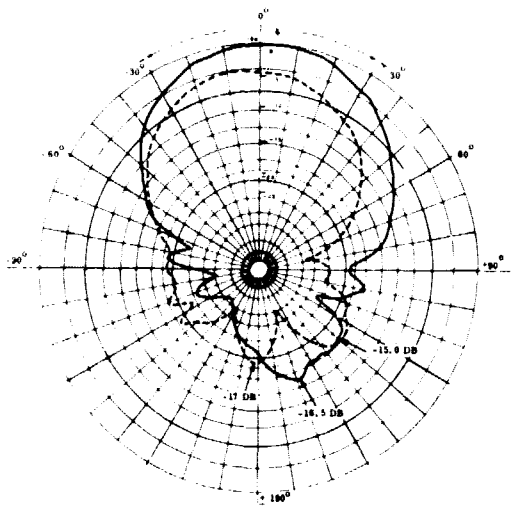

Figure 3.3-3. Feed Pattern in $\phi = 0^{O}$ Plane Using 4-Turn Helix Feed; Axial Ratio = 2.5 DB for $\psi = 0^{O}$ Direction, f = 7.5 GHz

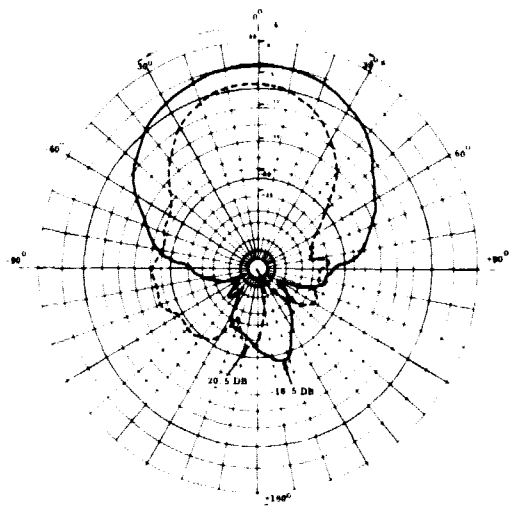

Figure 3.3-4. Feed Pattern in $\phi = 90^{O}$ Plane Using 4-Turn Helix Feed; Axial Ratio = 2.5 DB for $\psi = 0^{O}$ Direction, f = 7.5 GHz

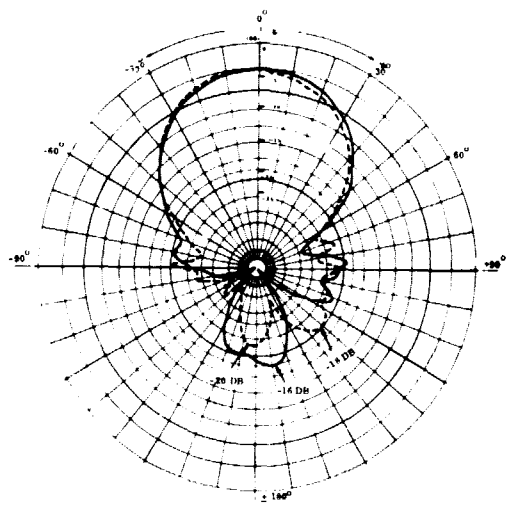

Figure 3.3-5. Feed Pattern in $\phi = 0^{O}$ Plane for 5-Turn Helix Feed; Axial Ratio = 2.0 DB for $\psi = 0^{O}$ Direction, f = 7.5 GHz

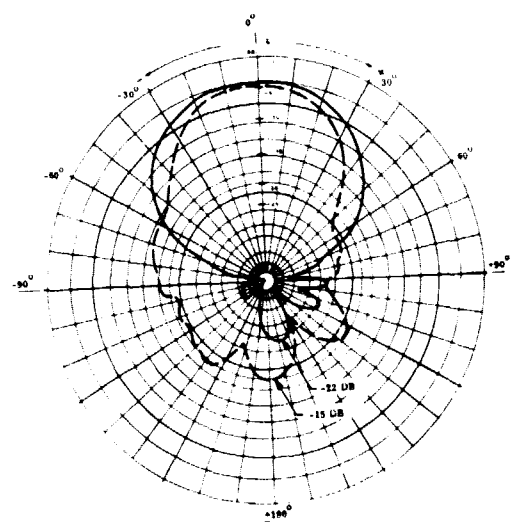

Figure 3.3-6. Feed Pattern in $\phi = 90^{O}$ Plane Using 5-Turn Helix Feed; Axial Ratio = 2.0 DB for $\psi = 0^{O}$ Direction, f = 7.5 GHz

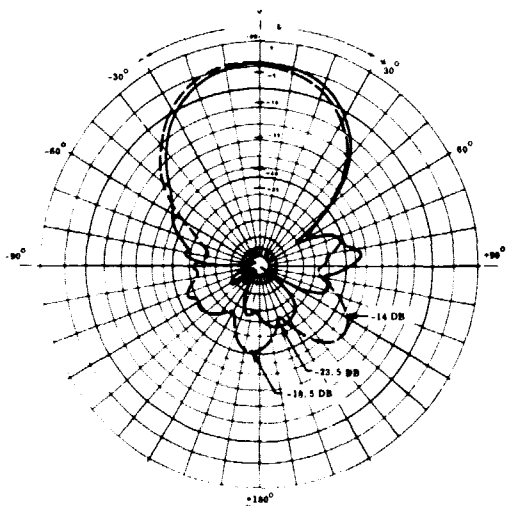

Figure 3.3-7. Feed Pattern in $\phi = 0^{O}$ Plane Using 6-Turn Helix feed; Axial Ratio = 1.9 DB for $\psi = 0^{O}$ Direction, f = 7.5 GHz

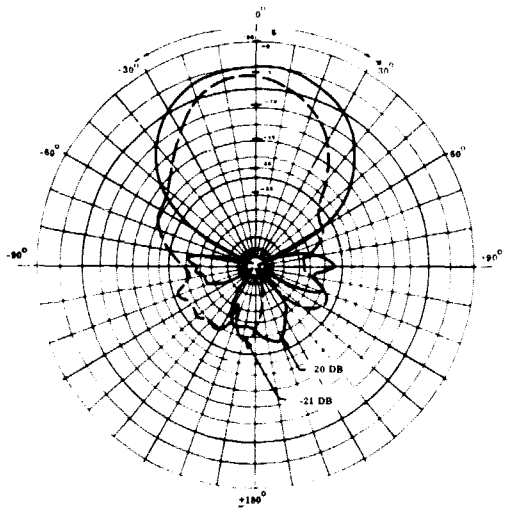

Figure 3.3-8. Feed Pattern in $\phi = 90^{O}$ Plane Using 6-Turn Helix Feed; Axial Ratio = 1.9 DB for $\psi = 0^{O}$ Direction, f = 7.5 GHz

LEGEND:
—— VERTICAL POLARIZATION
- - - HORIZONTAL POLARIZATION

power level of the vertically and horizontally polarized patterns are not relative power levels in these figures.) The patterns display a marginal degree of symmetry within the conical angle of 128 degrees; the nominal half-power beamwidths for the 4-turn, 5-turn and 6-turn helices are 61, 54 and 47 degrees, respectively. All of the patterns exhibit asymmetric backlobe radiation which varies from -15 to -23.5 db in peak-level (relative to the main beam maximum) over the paraboloid angular interval $15^{o} \geq \theta \geq -15^{o}$.

3.4 PREDICTION OF PARABOLOID PATTERNS

The vertically and horizontally polarized patterns for each helix feed were averaged and a nominal feed pattern constructed. To this was added the space attenuation loss factor to generate the average aperture illuminations for the paraboloid. Figures 3.4-1 through 3.4-3 illustrate these illuminations for the 4, 5 and 6 turn helices, respectively; in order, their edge illumination (at the subtended angle from the focus of $\pm 64^{o}$) was -16 db, -20 db and -23 db. These aperture distributions were then approximated by expressions of the form $A(r) = K_1 + K_2 (1 - r^2)^M$, (where r is the normalized aperture radius), to calculate predicted patterns. Two expressions, one straddling the average aperture distribution as an upper bound and the other as a lower bound, were used. For the 4-turn helix, $K_1 = 0.16$, $K_2 = 0.84$ and $M = 2.0$ represented the upper bound and $M = 2.5$ the lower bound. In the case of the 5-turn helix, $K_1 = 0.096$, $K_2 = 0.904$ and the upper and lower bound expressions utilized $M = 2.5$ and 3.0, respectively; the 6-turn helix used $K_1 = 0.068$, $K_2 = 0.932$ with the upper bound employing $M = 3.0$ and the lower bound $M = 3.5$.

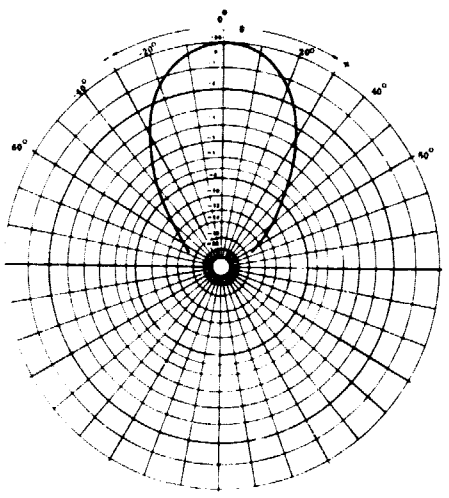

Figure 3.4-1. Paraboloid Aperture Illumination (Including Space Loss) Using Average Pattern for 4-Turn Helix

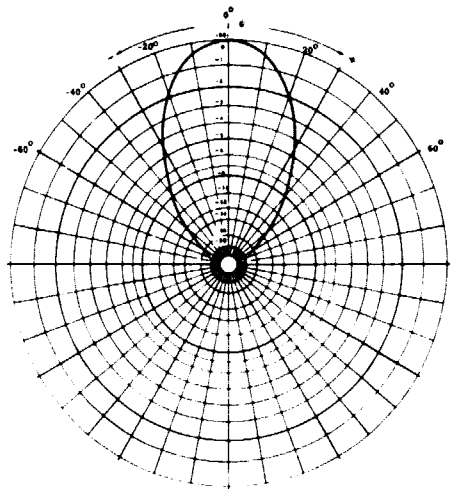

Figure 3.4-2. Paraboloid Aperture Illumination (Including Space Loss) Using Average Pattern for 5-Turn Helix

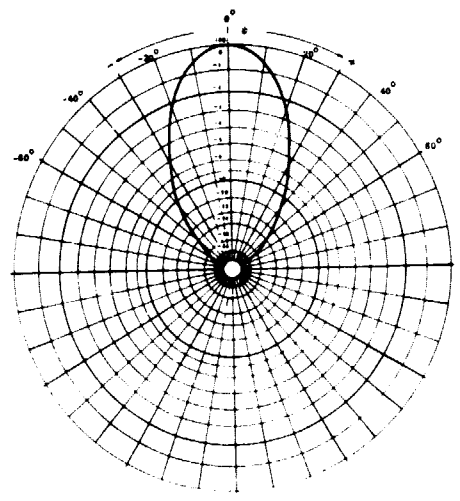

Figure 3.4-3. Paraboloid Aperture Illumination (Including Space Loss) Using Average Pattern for 6-Turn Helix

The two paraboloid patterns for each helix feed are given in Figure 3.4-4. The patterns neglect feed blockage and feed backlobe effects. The patterns associated with the 4-turn helix feed exhibited a half-power beamwidth of 5.9 degrees, a null-to-null mainlobe beamwidth of either 16 or 17.4 degrees and a single sidelobe above -40 db within $15^{o} \geq \theta \geq -15^{o}$. The 5- and 6-turn helix feeds produced patterns with broader mainlobes and no sidelobes above -40 db within this θ interval; a half-power beamwidth of 6.2 degrees and a null-to-null beamwidth of 19.2 to 24.4 degrees characterized the main lobe for the 5-turn helix feed while values of 6.6 degrees and 22.8 to 25.6 degrees reflected the same for the 6-turn feed. As such, the 4-turn helix is preferred because of its narrower mainlobe.

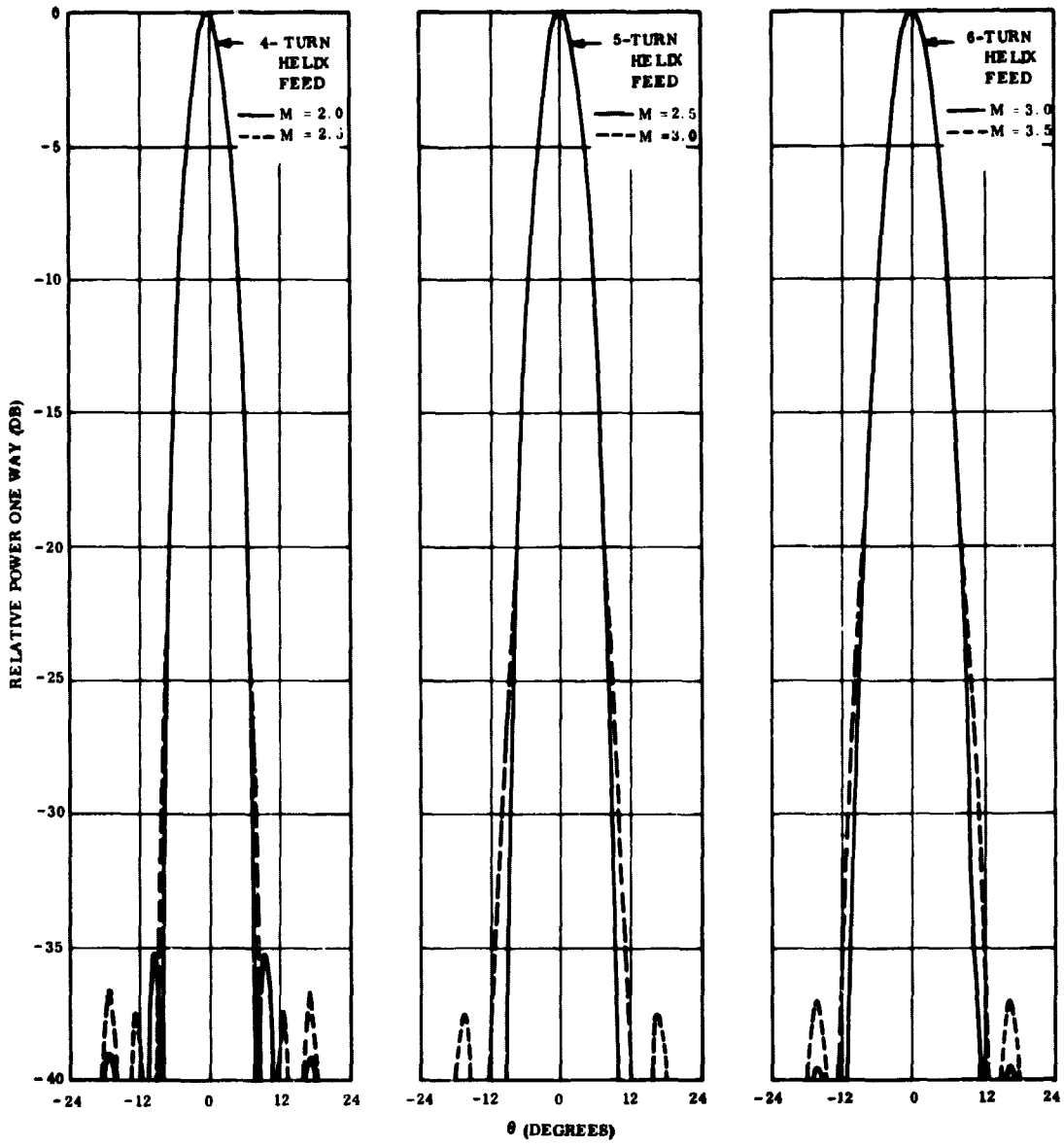

Figure 3.4-4. Predicted Paraboloid Pattern Response from a 4-Turn, 5-Turn, and 6-Turn Helix Feed

3.5 MEASUREMENTS OF PARABOLOID PATTERNS

Paraboloid patterns were measured using each of the above feeds. (The patterns for the 5 and 6-turn feeds are given in Appendix D) Pattern performance was determined by following a twofold procedure. First, the feed position was axially changed to locate the focal position of 19.6 cm. Here, patterns were taken at each location in the $\phi = 0^{o}$ plane for both vertical

and horizontal polarization; that pair of patterns providing the closest agreement with prediction established the focal position. Second, at the established focal position, paraboloid patterns were recorded at intervals of 30 degrees in other azimuth planes to assess pattern symmetry.

3.5.1 4-TURN HELIX FEED

In Figures 3.5-1 and 3.5-2 the pattern response of the paraboloid using a 4-turn helix feed is shown for several feed positions, d. This feed position is the axial distance from the apex of the paraboloid to the front edge of the feed cup as illustrated in Figure 3.5-3. From

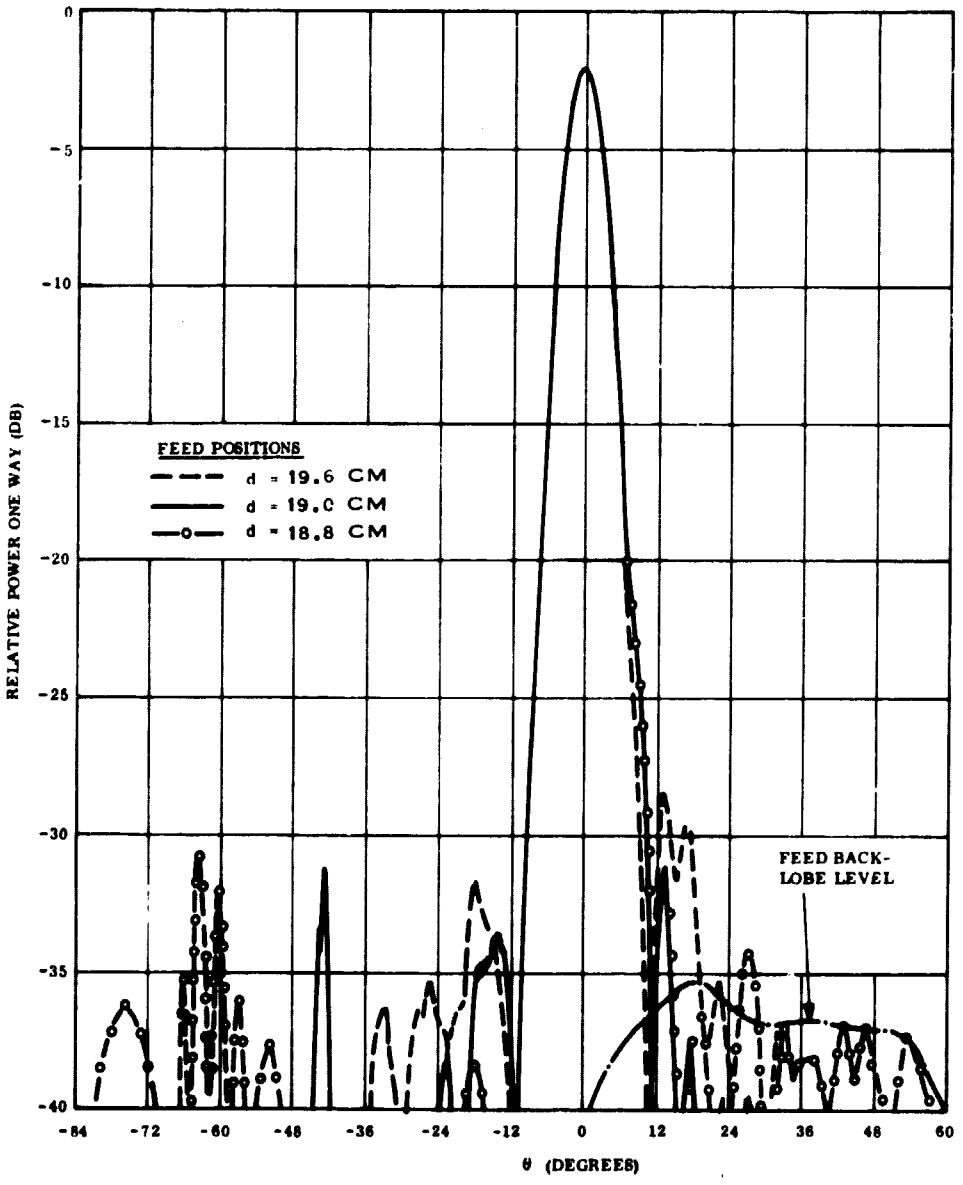

Figure 3.5-1. Paraboloid Patterns in $\phi = 0^{o}$ Plane as a Function of 4-Turn Helix Feed Position Using Vertical Polarization

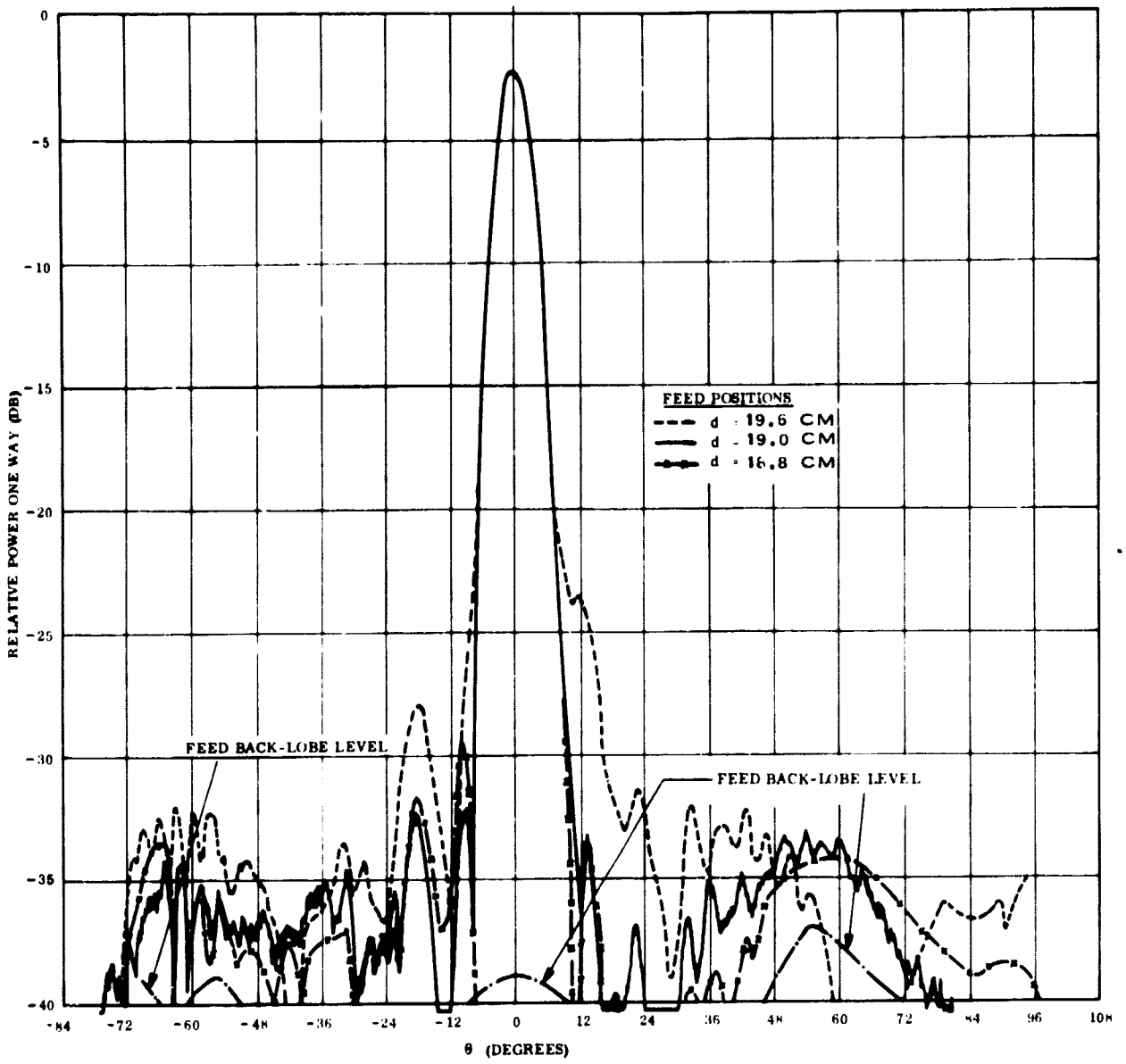

Figure 3.5-2. Paraboloid Patterns in $\phi = 0^{o}$ Plane as a Function of 4-Turn Helix Feed Position Using Horizontal Polarization

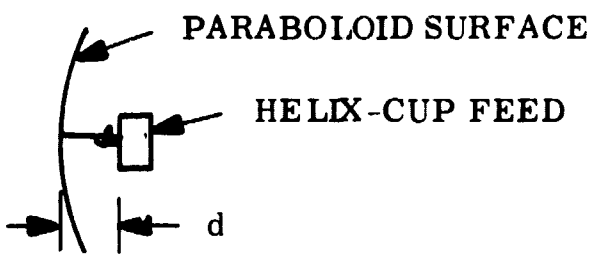

Figure 3.5-3. Parameter d for Helical Feed Position

these data, it became apparent that feed defocusing did not provide adequate sidelobe suppression. Additionally, the apparent in-focus feed position occurred for d = 19 cm which placed the focal point inside the helix cup. This feed location was considered as only apparent because two factors, both exclusive of feed defocusing, were influencing these radiation patterns. These were:

a. Aperture blockage by the feed and

b. Backlobe radiation from the feed

Calculations of feed blockage indicated it was at a level of -39.2 db relative to the peak of the paraboloid pattern. In the angular region $+15^{o} \geq \theta \geq -15^{o}$, this blockage produced a constant amplitude pattern which is out-of-phase with the paraboloid mainlobe and in-phase with its first sidelobe. As such, it can begin to perturb the paraboloid mainlobe by 1 db at the -21 db power level, and can raise a -35 db sidelobe to about -31 db.

Measurements of the feed and paraboloid gain showed the backlobe radiation from the feed to be a more dominant influence on the paraboloid patterns. The helix feed has a measured gain of 6.0 db for vertical polarization and 7.8 db for horizontal polarization; the corresponding gains for the paraboloid were 22.8 db and 27.6 db, respectively. The angular position and intensity of backlobe radiation, as depicted in Figures 3.5-1 and 3.5-2 was derived from the feed patterns in Figure 3.4-2. In Figure 3.5-1, this radiation is capable of altering the main lobe by 1 db at the -20 db power level and could raise the predicted sidelobe level of -35 db (see Figure 3.4-4) by about 6 db; in addition, if the backlobe radiation and blockage patterns were additive, the -35 db sidelobe would be increased by about 8.5 db. In Figure 3.5-2 the back-lobe radiation appears to account for most of the sidelobe structure. Its level about broadside can increase the predicted -35 db sidelobe to about -31 db.

A set of paraboloid patterns were taken using d = 19 cm. The set consisted of vertically and horizontally polarized patterns at azimuth intervals of 30 degrees. These data, shown in Figures 3.5-4 and 3.5-5, indicate a marginally symmetric pattern which has been modified by blockage and backlobe radiation from the feed.

Data for all three helix feeds (See Appendix D) supported the need to minimize and/or symmetrize the backlobe radiation before using an active zone or blockage compensation technique for sidelobe suppression. The data also discounted the employment of the defocusing technique as an adequate sidelobe suppresser.

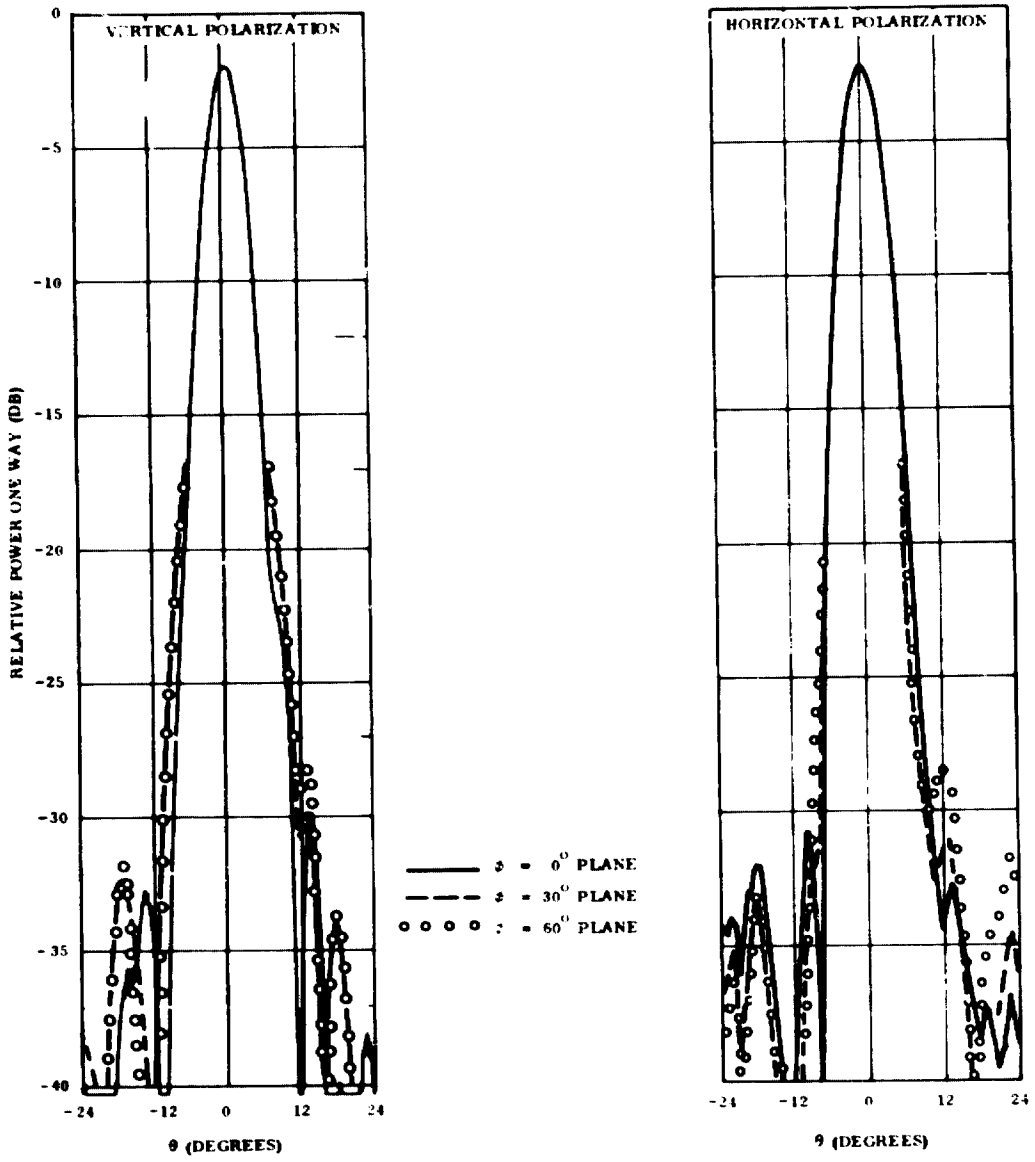

Figure 3.5-4. Pattern Response of Paraboloid in $\phi = 0^{o}$, 30^{o} 60^{o} Planes Using a 4-Turn Helix Feed

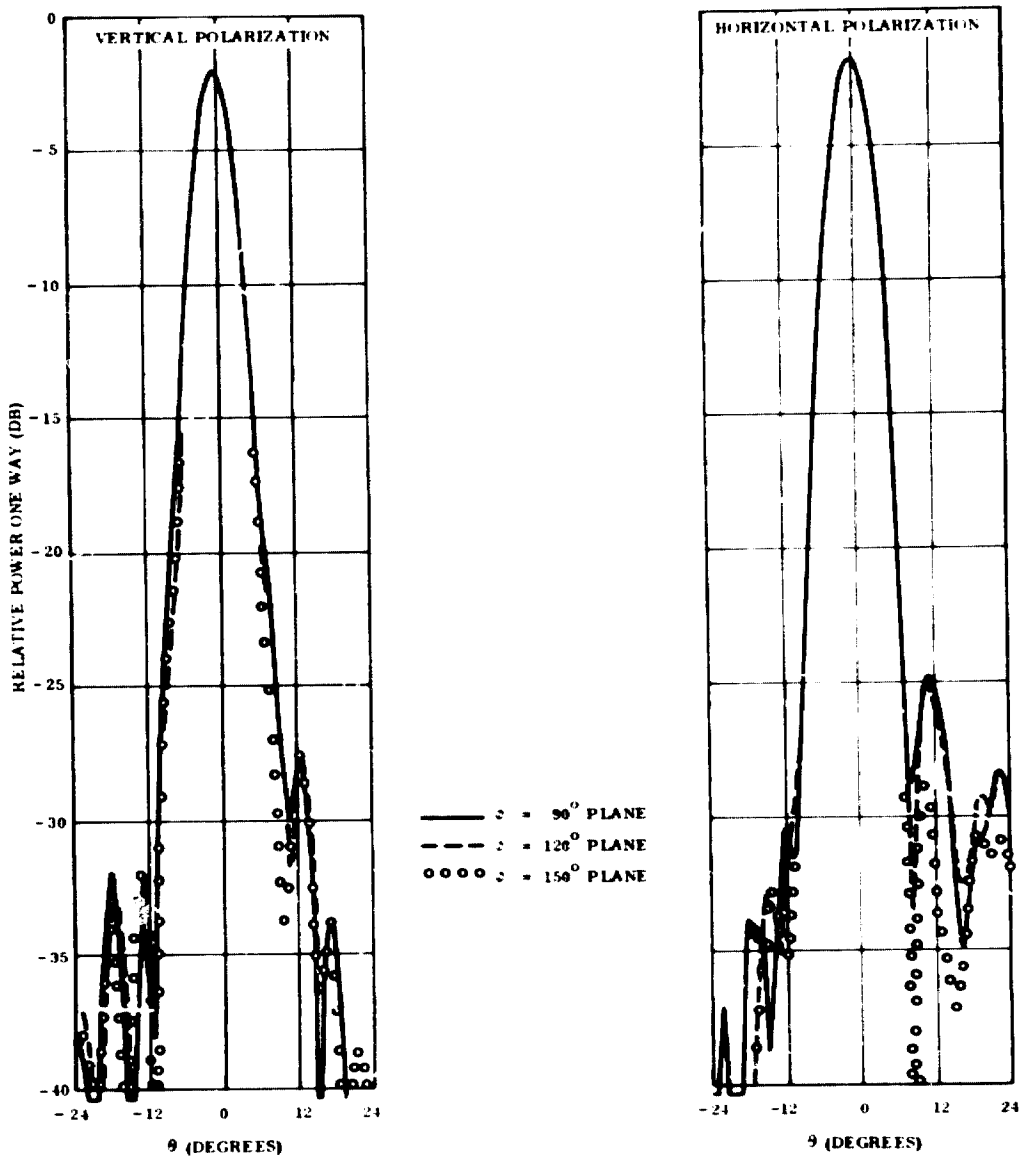

Figure 3.5-5. Pattern Response of Paraboloid in $\phi = 90^{o}$, 120^{o}, 150^{o} Planes Using a 4-Turn Helix Feed

3.5.2 BACKLOBE SUPPRESSION OF 4-TURN HELIX FEED

From the results of the aforementioned analysis and experimentation, the 4-turn helix feed design was chosen as the preferred feed because it provided the narrowest paraboloid main-lobe, including its null-to-null beamwidth.

This feed (see Figure 3.3-3) had peak backlobe radiation which varied between -17 db for horizontal polarization to -18 db for vertical polarization (relative to the peak intensity of the helix pattern) over the paraboloid pattern angular interval $15^{o} \geq \theta \geq -15^{o}$. As such, an investigation was undertaken to suppress this radiation within this angular interval. This included the design and testing of several feed cup chokes and feed cup rear covers; the latter were attached to the rear of the cup to symmetrize the backlobe radiation. A single choke (4.05 cm-diameter) was found to suppress the backlobe radiation relative to isotropic to -20 db for vertical polarization and -15 db for horizontal polarization; a double choke (4.64 cm-diameter) provided about -20 db suppression for both polarizations. With a rear cover on the feed, the backlobe radiation was increased by about 2 db for each choke design.

From these results, the double choke design was chosen (see Figure 3.5-6) even though it raised the feed aperture blockage to a level of -34 db with respect to the paraboloid pattern peak. This was done because aperture blockage could be compensated more readily than feed backlobes.

Figure 3.5-6. Double Choke Configuration for 4-Turn Helix Feed

3.6 DUAL PHASE CENTER OBSERVED

The pattern data using the 4-turn, 5-turn, and 6-turn helix feeds were primarily used to confirm a preferred helix feed. Having chosen the 4-turn helix, a more accurate determination of its focal position in the $\phi = 0$ degree plane was conducted. For these measurements the feed choke was not used. Patterns for vertical and horizontal polarization were taken at 0.16 cm feed displacements throughout a 3.80 cm feed travel. These pattern data revealed two different focal positions for vertical and horizontal polarization. The former was located at $\underline{d}$ = 20.6 cm (as measured from the front edge of the helix cup to the apex of the paraboloid); the latter occurred at $\underline{d}$ = 19.4 cm. The patterns taken at these two feed positions are compared with the predicted pattern in Figure 3.6-1. Both in-focus patterns show good agreement with prediction for the main lobe and for the angular location of several of the sidelobes within $15^{o} \geq \theta \geq -15^{o}$. The asymmetries in the sidelobe structure on both sides of the main beam indicate the influence of the helix feed backlobe radiation.

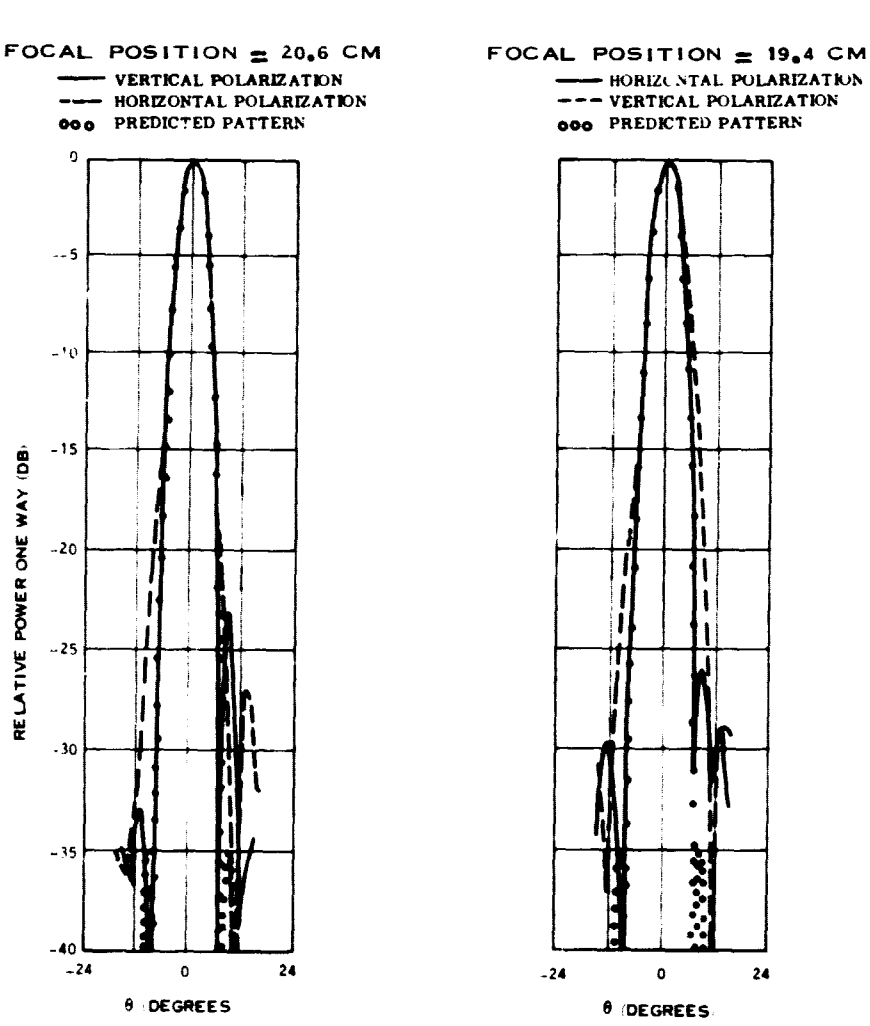

Figure 3.6-1. Measured Patterns of Paraboloid in $\phi = 0^{o}$ Plane Showing Dual Phase Center for 4-Turn Helix Feed

The polarization dependence of the phase center of the helix feed indicates that it does not have a unique phase center for circular-polarization. This condition causes the helix to always operate at a defocussed axial position and give rise to improper phase illumination across the paraboloid aperture. The resulting paraboloid pattern contains deformations in the main beam and null-filling in the sidelobe region which can only marginally be corrected by circularly polarized suppressor elements. Consequently, substantial sidelobe reduction cannot be realized for circular polarization. However, sidelobe suppression can be demonstrated for a linear polarization by locating the helix at the unique focal position corresponding to that linear polarization.

The dual phase center problem can be obviated by additional design effort with the helix feed or by using another feed with a unique phase center for circular polarization. Such detail design was beyond the scope of this study.

3.7 SIDELOBE SUPPRESSION FOR VERTICAL POLARIZATION

The in-focus pattern for vertical polarization in the $\phi = 0$ degree plane was arbitrarily chosen for this demonstration. A systematic procedure was employed to attempt to realize the pattern suppression. This consisted of:

a. Placing an rf choke on the feed to minimize its backlobe radiation.

b. Readjusting the feed-with-choke to be at the focal position of the paraboloid for vertical polarization.

c. Applying the blockage compensation technique to correct for aperture blockage of the feed plus additional sidelobe suppression within $15^{o} \geq \theta \geq -15^{o}$.

d. Applying the active zone suppressor to reduce the remaining sidelobes to the lowest average level within $15^{o} \geq \theta \geq -15^{o}$.

3.7.1 RF-CHOKE

A double choke was mounted around the front edge of the helix cup to reduce the peak backlobe radiation to about -44 db (relative to the peak of the paraboloid pattern) for vertical polarization and -46 db for horizontal polarization. The choke contained two, 0.25 cm wide

and λ/4 deep circular channels (λ is a free space wavelength). Its presence enhanced the aperture blockage to -34 db relative to the peak of the paraboloid pattern and modified the predicted paraboloid pattern to that shown in Figure 3.7-1.

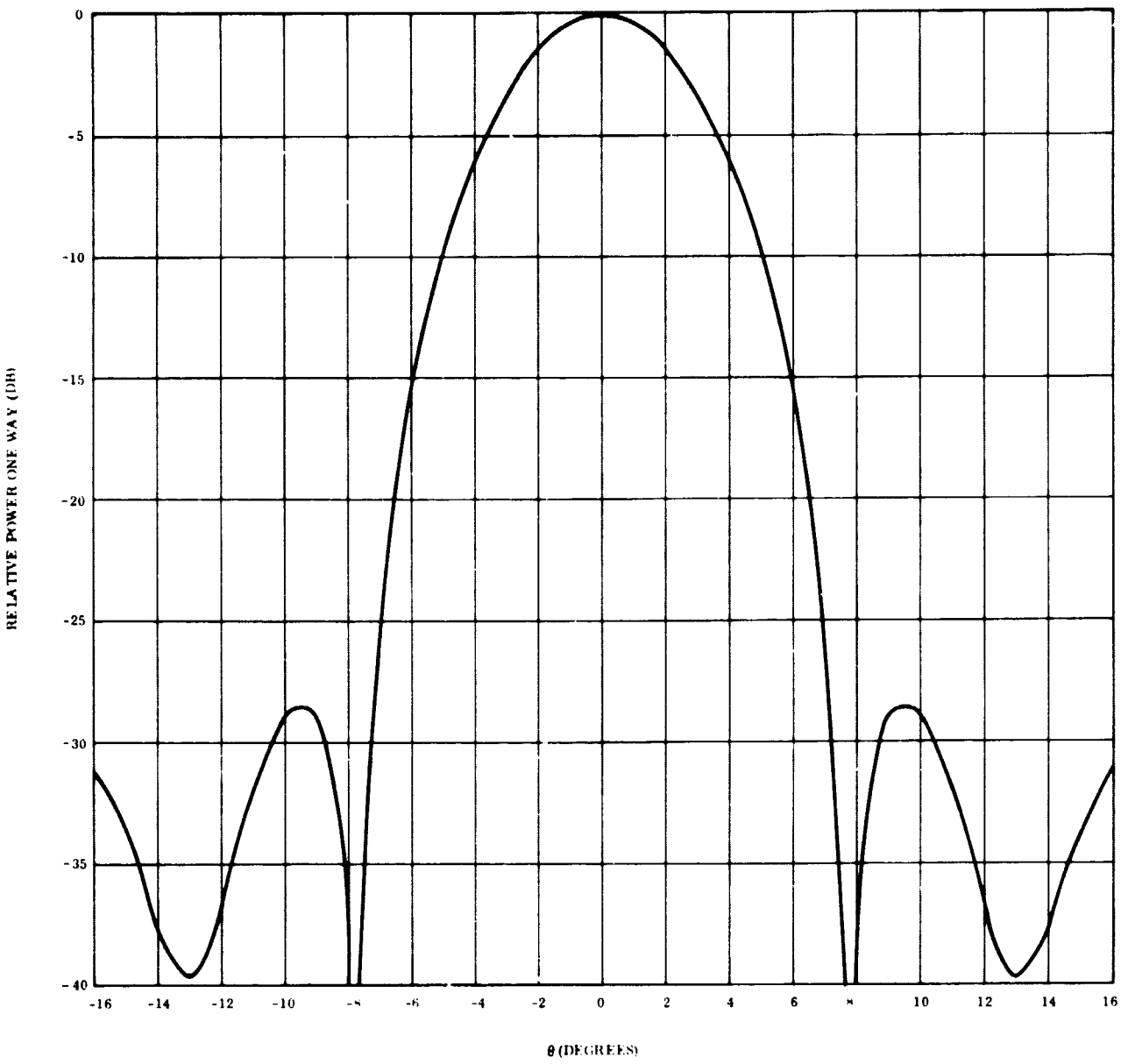

Figure 3.7-1. Predicted Paraboloid Pattern with -34 DB Aperture Blockage

3.7.2 FEED-ADJUSTMENT

The addition of the choke to the helix feed required that the feed be moved to $\underline{d}$ = 20.3 cm to be in-focus.

3.7.3 BLOCKAGE COMPENSATION TECHNIQUE

The blockage compensator was a 4-turn helix mounted in a cup and physically located about 61 cm directly above the axis of symmetry of the paraboloid (see Figure 3.7-2). This location was chosen in order to facilitate testing of this technique, while not detracting from its performance at its preferred location; namely, on the back-side of the primary feed. The blockage compensator helix was counter-wound to that of the helix feed, and its amplitude

and phase were independently adjustable. The element produced a near-constant amplitude pattern in the vicinity of $\theta = 0$ degrees. Its phase was experimentally adjusted to be in-phase with the paraboloid main beam and its amplitude was set to reduce the sidelobe structure of the paraboloid pattern to the lowest overall level within $15^{o} \geq \theta \geq -15^{o}$.

3.7.4 ACTIVE ZONE SUPPRESSION TECHNIQUE

The active zone suppressor consisted of two counter wound 4-turn helices in cups separated by 12.1λ or 48.5 cm. The suppressor was horizontally arrayed with its center coincident with the location of the blockage compensation element as seen in Figure 3.7-2. Both elements were fed in-phase and produced equal-intensity beams at $\theta = 0^{o}$, $\pm 4.7^{o}$, $\pm 9.5^{o}$ and $\pm 14.3^{o}$. The phase and amplitude of the signal energizing these elements was also independently controlled. The phase was adjusted to have the beams at $\theta = 0^{o}$, and $\pm 9.5^{o}$ be in-phase with the paraboloid mainlobe, the amplitude was varied to minimize the paraboloid sidelobe structure within $15^{o} \geq \theta \geq -15^{o}$.

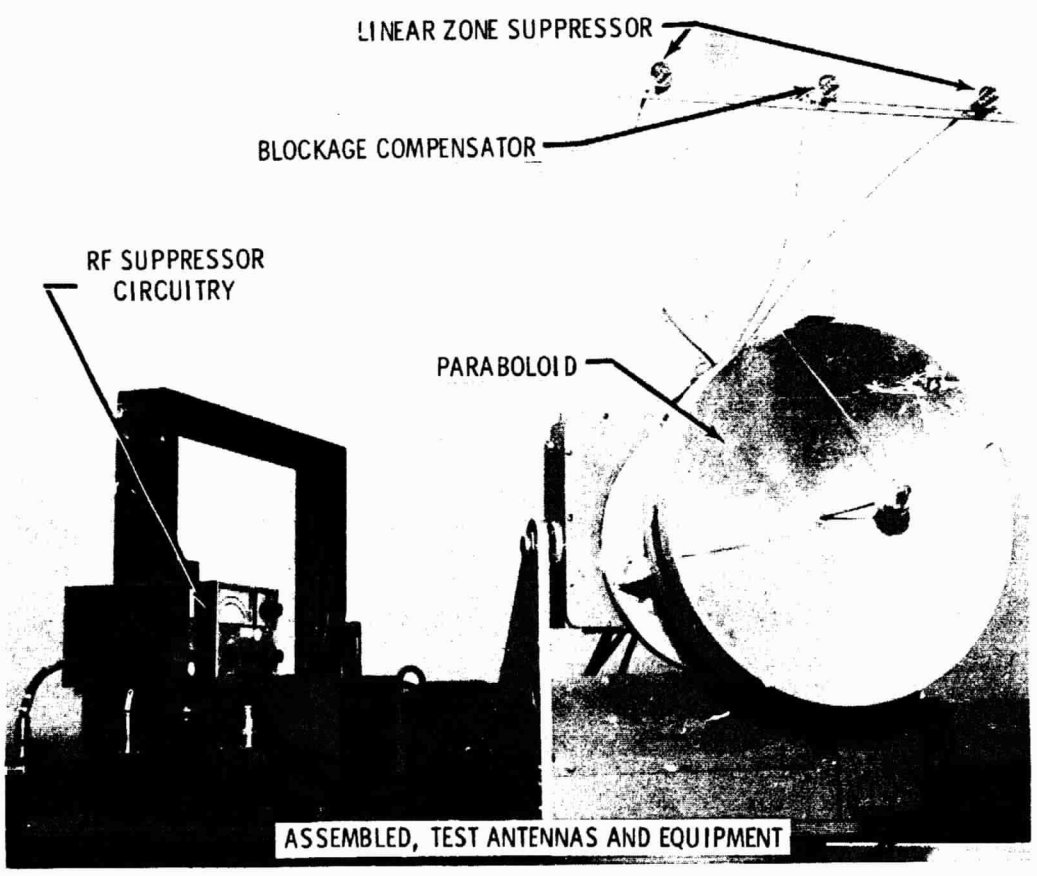

Figure 3.7-2. Experimental Setup for Evaluating Sidelobe Suppression Techniques

3.7.5 RF-CIRCUITRY

An rf circuit was used to combine the paraboloid signal with the two suppressor signals to demonstrate sidelobe suppression. The rf circuit location is indicated in Figure 3.7-2; a close-up photograph and schematic of this circuit is shown in Figures 3.7-3 and 3.7-4, respectively. The rf circuit utilized precision phase shifters and attenuators to control the amplitude and phase of the two suppressor signals; three magic tees maintained isolation between all signal subchannels and were used to sum the signals at appropriate circuit points.

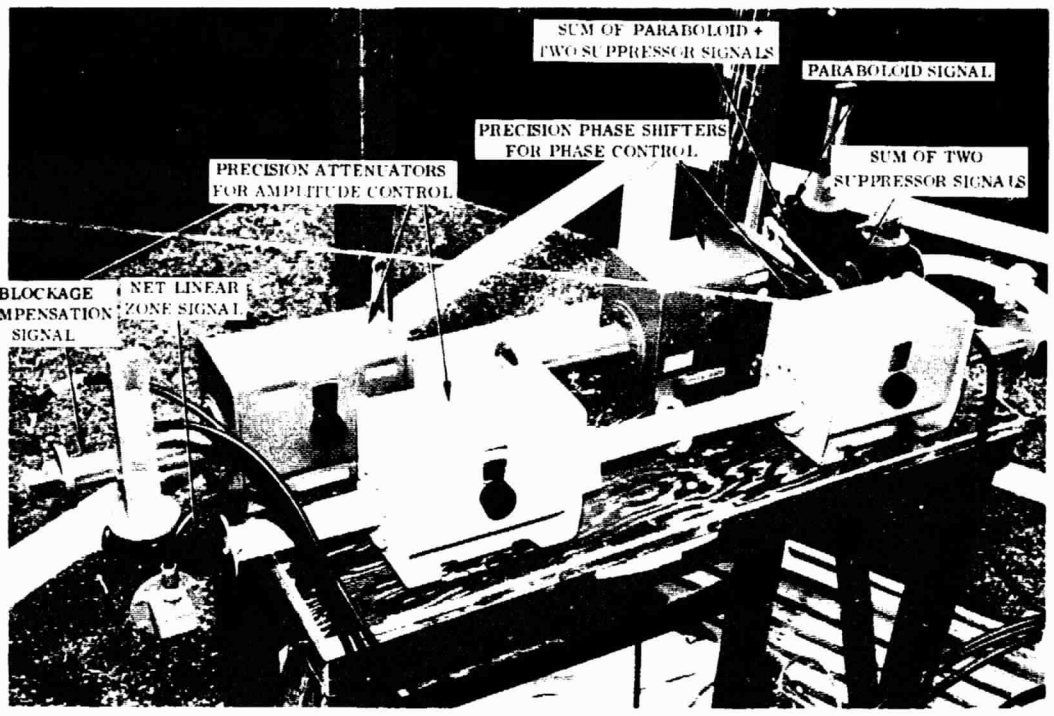

Figures 3.7-3. Implementation of RF Suppressor Circuitry

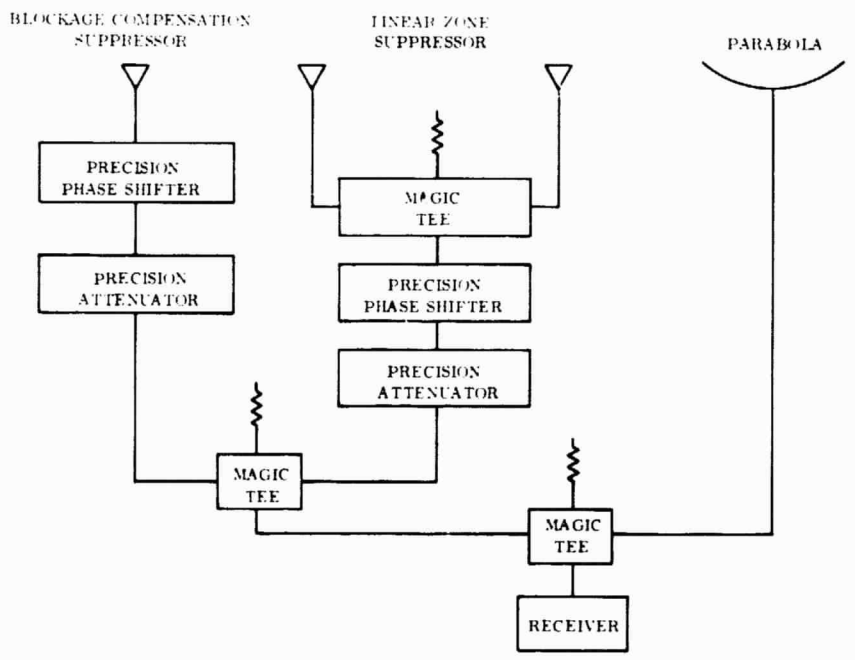

Figures 3.7-4. Schematic of RF Suppressor Circuitry

3.7.6 SIDELOBE SUPPRESSION PATTERNS IN THE $\phi = 0^{O}$ PLANE

The vertically polarized pattern for the paraboloid alone was measured in the $\phi = 0^{O}$ pattern plane shown in Figure 3.7-5 for no blockage compensation. The pattern exhibited about -30 db first sidelobes. The blockage compensation element was then adjusted to be in-phase with the paraboloid main lobe and to have successive pattern amplitudes of -36.7 db and -34.5 db relative to peak.

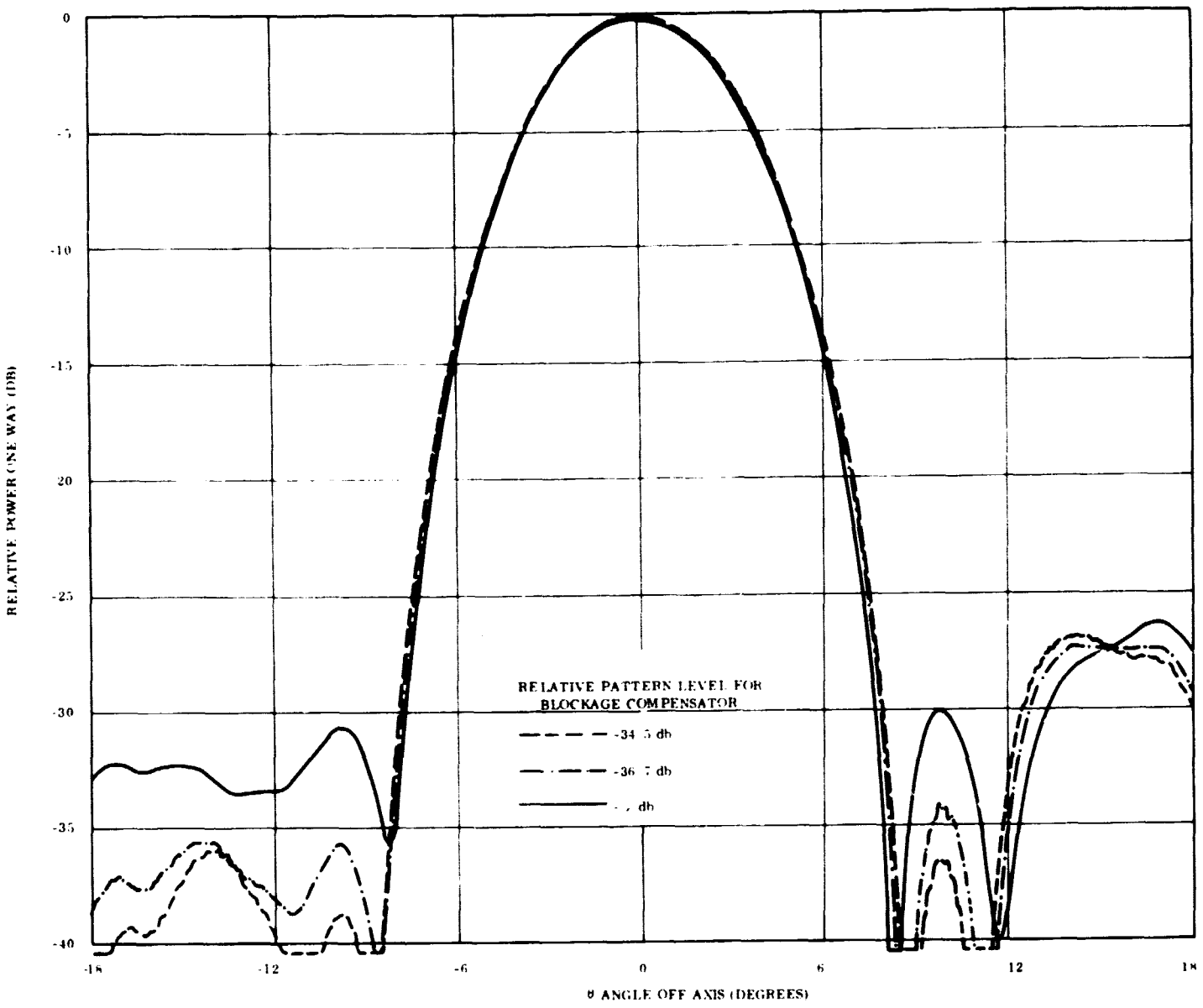

Figure 3.7-5. Sidelobe Reduction of Paraboloid Pattern as a Function of Blockage Compensation Amplitude in the $\phi = 0^{O}$ Pattern Plane

As shown in Figure 3.7-5 the paraboloid sidelobe structure on the left side and the first sidelobe on the right side progressively decreased, indicating that the blockage pattern and sidelobes of the paraboloid pattern were being suppressed. Then, with the blockage compensator amplitude increased to -32.5 db, the in-phase active zone suppressor was introduced and adjusted to a pattern amplitude of -41 db. At this amplitude, the second and third sidelobes of the active-zone suppressor were aligned with the first and second side-

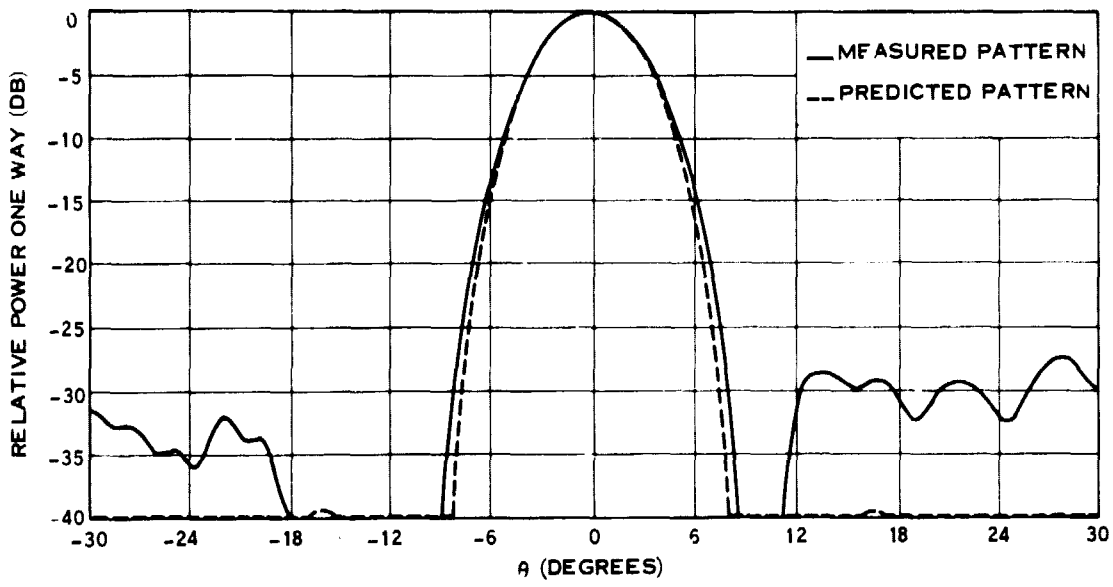

Figure 3.7-6. 60^{O} Pattern of Paraboloid with Suppressed Sidelobe Structure in $\phi = 0^{O}$ Pattern Plane

lobes of the paraboloid pattern; this produced additional suppression as indicated in Figures 3.7-6 and 3.7-7. As shown in Figure 3.7-6, the sidelobe structure was $\leq$ -40 db within $11.3^{O} \geq \theta \geq -18^{O}$. The half-power beamwidth was in good agreement with theory and the null-to-null beamwidth (at the -40 db power level) was 1.2 degrees greater than predicted. (This pattern was reconstructed several times to verify its accuracy.) In addition, the 360 degree azimuth pattern in Figure 3.7-7 shows that the asymmetric pattern goal (as indicated by the dashed line) had been satisfied in one complete pattern plane of the paraboloid. These results demonstrated the effectiveness of applying these suppressor techniques.

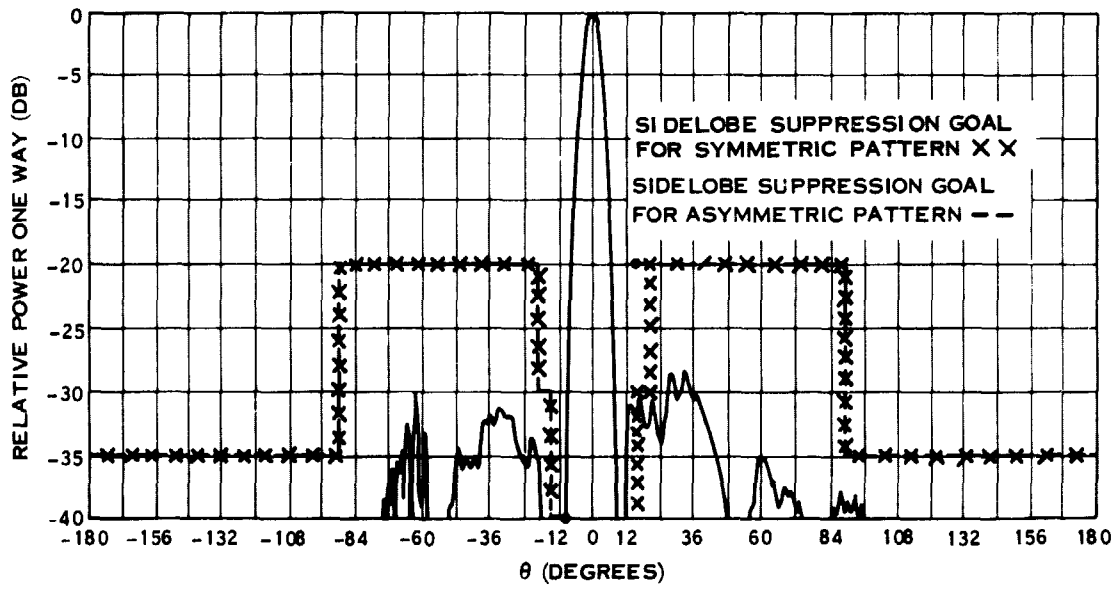

Figure 3.7-7. 360^{O} Pattern of Paraboloid with Suppressed Sidelobe Structure in $\phi = 0^{O}$ Pattern Plane

To indicate the pattern levels for the suppressor techniques relative to the suppressed paraboloid pattern peak, the pattern data shown in Figure 3.7-8 were taken. The broad lobe of the blockage compensator element is shown to be at a level of -32.5 db; the multiple beams of the active zone suppressor operated at a peak level of -41 db and displayed the angular location in space needed for sidelobe suppression. As can be noted, the sidelobe structure on the left side of the paraboloid pattern was suppressed several db below -40 db.

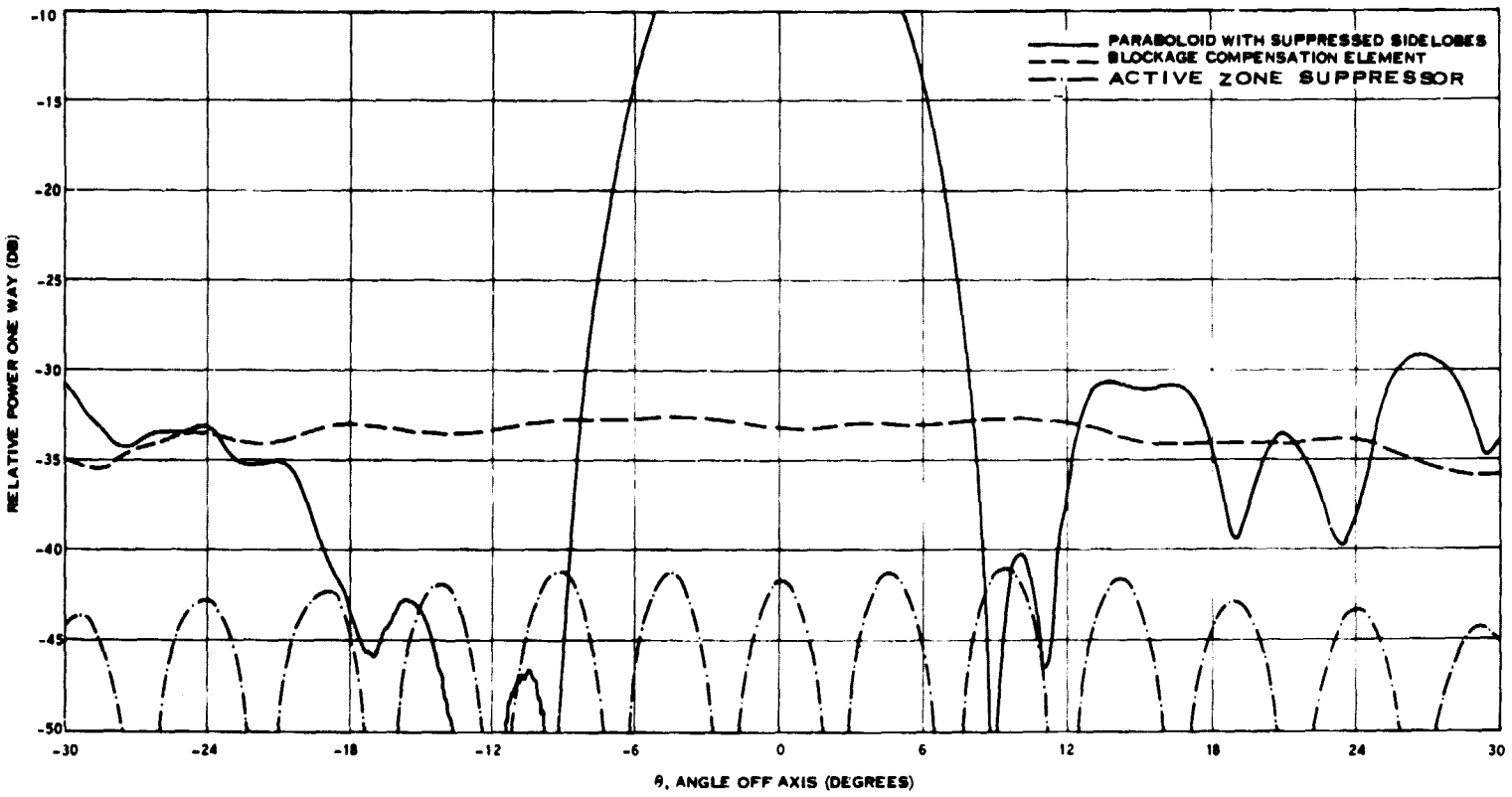

Figure 3.7-8. Relative Levels of Paraboloid Pattern with Sidelobe Suppression and the Two Suppression Patterns in $\phi = 0^{o}$ Pattern Plane

3.7.7 OTHER LINEAR POLARIZATION PATTERNS IN THE $\phi = 0^{o}$ PLANE

In addition to the patterns for vertical polarization in the $\phi = 0^{o}$ plane, patterns were also taken for inclined linear polarizations at angles of $\pm$ 60 degrees relative to vertical polarization. For each inclined linear polarization, patterns were recorded of the paraboloid alone, the paraboloid plus the blockage compensator element, and the paraboloid plus both suppressor techniques; when used, the amplitude and phase of excitation of the suppressor elements were identical to that of the vertically polarized patterns. These data are given in Figures 3.7-9 through 3.7-14. The broadened mainlobe-to-null beamwidth and the masking of the first sidelobe of the paraboloid pattern (See Figure 3.7-9) indicates that the

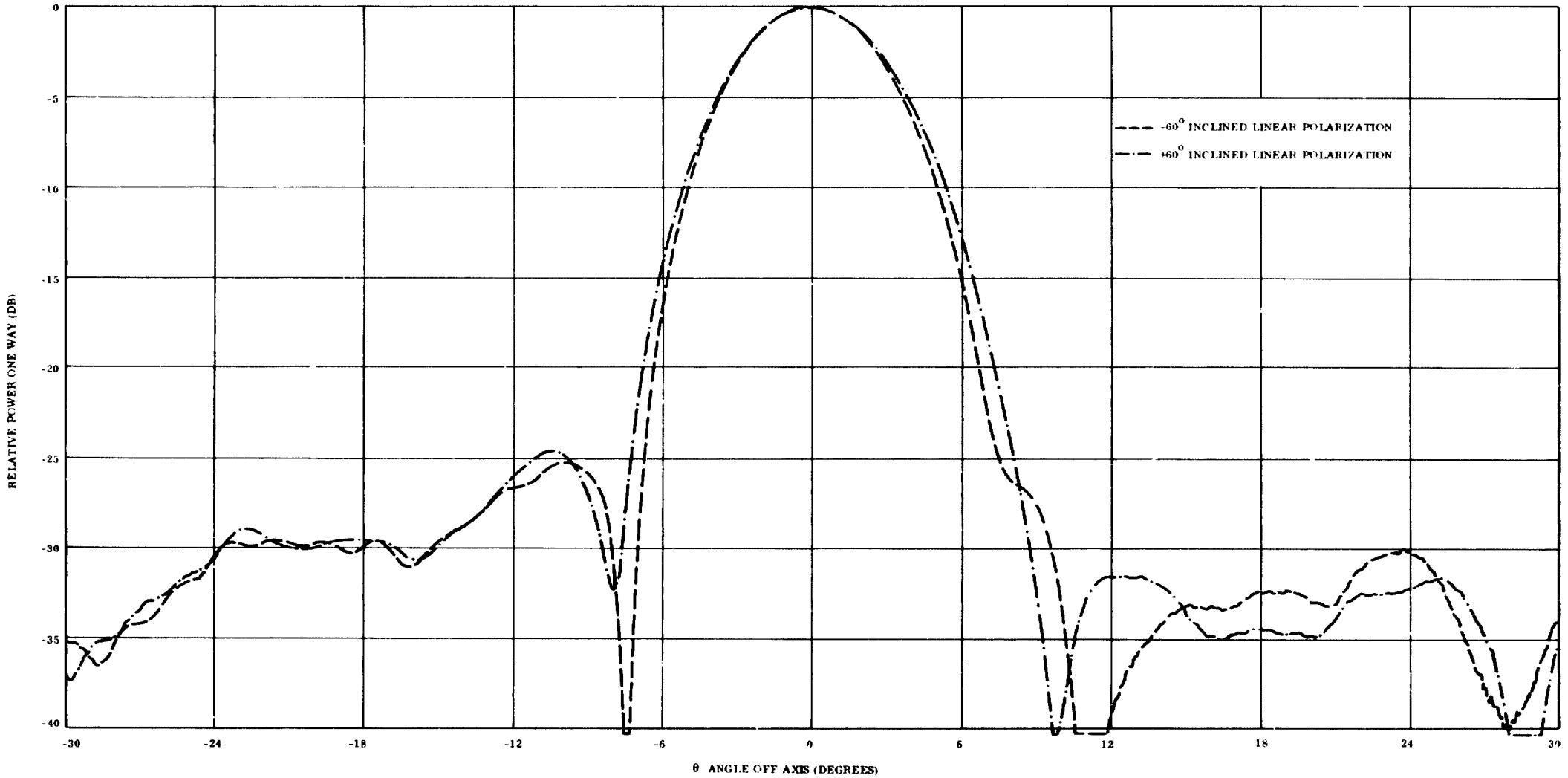

Figure 3.7-9. 60^{O} Pattern of Paraboloid Alone Using $\pm 60^{O}$ Inclined Linear Polarizations in $\phi = 0^{O}$ Pattern Plane

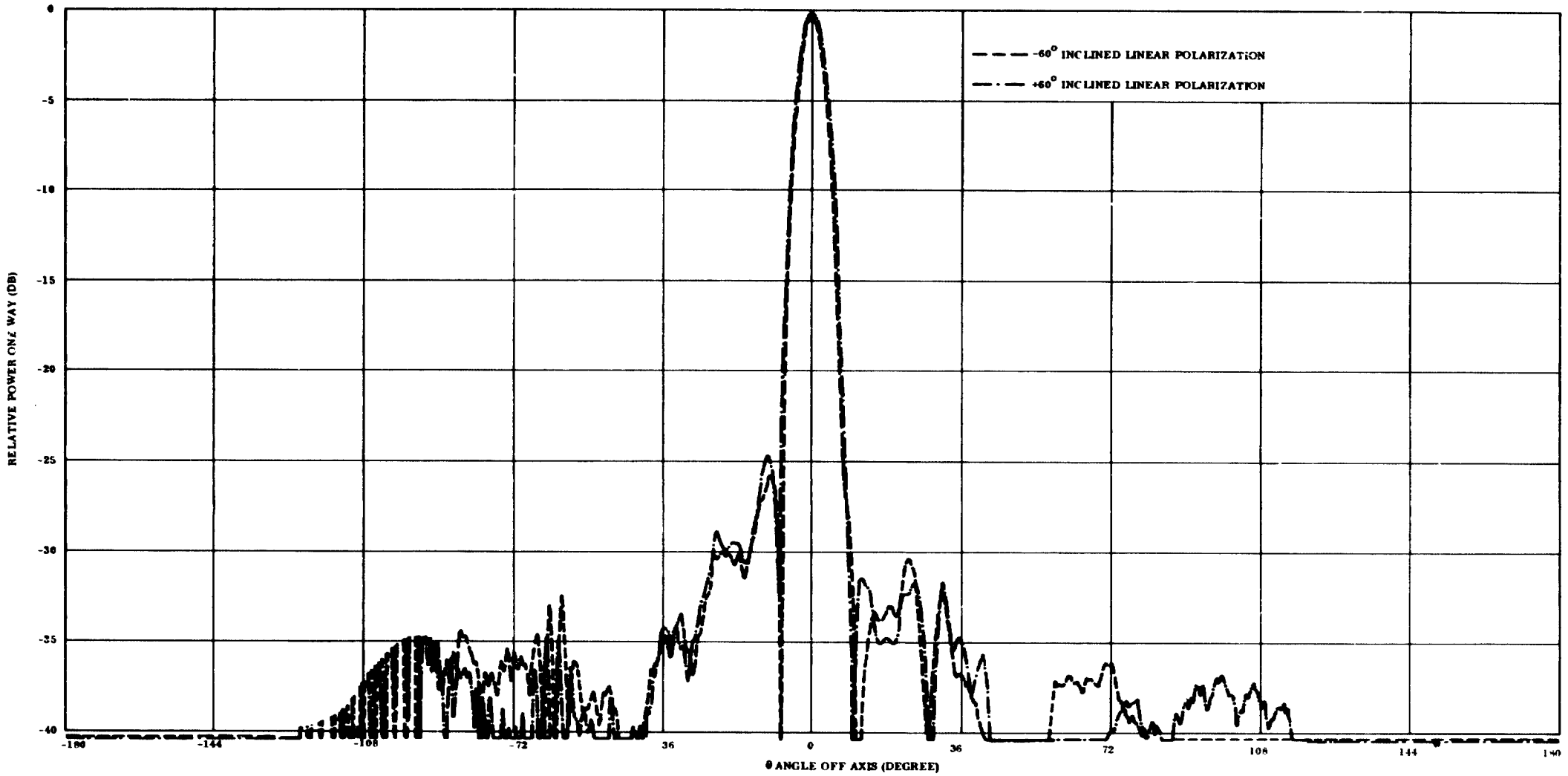

Figure 3.7-10. 360° Pattern of Paraboloid Alone Using ± 60° Inclined Linear Polarization in $\phi = 0^{o}$ Pattern Plane

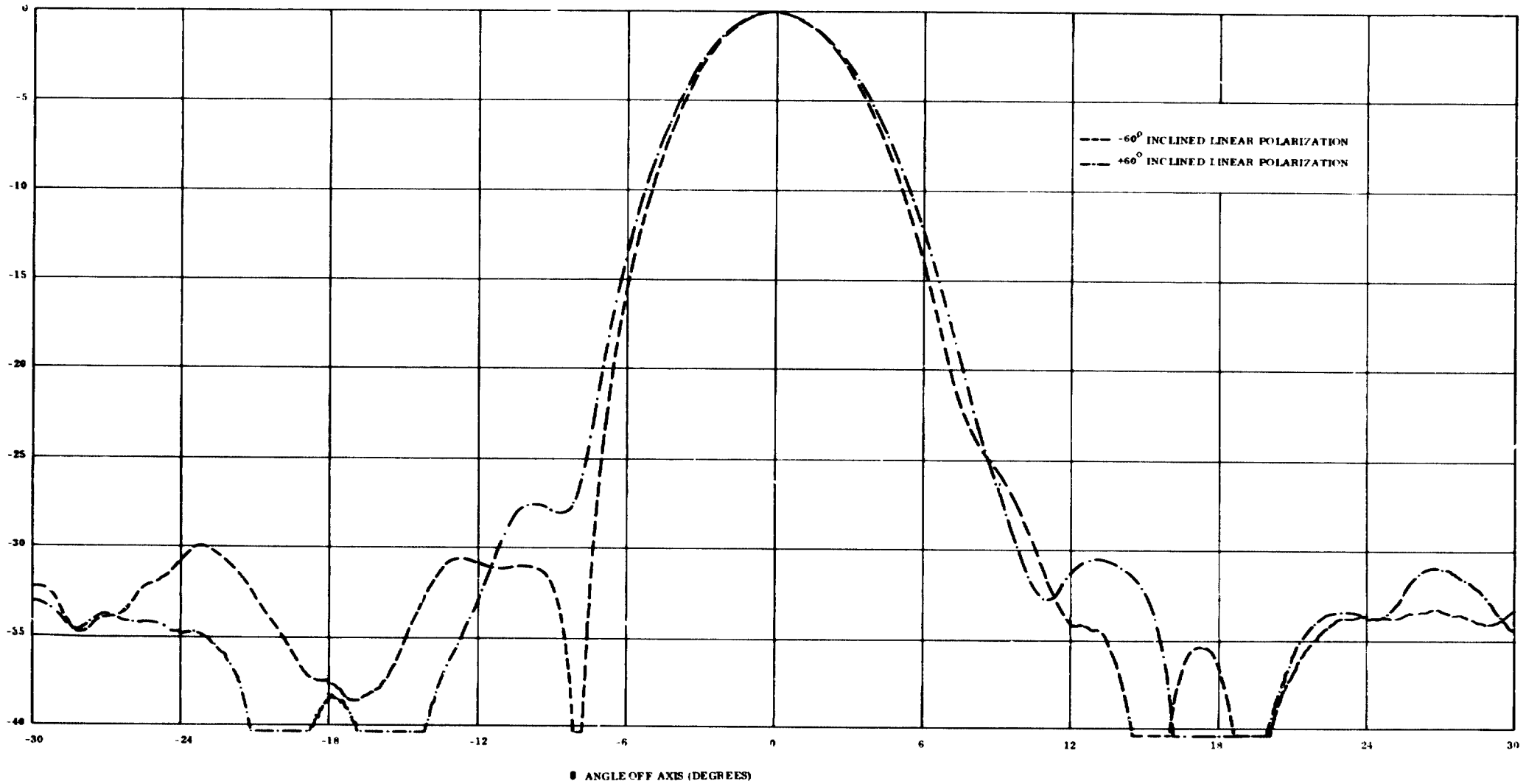

Figure 3.7-11. 60^{O} Pattern of Paraboloid Plus Blockage Compensator Using Inclined Linear Polarizations in $\phi = 0^{O}$ Pattern Plane

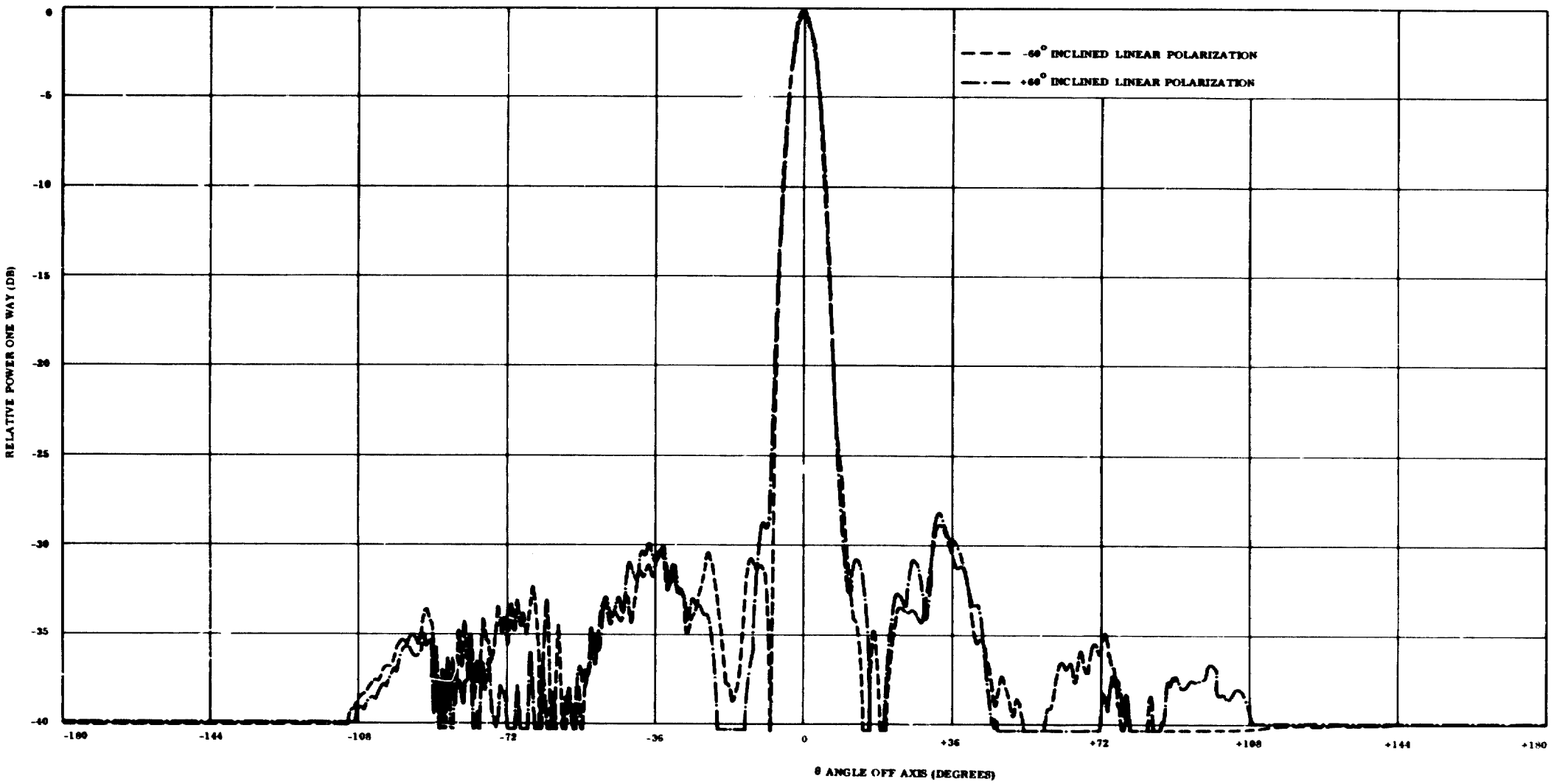

Figure 3.7-12. 360° Pattern of Parabola Plus Blockage Compensator Using Inclined Linear Polarizations in $\phi = 0^{o}$ Pattern Plane

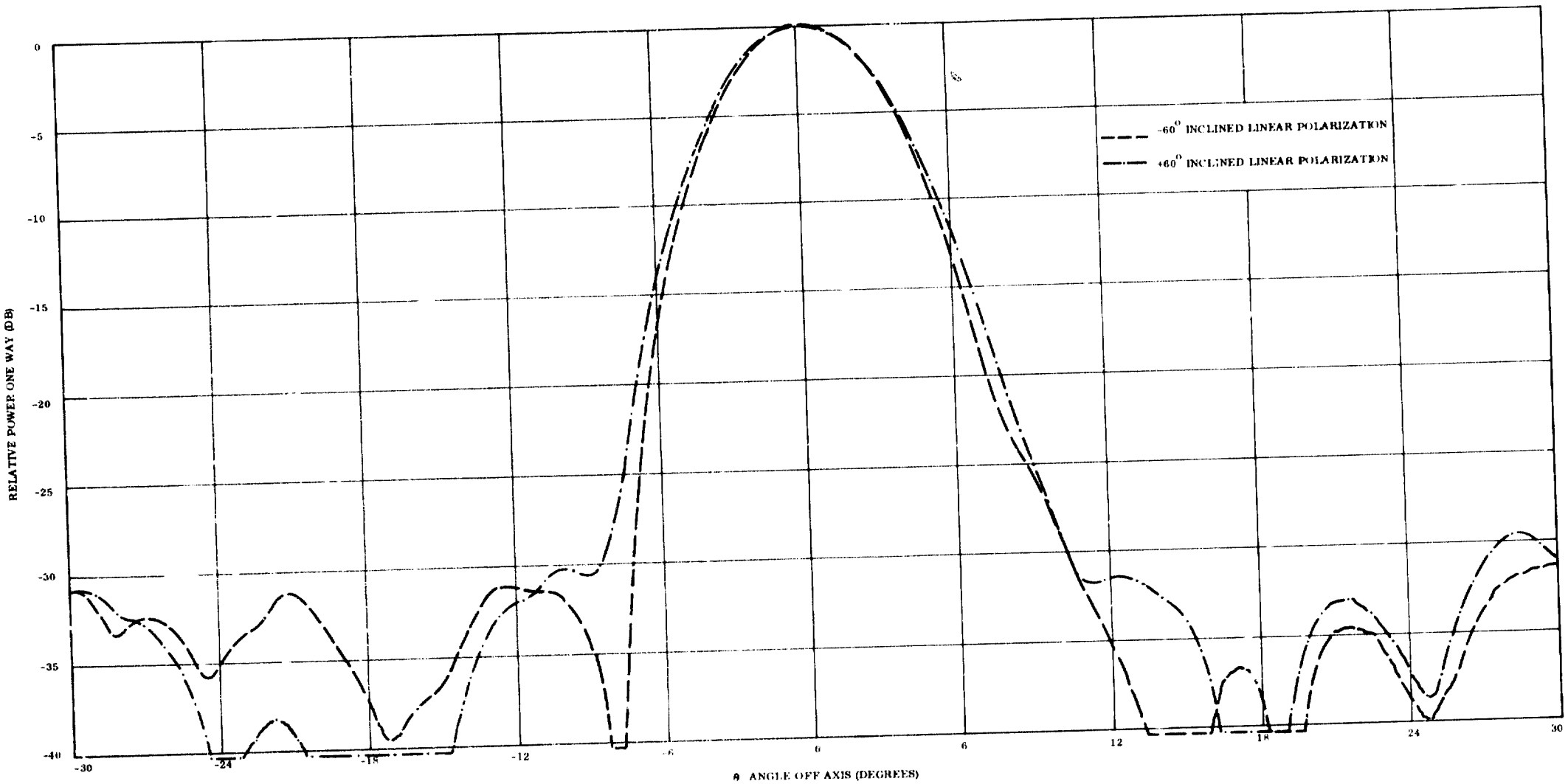

Figure 3.7-13. 60^{O} Pattern of Paraboloid Plus Both Suppressor Techniques Using Inclined Linear Polarization in $\phi = 0^{O}$ Pattern Plane

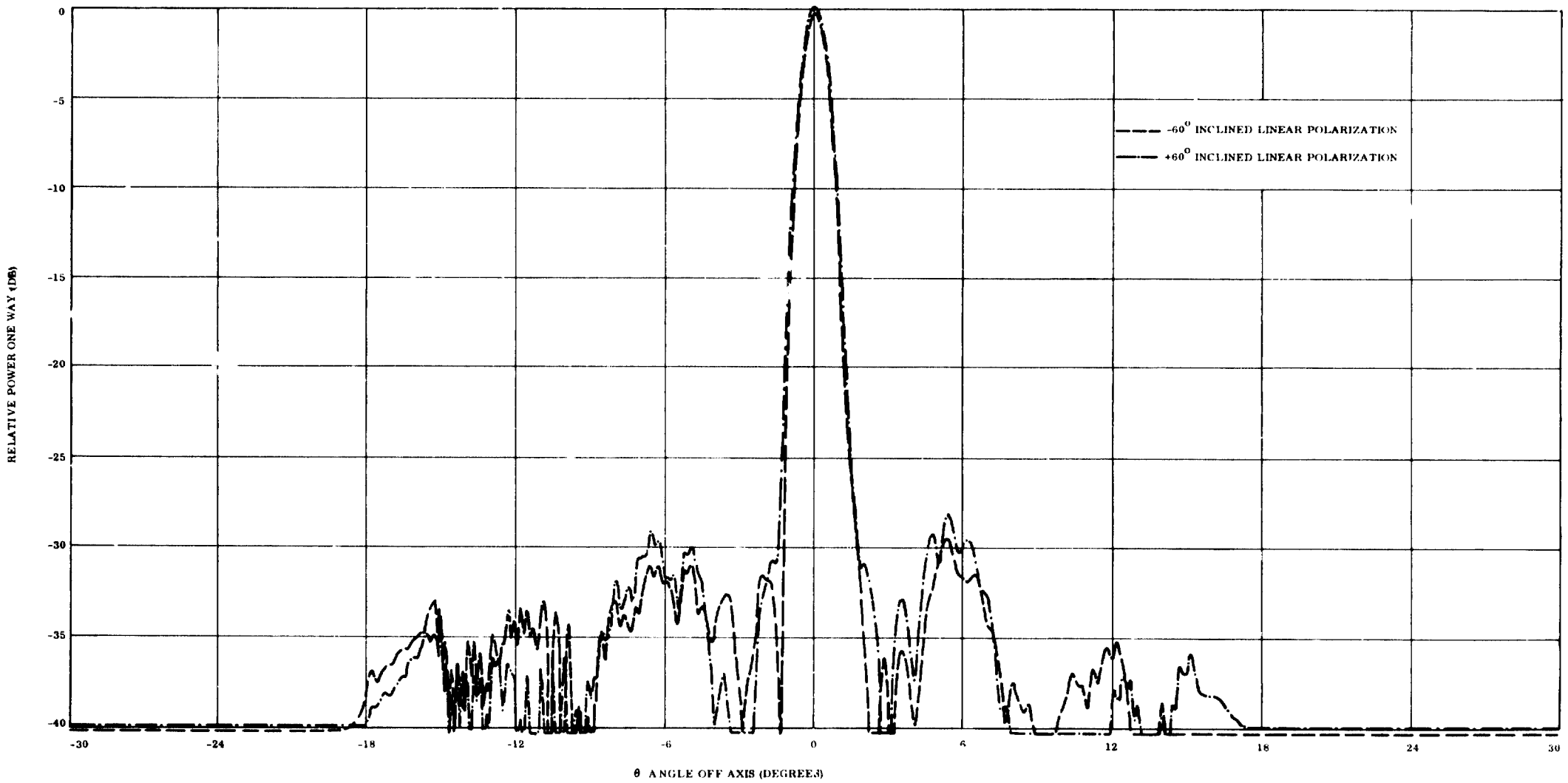

Figure 3.7-14. 360° Pattern of Paraboloid Plus Both Suppressor Techniques Using Inclined Linear Polarization in $\phi = 0^{\circ}$ Pattern Plane

helix is in a defocussed axial position for both inclined linear polarizations. With the application of the blockage compensation element (See Figure 3.7-11) the sidelobes to the left of broadside exhibit some reduction in amplitude, but this is accompanied by a broadening of the main lobe to the right of broadside. Further sidelobe reduction on the left side is in evidence in Figure 3.7-13, when the active zone suppressor is utilized. In general though, these patterns show limited sidelobe reduction with the application of the suppressor techniques, as expected.

3.8 GAIN MEASUREMENT AND DISTRIBUTION OF POWER FOR SUPPRESSION

The gain of the paraboloid alone, the paraboloid with blockage compensation and the paraboloid with both suppressor techniques was measured using $\underline{d} = 20.3$ cm. These gain figures, which have been corrected for a feed insertion loss of 1.4 db, are listed in Table 3.8-1. The gain of the paraboloid alone represents an overall efficiency of 60 percent. The predicted efficiency for a 16 db taper across the paraboloid aperture is 77 percent. Most of this reduction in efficiency can be attributed to the existence of a dual phase center for the helix feed.

Table 3.8-1. Gain Measurements

Antenna Configuration	Peak Gain at $\theta = 0^{o}$ (db)		
	Vertical Polarization	Horizontal Polarization	Elliptical Polarization
Paraboloid Alone	23.5	25.9	27.9
Paraboloid Plus Blockage Compensator	23.7	26.1	28.1
Paraboloid Plus Blockage Compensator and Active Zone Supressor	24.0	26.2	28.2

Note that the gain increased slightly in the broadside direction (i.e., $\theta = 0^{o}$) as the suppressor techniques were applied; this shows that the suppressor techniques were in-phase with the paraboloid main lobe. The gain of 28.2 db using both suppressor techniques represents an overall efficiency of 63 percent.

The distribution of power among the paraboloid and the two suppressor techniques was calculated for the sidelobe suppression results realized in this program. The calculations were made using the equations to be derived below.

The total power P_T to be radiated by a lossless antenna system consists of

$$P_T = P_p + P_{BC} + P_Z \tag{3.8-1}$$

wherein,

P_p is the power distributed to the paraboloid

P_{BC} is the power distributed to the blockage compensator

P_Z is the power distributed to the zone supressor

The power distributed to each radiator is related to its radiated power by means of the gain expression,

$$P_{R_i} = \frac{G_i P_i}{4\pi} \tag{3.8-2}$$

wherein, P_{R_i} is the power radiated per unit solid angle in a particular direction in space for the ith radiator and G_i is its gain in that direction.

At broadside (i.e., $\theta = 0^{o}$) let us consider the ratios:

$$\frac{P_{R_{BC}}}{P_{R_p}} = K_1^2 = \frac{G_{BC}}{G_p} \quad \frac{P_{BC}}{P_p} \tag{3.8-3}$$

and

$$\frac{P_{R_Z}}{P_{R_p}} = K_2^2 = \frac{G_Z}{G_p} \quad \frac{P_Z}{P_p}$$

These ratios have been measured (see Figure 3.7-8) and have values represented by the constants K_1^2 and K_2^2.

Rearranging Equations 3.8-3 yields,

$$P_{BC} = K_1^2 \quad \frac{G_p}{G_{BC}} \quad P_p$$

$$P_Z = K_2^2 \quad \frac{G_p}{G_Z} \quad P_p \tag{3.8-4}$$

As can be discerned from Equations 3.8-3, the power to be distributed to a suppressor technique is inversely related to the gain of the suppressor elements; thus, for a specified K^2 needed for sidelobe suppression, the greater the suppressor gain the less the suppressor power required.

Substituting Equation 3.8-4 intc 3.8-1 gives,

$$P_T = \left[1 + K_1^2 \quad \frac{G_p}{G_{BC}} \quad + K_2^2 \quad \frac{G_p}{G_Z}\right] \quad P_p \tag{3.8-5}$$

Then, dividing Equations 3.8-4 by Equation 3.8-5, the relative distribution of power to the three radiators is specified by:

$$\frac{P_p}{P_T} = \frac{1}{1 + K_1^2 \frac{G_p}{G_{BC}} + K_2^2 \frac{G_p}{G_Z}}$$

$$\frac{P_{BC}}{P_T} = \frac{K_1^2 \frac{G_p}{G_{BC}}}{1 + K_1^2 \frac{G_p}{G_{BC}} + K_2^2 \frac{G_p}{G_Z}} \qquad (3.8\text{-}6)$$

$$\frac{P_Z}{P_T} = \frac{K_2^2 \frac{G_p}{G_Z}}{1 + K_1^2 \frac{G_p}{G_{BC}} + K_2^2 \frac{G_p}{G_Z}}$$

The data obtained for the parameters in Equation 3.8-6 for vertical polarization are,

K_1^2 = 0.000562 (i.e., -32.5 db)

K_2^2 = 0.0000795 (i.e., -41.0 db)

G_p = 224 (i.e., 23.5 db)

G_{BC} = 3.97 (i.e., 6.0 db)

G_Z = 7.94 (i.e., 9.0 db)

Applying these data in Equations (3.8-6) reveals that

$$\frac{P_p}{P_T} = 96.7\%$$

$$\frac{P_{BC}}{P_T} = 3.1\%$$

$$\frac{P_Z}{P_T} = 0.2\% \qquad \text{and}$$

thus, only 3.3 percent of the total power to be radiated using vertical polarization is needed to suppress the sidelobe structure to the levels attained. This result is not surprising because the sidelobes were initially at a level of -30 db.

SECTION 4

SPACECRAFT CONSTRAINTS

The antenna techniques investigated in this program are intended for use on future spacecraft. For these applications, certain constraints may be imposed upon the suppression techniques. These constraints are listed in Table 4-1 and applied to the blockage compensation

Table 4-1. Compatibility of Suppression Techniques with Spacecraft Constraints

Spacecraft Constraint	Compatible	
	Blockage Compensator Technique	Active Zone Technique
2 HPBW Steering	Yes, Antenna Steering No, Feed Motion	Yes, Antenna Steering No, Feed Motion
10% Maximum Increase in Antenna Weight	Yes (3%)	No (110%)
20 KW RF Power For L-Band; 7 KW RF Power For S, X-Band	Yes	Yes
Radiation Heat Rejection Only	Dependent Upon Spacecraft Design	
No Organic Material Near High Fields	Yes	Yes
Same Deployment Reliability	Yes	Yes
$.08^2$/CPS Vibration and $\pm$15 g Longitudinal Acceleration and $\pm$2.5 g Normal and Lateral Acceleration	Yes	Yes
10% Maximum Increase in Launch Volume	Yes (0.3%)	Yes (4.0%)

technique and active zone suppressor technique. The table indicates the compatibility of each suppressor technique to meet spacecraft constraints, based upon the current information available.

The table is self-explanatory. However, additional comments on scanning the feed ± two half-power beam widths are in order. It is theoretically possible to achieve the desired sidelobe envelope for an unperturbed reflector aperture by modifications of the aperture distribution and/or the feed system radiation characteristics and, at the same time, maintain a reasonable aperture efficiency. Further, it has been demonstrated that substantial sidelobe suppression can be realized for a given, single beam position for a paraboloid reflector. However, an attempt to maintain the same performance over a significant beam scan range would be self-defeating, since the amplitude and phase of the very suppression techniques, introduced for a given beam direction, now become undesirable elements of disturbance.

An obvious, but extremely complicated approach to overcome this impasse is to employ techniques which are variable and thus adaptable to any desired scan angle.

The application of the sidelobe suppression techniques to existing spacecraft antennas will have an impact on antenna weight and size. Estimates of this impact have been calculated by assuming, as a mathematical model, a 4 meter diameter paraboloid with an F/D = 0.4 and an operating frequency of 860 MHz (its half-power beam width is 6 degrees.) The weight of the paraboloid was 22.4 kilograms and its package volume 8.0 cubic meters.

The active zone technique, when implemented for sidelobe suppression in all azimuth planes of a paraboloid, takes the form of a ring or annulus of 20 helices having a diameter of 4.7 meters.* Assuming that each helix is individually attached about the paraboloid and a 20-way power divider with cables extending to each element is used as the feed system, the estimated increase in weight and package volume becomes 25 kilograms and 0.33 cubic meter, respectively. These values constitute a 110 percent increase in antenna weight and a 4 percent increase in package size.

The blockage compensation technique should present no deployment problems; its operational

---

*See Appendix E for description of ring zone design

reliability should be consistent with that provided by a conventional paraboloid antenna system. The active zone suppression technique would have deployment problems because of the complexity of using a ring of twenty helices and associated feed circuitry. It is anticipated that this problem is solvable with the adoption of a suitable mechanical design. The operational reliability of this technique is estimated as being somewhat less than that for the other two techniques, but acceptable nevertheless.

A minor degree of mechanical modification is anticipated for the implementation of the blockage compensation technique; major mechanical design changes are envisioned with the use of the active-zone suppressor technique. These design changes are feasible and represent work within the state of the art.

SECTION 5

CONCLUSIONS AND RECOMMENDATIONS

An analytical and experimental investigation of four sidelobe suppression techniques for reflector-type antennas was performed. The application of the heavy taper, blockage compensation and active zone suppression techniques was shown to meet the pattern goal requirements for near axis sidelobe suppression (including - 40 db sidelobes) in one pattern plane of a paraboloid. This achievement was obtained for linear polarization and required only 3.3 percent of the total RF power radiated to be used by the suppressor elements. Although certain feed problems precluded demonstration of sidelobe suppression for circular polarization, these achievements clearly indicate that blockage compensation, and/or active zone suppression can provide substantial sidelobe suppression for this polarization.

The blockage compensation technique offers a simple but effective method to correct for aperture blockage and to significantly suppress the sidelobe sturcture. Active-zone suppression is a more complex, larger, and heavier method. However, it is capable of suppressing more of the sidelobe structure.

The results of this program suggest that additional work be done to more fully exploit and develop these techniques. It is recommended that this work include:

a. The design and development of a circularly-polarized feed which inherently provides better symmetric illumination of a reflector antenna and possesses a unique phase center.

b. The design and development of an integral feed unit containing a blockage compensator to provide aperture blockage correction and sidelobe suppression in all reflector planes for circular polarization.

APPENDIX A

REVIEW OF LITERATURE

Appendix A is a compilation of the literature surveyed. Each document surveyed is appropriately referenced and abstracted to indicate the overall scope of the survey and applicability to the desired program objective.

E.M.T. Jones, "Low Side Low Side Lobes in Pencil-Beam Antennas," IRE National Convention Record, Part 2, pp. 64-67, March 1953.

The paraboloid reflector and the hyperboloid dielectric lens are considered, using three feed types. These are

a. Short electric dipole

b. Short magnetic dipole

c. Plane wave source

Insofar as the reflector is concerned, emphasis is placed upon cross-polarized radiation. It is shown that small feed horns, which approximate plane wave sources, are superior to the dipoles in maintaining low cross-polarized side lobes.

R.J. Adams and K.S. Kelleher, "Pattern Calculations for Antennas of Elliptical Apertu e," Proceedings of the IRE, Vol 38, pp. 1052, September 1950.

A method is presented for determining the pattern of a paraboloid antenna of elliptical aperture from a knowledge of the characteristics of the reflector and feed horn. Measured data are converted to an analytical function by means of a Fourier series approximation, and the corresponding pattern is expressed as a sum of Lambda functions. Good agreement is shown between calculated and measured patterns.

A. Ksienski, "Derivative Control in Shaping Antenna Patterns," IRE International Convention Record, Part 1, pp. 3-12, March 1960.

This paper describes a method of array synthesis, using the related polynomial expressions and their derivatives, which is capable of matching limited portions of the desired pattern to any prescribed degree of accuracy. Comparison is made with the conventional Fourier and Woodward Techniques which are based upon RMS error minimization. The method is applicable to arrays with complex excitation coefficients. It is seminumerical in nature and may involve several perturbations depending upon how closely one desires to approach the optimum. Numerical examples and experimental verification are presented.

P. T. Hutchison, "The Image Method of Beam Shaping," IRE Trans. on Antennas and Propagation, Vol AP-4, pp. 604-609, October 1956.

The image method of beam shaping applies to a paraboloid with offset feed, the image being provided by the ground plane near the feed giving the effect of multiple feeds. Since the real feed is slightly offset from the focus, a variety of patterns may be obtained by superposition. Cosecant squared patterns result from the use of reflectors no larger than those required to give pencil beams of commensurate width. Measured and computed patterns show good agreement.

J. Perini, "Side-Lobe Reduction by Beam Shifting," IEEE Transactions on Antennas and Propagation, Vol AP-12, pp. 791-792, November 1964.

The method described is a version of the well-known Woodward Technique for pattern shaping with a rectangular aperture. In this case the phases and amplitudes of the various $\frac{\sin x}{x}$ components are chosen by a straightforward procedure to produce the desired side lobe level.

J. Ruze, "Circular Aperture Synthesis," IEEE Transactions on Antennas and Propagation, Vol AP-12, pp. 691-694, November 1964.

In this paper, the Woodward technique for rectangular apertures is extended to the case of a circular aperture. Expressions for the pattern and corresponding aperture illumination are given, and an example is shown for flat-top beam shaping.

Non-rotationally symmetric patterns can be synthesized by a generalization of the technique; the procedure for doing this is outlined.

J.F. Kauffman, "The Calculated Radiation Patterns of a Truncated Gaussian Aperture Distribution," IEEE Transactions on Antennas and Propagation, Vol AP-13, pp. 473-474, May 1965.

A computed pattern is shown for a circular aperture with a truncated $e^{-\alpha\rho^2}$ aperture distribution. While the pattern integral can be evaluated analytically, the result is a slowly converging infinite series which cannot be calculated accurately on a digital computer. The result given was obtained by means of an analog computer; for a 50 λ aperture the beamwidth is 1.8 degrees and the sidelobe level is -51 db.

C.C. Allen, "Radiation Patterns for Aperture Antennas with Non-Linear Phase Distributions," IRE National Convention Record, Part 2, pp 9-17, March 1953.

Two-dimensional antenna patterns are determined for several aperture distributions having symmetrical amplitude and non-linear phase using a computer.

A. F. Sciambi, "The Effect of the Aperture Illumination on the Circular Aperture Pattern Characteristics," Microwave Journal, Vol. 8, pp 79-84, August, 1965.

Patterns and aperture efficiencies are computed for circular apertures using various parameters in the general illumination expression $C + (1 - r^2)^n$.

H. E. Bartlett and R. E. Moseley, "Dielguides - Highly Efficient Low Noise Antenna Fields", Microwave Journal, Vol. 9, pp. 53-58, December 1966.

Dielectric structures providing total internal reflection are used to support both prime focus feeds and Cassegrain subreflectors. Due to the control of feed radiation the subreflector may be made smaller than those used in conventional Cassegrain designs. Higher antenna efficiencies and superior low noise characteristics are claimed as a result of this technique which, it is suggested, may afford solutions to other antenna problems.

G. Hampton and R. Thomas, "Design Techniques for Shaped Beam Antenna," Twelfth East Coast Conference on Aerospace and Navigational Electronics, October 1965.

A study was made to determine the best design for a high gain narrow pulse radar antenna having a rectangular shape in the vertical plane. Hardware portions were built to verify critical concepts; measured results are given, along with calculated performance of the entire antenna. Both resonant and nonresonant slot arrays were considered; the design was based upon a truncated $\frac{\sin x}{x}$ aperture distribution.

D. J. Lewis, "Fourier Transform Synthesis of Sector Beam Radiation Patterns," Microwave Journal, Vol. 9, pp. 71-74, December 1966.

The discussion is restricted to aperture distributions that produce sector beams in a single plane. A modification of the Fourier derived aperture distribution is presented which permits the reduction of ripple and sidelobe level to any desired degree at the expense of a decrease in the slope of the beam edge.

T. T. Taylor, "Design of Circular Apertures for Narrow Beamwidth and Low Sidelobes," IRE Trans. on Antennas and Propagation, Vol. AP-8, pp. 17-22; January 1960.

This article extends a method of antenna design originally developed for line-source antennas. A family of continuous circular aperture distributions is developed in such a way as to involve only two independent parameters, A, a quantity uniquely related to the design sidelobe level and $\bar{n}$ a number controlling the degree of uniformity of the sidelobes. Formulas relating pattern to aperture distribution are given.

J. Ruze, "Lateral-Feed Displacement in a Paraboloid," IEEE Trans. on Antennas and Propagation, Vol. AP-13, pp. 660-665; September 1965.

The beam shift and degradation of a paraboloidal reflector with an offset feed is analyzed by the scalar plane wave theory. Higher order coma terms are included with the feed at its optimum axial position. The beam characteristics for a tapered circularly symmetric illumination are presented. Equations are given which permit gain evaluation and pattern computation.

R. C. Johnson, "Reducing Wide-Angle Side Lobes in Radar Antennas," Microwave Journal, Vol. 9, pp. 48-49, 94-96, August 1966.

Techniques are demonstrated for reducing wide angle sidelobes by feed modification. This was done for the SPS-10 for beam and for the SPN-6 pencil beam antennas by attaching a pair of blinders to the sides of the feed horn to reduce spillover radiation. In the case of the SPN-6, absorbing material was also placed behind the reflector to reduce back radiation. Both radars are horizontally polarized; the measured reduction was approximately 10 db in the plane of polarization.

K. Green, "Modified Cassegrain Antenna for Arbitrary Aperture Illumination," IEEE Trans. on Antennas and Propagation, Vol. AP-11, pp. 589-590; September 1963.

Well-known techniques for designing shaped reflectors, based upon energy conservation principles, are applied to the subreflector of a Cassegrain antenna in order to produce a Taylor distribution. This introduces a phase error in the aperture plane which is circumvented by correcting the main reflector by the amount necessary to maintain equal path lengths for all the rays from the focus to the aperture plane. Spillover can be reduced since the subreflector can be designed to intercept nearly all the primary pattern main lobe. Design equations are given.

The same technique is described in the following reference:

W. F. Williams, "High Efficiency Antenna Reflector," Microwave Journal, Vol. 8, pp. 79-82, July, 1965.

AD 405 824, L. Peters, Jr. and R.C. Rudduck "RFI Reduction by Control of Antenna Sidelobes," RADC-TRD-63-133, May 1963.

The reduction of direct feed radiation and edge diffracted radiation is treated for three types of antennas: (1) Horn, (2) Reflector (3) Luneberg Lens. For the reflector, an optimum F/D ratio is derived on the basis of minimum direct feed radiation. Another optimum is derived for minimum edge diffraction. The two values indicate that small values of F/D are preferable in this respect. The use of absorbing material and methods of feed modification are considered; some measured results are given.

AD 623 074, Leon Peters, Jr. et al., "Antenna Lobe Suppression, Vol III - Radiating Mechanisms in a Reflector Antenna System," RADC-TR-65-186, October 1965.

Direct and diffracted feed radiation may be reduced considerably by small adjustments in reflector size, provided the feed pattern has a large slope in the direction of the edge of the reflector and that it has low backlobes. The boundary determined by the phase center of the feed and the edges of the reflector is known as the shadow boundary. From optics, it is known that the antenna pattern is approximately 6 db below the feed pattern at this angle. Experimental measurements show 7 db, using an offset feed horn, with corrugated walls in the E-plane, having nearly identical E and H plane patterns. The level of the direct radiation is related by the gain of the reflector and of the feed antenna. The maximum diffracted radiation can be directed in the main beam region by an appropriate choice of reflector geometry.

AD 623 076, R.E. Lawrie, "Antenna Lobe Suppression, Vol V - Grated Reflector Antennas for Spurious Radiation Reduction," RADC-TR-65-186, October 1965.

The suppression of higher harmonic radiation by grating techniques is treated in this report. The discrimination between fundamental and second harmonic in a conventional strip grating is 6 db, which is insufficient for the purpose. This leads to consideration of a reflector composed of edge strips the broad dimension of which is in the direction of propagation. When arranged parallel to the incident E vector, they function as below cut-off waveguides for the fundamental. Radial wedge versions are described; the harmonic discrimination is better than 20 db. The harmonic energy of course appears behind the reflector.

AD 607 321, R.E. Moseley et al., "Study of Special Beamshaping Antennas," Final Report-Contract DA 36-039 AMC-03310(E), July 30, 1964.

This report is concerned with beamshaping of end-fire antennas intended for use as array elements. A theoretical analysis leads to a useful design procedure based on ray tracing. From this is evolved a "Foamrod Antenna" which is actually a combination of end-fire and broadside concepts in that the element is flared into an aperture in the same manner as a horn. In this case the antenna consists of a solid dielectric cone having an order of magnitude greater gain than conventional end-fire dielectric elements. Investigations of the applicability of these elements as primary feeds for lenses and reflectors are described. It is an ideal Cassegrain feed; one model was constructed which had 70 percent aperture efficiency.

AD 617 123, W.R. Lind, "Out of Band Performance of Antennas," Technical Report No. RADC-TR-65-43, May 1965.

This report is a summary of the available information on the performance of antennas outside of their design band. It covers the following types:

a. Cylindrical
b. Biconical
c. Horn
d. Parabolic

Both measured and theoretical data are presented. The antenna parameters covered are radiation and input impedances, gain, and radiation patterns:

These data for circular aperture parabolic antennas are based on the use of double dipole feeds. The properties of these antennas are summarized as follows:

a. Out-of-band gain tends to remain constant
b. Out-of-band beamwidth is relatively constant, with a tendency to decrease with increasing frequency.
c. Beam tilt is not a function of frequency.

d. Front-to-back ratio tends to remain constant.

e. Sidelobe level tends to remain constant.

f. VSWR to generally below 5:1

g. The H-plane patterns are symmetrical about the antenna axis.

A particular type of elliptical aperture antenna, the AN/FPS-8. was also studied, leading to the following conclusions:

a. The gain tends to remain constant above the third harmonic, except for a peak at the seventh harmonic.

b. The beamwidth remains constant up to the tenth harmonic

c. The radiation pattern breaks up into many lobes above the fourth harmonic.

AD 623 072, C. Davis et al., "Antenna Lobe Suppression, Volumes I through IV, Contract AF 30 (602) - 3269, October 1965.

Three mechanisms for reducing backlobes of horn antennas are described. These prevent the energy from illuminating the edges from which it is diffracted into the back region. The three mechanisms for forcing energy away from these edges are

a. The use of microwave absorber
b. Choke slots
c. Corrugated surfaces

These devices lead to a smooth main beam with very low sidelobes.

The use of absorber to line the horn walls introduces excessive attenuation, and so the principal techniques of interest are limited to the chokes and to the corrugated surfaces. The use of the latter produces a greater backlobe reduction than do the chokes but results in a slight increase in beamwidth. The usable bandwidth of the modified horns is at least as great as the bandwidth of the waveguide feeding the horn. Using chokes, the backlobe improvement varies from 12 db at the low end to 3 db at the high end. With corrugations, the corresponding improvements are 13 to 6 db.

AD 646 225, F.I. Sheftman, "Experimental Study of Subreflector Support Structures in a Cassegrainian Antenna," Lincoln Laboratory Technical Report 416, September 23 1966.

This report covers the experimental investigation of various subreflector support structures insofar as gain and sidelobe levels are concerned. Sidelobe disturbances are shown to decrease rapidly for perpendicular polarization when the cross-sectional dimensions are reduced to less than one-half wavelength. The on-axis geometrical shadowing due to the support members does not give the correct level and shape of the wide angle radiation. Account must be taken of the polarization and orientation of the members relative to the antenna axis. The performance of dielectric members is shown to be generally poorer than that of metallic members. The alternative of supporting the subreflector with a thin-wall axial dielectric cylinder is shown to be electrically acceptable for thicknesses of the order of 0.01 wavelength. The peak gain and E-plane pattern, using this device, are affected negligibly. The H-plane sidelobes increased up to 5 db at some intermediate angles, the level of the close-in and far-out lobes being essentially unchanged.

AD 418 367, R.E. Franks and C.F. Hummel, "Side Lobe Power Level Probabilities for Matched and Unmatched Polarizations," Tech. Memo. EDL-M560, Contract DA 36-039 AMC-00088(E), April 22 1963.

A probability analysis was made to determine side lobe effects upon system performance, and curves are presented which exhibit the results. Experimental data on specific reflector antennas were taken in order to provide inputs to the analysis. The following antennas were used:

Reflector	Frequency	Gain
6'	2.8 GHz	30 db
6' (Solid)	4.8 8.5	38
28' (mesh)	187 MHz	21

Measured results show that, in general, the mean value of radiation in the sidelobe region is about -10 db. The principal source is feed spillover.

AD 152 394, "Final Report on Theoretical and Experimental Investigations In Methods of Reducing Antenna Sidelobes," AFCRC-TR-58-139, June 26, 1956 to June 15, 1958.

This report is principally concerned with the reduction of far-out sidelobes in order to improve radar resistance to jamming. Several antenna types were evolved with the first five sidelobe regions below -25 db and the remaining portion below -40 db. A large part of the spacial radiation pattern is less than -50 db below the main lobe maximum. The antenna types or techniques evaluated were:

a. The parabolic horn
b. The parabolic horn with a correcting lens
c. The shaped horn reflector
d. The cylindrical antenna fed by a half pillbox feed.
e. The shaped cylindrical antenna fed by a half pillbox feed.
f. The dual reflector antenna
g. High dielectric constant rod arrays
h. High dielectric constant rod arrays
i. The tunnel antenna technique.

The study opens with the comment that many other previous study programs have been directed towards the suppression of sidelobes with only marginal success. In general, these programs were mainly concerned with the reduction of near-in diffraction lobes to magnitudes of less than -25 to -30 db. In this the programs they were partially successful, although the mechanical tolerances necessary to maintain these levels were extremely tight.

APPENDIX B

LOW BLOCKAGE FEED FOR REFLECTOR ANTENNAS

APPENDIX B

LOW BLOCKAGE FEED FOR REFLECTOR ANTENNA

For a given reflector diameter and edge illumination, the feed aperture increases with the F/D ratio because its pattern in required to become more directive under these circumstance. This leads to increased blockage when broadside feeds such as horns are used, with the attendant degradation in gain and sidelobe level.

In order to avoid this effect we may consider the use of an end-fire type of feed element such as a helix, for example, because this obviously produces less physical blockage for a given directivity. To evaluate the electrical effects, let us assume that the feed has gain G_F and unity axial ratio in right-hand circular polarization. Looking in the axial direction of propagation, we will represent its transmitted wave by $E(\bar{U}_y + j\bar{U}_x)$ where $\bar{U}_y$ and U_x are respectively unit vectors in the y and x directions. This will be returned by the reflector as a left-hand circularly polarized wave which, as seen by the feed, may be described in $E'(\bar{U}_y + j\bar{U}_x). = a_1 e^{j\phi 1} E(\bar{U}_y + {}_j\bar{U}_x)$. These relationships are shown in A and B of Figure B-1 which is a conceptual representation of the fields and antenna components. In C it is shown that the energy collected by the feed, in B, will be reradiated as left hand circular polarization since each received component undergoes an effective short circuit due to the opposite phase of the other component. Upon returning from the reflector, the reradiated energy is right-hand circularly polarized and may be absorbed by the feed load. Further multiple reflections are neglected.

It is seen that two electrical effects are produced:

a. The reflector field consists of both left and right-hand components, thus producing elliptical polarization.

b. Some power is absorbed by the load, which may lead to a mismatched condition.

Both of these effects will be analyzed under the assumptions that the reflector is uniformly illuminated and that there is no spillover in order to simplify the calculations and thereby exhibit the basic relationships more clearly.

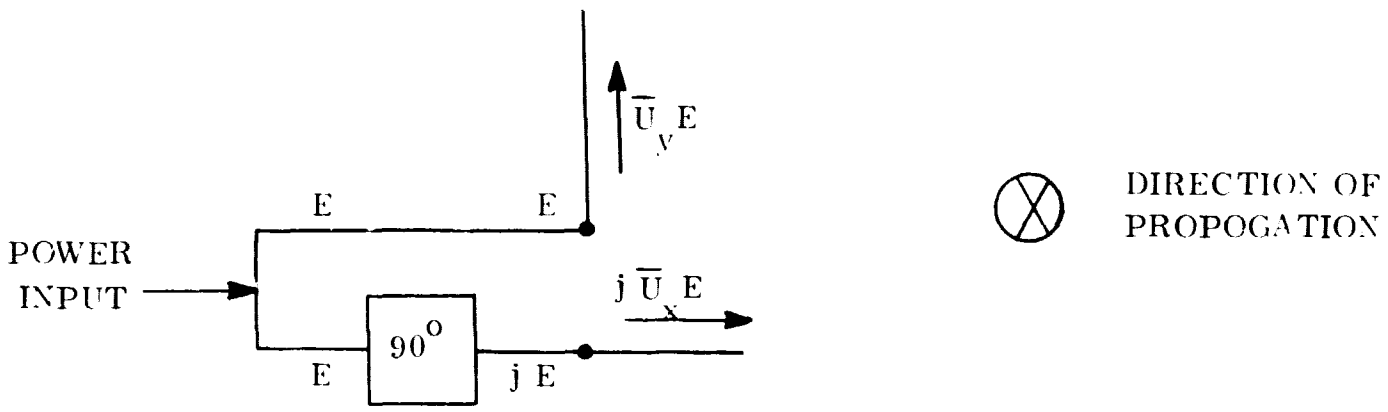

A. TRANSMIT RH CIRCULAR POLARIZATION

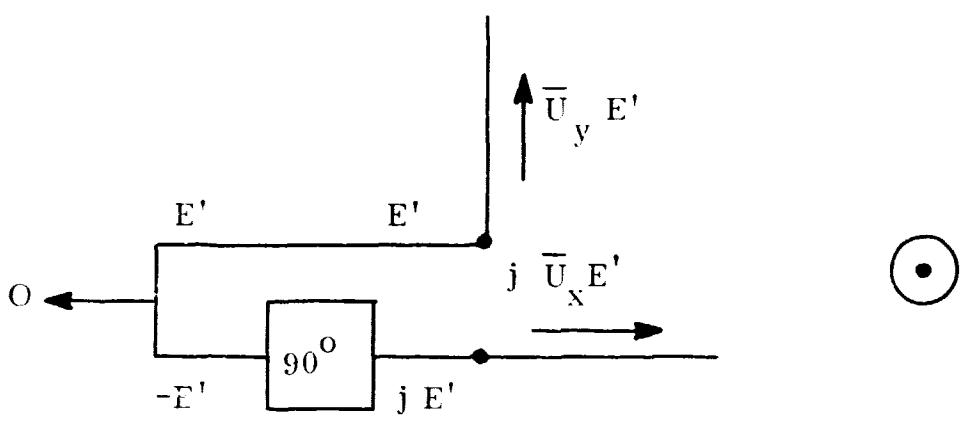

B. RECEIVE LH CIRCULAR POLARIZATION

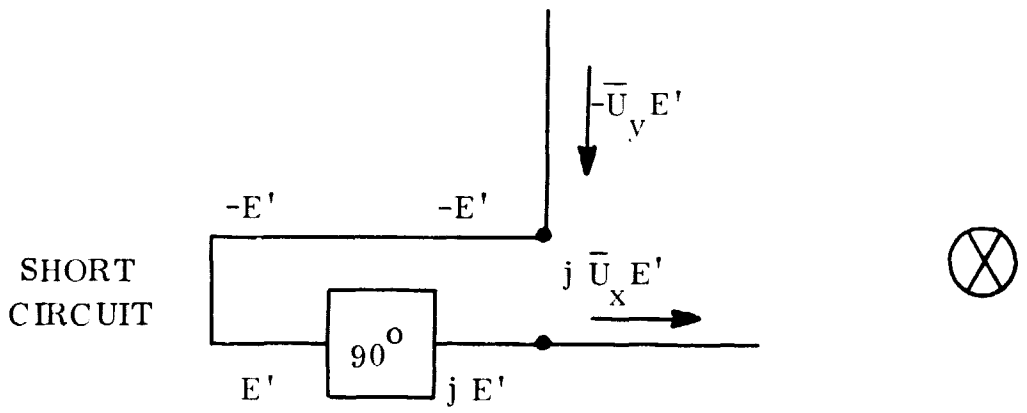

C. RERADIATE LH CIRCULAR POLARIZATION

Figure B-1. Conceptual Representation of Fields

B.1 ELIPTICAL POLARIZATION

In 1A the feed transmits power P in right-hand circular polarization. The reflected power density (left hand) is $4P/\pi D^2$ where D is the reflector diameter. The received power, in 1B, is $4\ P/\pi D^2 \times G_F\ \lambda^2/4\pi = P\ G_F/G_A$ where G_A is the aperture gain. The reradiated power (left hand), in 1C, is reflected as right-hand circular polarization with power density $P\ G_F/G_A \times 4/\pi D^2$. This reflected field, viewed from the feed, may be denoted as $a_2 e^{j\phi 2}$ $E\ (\bar{U}_y - j\bar{U}_x)$ where

$$a_2 = \sqrt{P\ G_F/G_A \cdot 4/\pi D^2}$$

$$\phi_2 = 2\pi/\lambda \times 4\ F, \text{ measured at F}$$

F = focal distance in wavelengths

This combines with the first reflected field (left hand) which was denoted by $a_1 e^{j\phi 1} E\ (\bar{U}_y + j\bar{U}_x)$ where

$$a_1 = \sqrt{4P/D^2} = a_2\sqrt{G_A/G_F}$$

$$\phi_1 = 2\pi/\lambda \quad x \quad 2F$$

The composite field, for purposes of polarization analysis, may be expressed as

$$\bar{E}_c = E\ (\bar{U}_y + j\bar{U}_x) + \sqrt{G_F/G_A} \cdot e^{j\ 4\pi F/\lambda} \cdot E\ (\bar{U}_y - j\bar{U}_x)$$

by putting $a_1 = 1$, $\phi_1 = 0$ as references.

The axial ratio is $\dfrac{1 + \sqrt{G_F/G_A}}{1 - \sqrt{G_F/G_A}}$. For

example, if $G_F = 10$ (10 db)

$G_A = 1000$ (30 db)

the axial ratio is $1.1/0.9 = 1.22$, or 1.7 db.

B.2 POSSIBLE MISMATCHED CONDITION

The reradiated field upon reflection (right hand) was shown to have power density $P\,G_F/G_A \times 4/\pi D^2$. The feed accepts $P\,G_F/G_A \times 4/\pi D^2 \times G_F\,\lambda^2 /4\pi = P\,G_F{}^2/G_A{}^2$; thus, the power reflection coefficient is $G_F{}^2/G_A{}^2$. For the example quoted previously where $G_F = 10$ and $G_A = 1000$, the effect is negligible.

B.3 CONCLUSIONS

The use of a circularly polarized end fire feed produces less effective blockage than does a broadside-type feed of equal gain. The energy associated with the feed capture area is redistributed over the reflector in a manner which produces a minor degradation of axial ratio, with no increase in side lobe levels.

APPENDIX C

APERTURE EFFICIENCY OF VARIOUS AMPLITUDE DISTRIBUTIONS

For a circular aperture of normalized radius 1 and amplitude distribution A(r), the aperture efficiency is

$$\eta = \frac{\left[\int_0^{2\pi}\int_0^1 A(r)\, r\,dr\,d\phi\right]^2}{\pi\int_0^{2\pi}\int_0^1 A^2(r)\, r\,dr\,d\phi}$$

$$= \frac{2\left[\int_0^1 A(r)\, r\,dr\right]^2}{\int_0^1 A^2(r)\, r\,dr}$$

Thus, if $A(r) = C$, $\eta = 1$ or 100 %

Table C-1. Aperture Efficiency Calculation

20 db reduction on Rings 13, 14, 15
11.8 λ aperture
$A(r) = 0.3 + 0.7(1-r^2)$

Ring	r	A(r)	$A^2(r)$	rA(r)	$rA^2(r)$	
1	0.05	0.998	0.997	0.050	0.050	
2	0.10	0.993	0.986	0.099	0.099	
3	0.15	0.984	0.969	0.148	0.145	
4	0.20	0.972	0.945	0.194	0.189	
5	0.25	0.956	0.914	0.239	0.229	
6	0.30	0.937	0.878	0.281	0.263	
7	0.35	0.914	0.836	0.320	0.293	
8	0.40	0.888	0.789	0.355	0.316	
9	0.45	0.858	0.737	0.386	0.332	
10	0.50	0.825	0.680	0.413	0.340	
11	0.55	0.788	0.621	0.433	0.342	
12	0.60	0.748	0.560	0.449	0.336	
-13	0.65	0.070	0.005	0.046	0.003	
-14	0.70	0.066	0.004	0.046	0.003	
-15	0.75	0.061	0.004	0.046	0.003	
16	0.80	0.552	0.305	0.442	0.244	
17	0.85	0.494	0.244	0.420	0.207	
18	0.90	0.433	0.187	0.390	0.168	
19	0.95	0.368	0.136	0.350	0.129	
20	1.00	0.300	0.090	0.300	0.090	
				5.407	3.781 →	4.672 for
			x 0.05	0.270	0.189	no absorber

$$\eta = \frac{2(0.270)^2}{0.189} = 0.77 \quad \text{aperture efficiency}$$

Factor due to power absorption loss $\frac{3.781}{4.672} = 0.81$

Overall efficiency = 0.77 x 0.81 = 0.62.

Table C-2. Aperture Efficiency Calculation
Ring 25 Active

$$A(r) = 0.3 + 0.7(1-r^2), \quad r \leq 1.0$$

$$A(1.25) = 0.247$$

Ring	r	rA(r)	$rA^2(r)$
1	0.05	0.050	0.050
2		0.099	0.099
3		0.148	0.145
4		0.194	0.189
5		0.239	0.229
6		0.281	0.263
7		0.320	0.293
8		0.355	0.316
9		0.386	0.332
10	0.50	0.413	0.340
11		0.433	0.342
12		0.449	0.336
13		0.458	0.322
14		0.460	0.302
15		0.455	0.276
16		0.442	0.244
17		0.420	0.207
18		0.390	0.168
19		0.350	0.129
20	1.00	0.300	0.090
		6.642	4.672
25	1.25	0.309	0.076
		6.951	4.748
	x 0.05	0.348	0.237

$$\eta = \frac{2(0.348)^2}{0.237} = \left(\frac{1}{1.25}\right)^2 = 0.65.$$

Table C-3. Aperture Efficiency of Taylor 25 db Circular

$\bar{n} = 3$

Ring	r	A(r)	$A^2(r)$	rA(r)	$rA^2(r)$
1	0.05	0.996	0.991	0.050	0.050
2	0.10	0.983	0.966	0.098	0.097
3	0.15	0.962	0.926	0.144	0.139
4	0.20	0.934	0.873	0.187	0.175
5	0.25	0.900	0.809	0.225	0.202
6	0.30	0.860	0.739	0.258	0.222
7	0.35	0.816	0.666	0.286	0.233
8	0.40	0.769	0.591	0.308	0.237
9	0.45	0.721	0.520	0.324	0.234
10	0.50	0.673	0.452	0.336	0.226
11	0.55	0.626	0.391	0.344	0.215
12	0.60	0.581	0.337	0.348	0.202
13	0.65	0.539	0.291	0.351	0.189
14	0.70	0.502	0.252	0.351	0.176
15	0.75	0.470	0.221	0.352	0.165
16	0.80	0.443	0.196	0.354	0.157
17	0.85	0.422	0.178	0.358	0.151
18	0.90	0.407	0.165	0.366	0.149
19	0.95	0.398	0.158	0.378	0.150
20	1.00	0.395	0.156	0.395	0.156
				5.813	3.525
			0.05	0.291	0.176

$$\eta = \frac{2(0.291)^2}{0.176} = 0.962$$

Table C-4. Aperture Efficiency of Taylor 35 db Circular

$\bar{n} = 4$

Ring	r	A(r)	$A^2(r)$	rA(r)	$rA^2(r)$
1	0.05	0.996	0.991	0.050	0.050
2	0.10	0.982	0.965	0.098	0.097
3	0.15	0.961	0.923	0.144	0.138
4	0.20	0.931	0.866	0.186	0.173
5	0.25	0.893	0.797	0.223	0.199
6	0.30	0.848	0.720	0.254	0.216
7	0.35	0.798	0.636	0.279	0.223
8	0.40	0.741	0.550	0.296	0.220
9	0.45	0.681	0.464	0.306	0.209
10	0.50	0.618	0.382	0.309	0.191
11	0.55	0.554	0.307	0.305	0.169
12	0.60	0.490	0.240	0.294	0.144
13	0.65	0.428	0.183	0.278	0.119
14	0.70	0.369	0.136	0.258	0.095
15	0.75	0.317	0 100	0.238	0.075
16	0.80	0.271	0.074	0.217	0.059
17	0.85	0.235	0.055	0.200	0.047
18	0.90	0.208	0.043	0.187	0.039
19	0.95	0.192	0.037	0.182	0.035
20	1.00	0.187	0.035	0.187	0.035
				4.491	2.533
			0.05	0.22455	0.12665

$$\eta = \frac{2(0.22455)^2}{0.12665} = 0.7963$$

Table C-5. Aperture Efficiency of Taylor 40 db Circular

$\bar{n} = 4$

Ring	r	A(r)	$A^2(r)$	rA(r)	$rA^2(r)$
1	0.05	0.995	0.989	0.050	0.049
2	0.10	0.979	0.958	0.098	0.096
3	0.15	0.953	0.908	0.143	0.136
4	0.20	0.918	0.843	0.184	0.163
5	0.25	0.875	0.766	0.219	0.192
6	0.30	0.825	0.681	0.248	0.204
7	0.35	0.769	0.592	0.269	0.207
8	0.40	0.709	0.502	0.284	0.201
9	0.45	0.645	0.416	0.290	0.187
10	0.50	0.579	0.335	0.290	0.168
11	0.55	0.512	0.262	0.282	0.144
12	0.60	0.445	0.198	0.267	0.119
13	0.65	0.381	0.145	0.248	0.094
14	0.70	0.320	0.102	0.224	0.071
15	0.75	0.265	0.070	0.199	0.053
16	0.80	0.217	0.047	0.174	0.038
17	0.85	0.178	0.032	0.151	0.027
18	0.90	0.149	0.022	0.134	0.020
19	0.95	0.132	0.017	0.125	0.016
20	1.00	0.126	0.016	0.126	0.016
				4.005	2.207
			0.05	0.20025	0.11035

$$\eta = \frac{2(0.20025)^2}{0.11035} = 0.7268$$

APPENDIX D

MEASURED PARABOLOID PATTERNS USING 5-AND 6-TURN HELIX FEEDS

D.1 5-TURN HELIX FEED

For the 5-turn helix feed, the pattern data for evaluating the defocusing technique and establishing the focal position d are shown in Figures D-1 and D-2. As shown, the defocusing technique did not suppress the sidelobe structure. The apparent in-focus feed position was d = 19.0 centimeters. This feed had a measured gain of 7.5 db for vertical polarization and 7.7 db for horizontal polarization; its aperture blockage is -38 db relative to the peak of the paraboloid pattern. This level of aperture blockage begins to perturb the main lobe of the parabola pattern by -1 db at about the -20 db power level and can raise a predicted -37.5 db first sidelobe to about -31.6 db. The angular position and intensity of backlobe radiation (see Figure 3.3-5) was as depicted in Figures D-1 and D-2. The vertically polarized backlobe contributed to null-filling at $\theta = +14$ degrees and is capable of raising the predicted sidelobe level of -37.5 db (at $\theta = \pm 16.5^{\circ}$) by about 10 db. The horizontally polarized backlobe is capable of altering the main lobe by 1 db at the -20 db power level and is a contributor to the wide angle sidelobe structure.

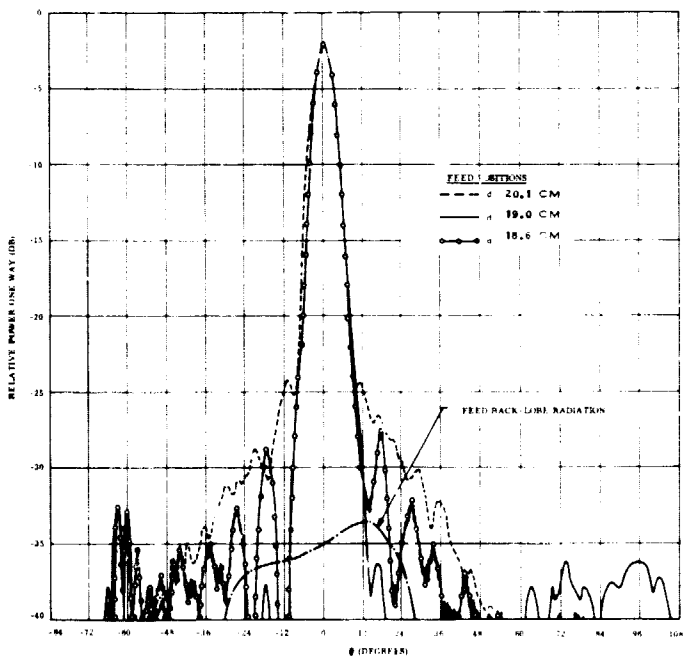

Figure D-1. Paraboloid Patterns in $\phi = 0^{\circ}$ Plane as a Function of 5-Turn Helix Feed Position Using Vertical Polarization

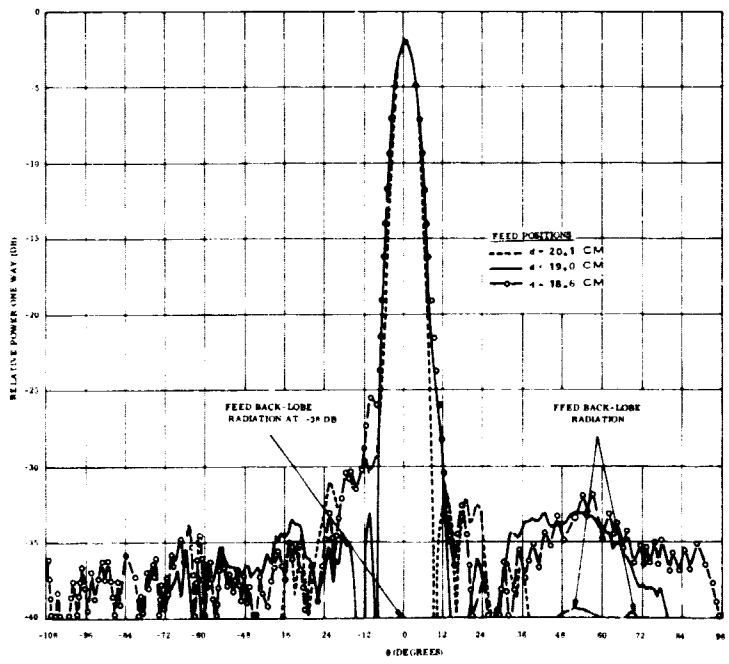

Figure D-2. Paraboloid Patterns in $\phi = 0^{\circ}$ Plane as a Function of 5-Turn Helix Feed Position Using Horizontal Polarization

A set of paraboloid patterns were taken at azimuth intervals of 30 degrees using d = 19.0 centimeters. These patterns are given in Figures D-3 and D-4 for vertical and horizontal polarization. All patterns agreed with prediction down to a power level of -15 db; below this level they were modified by marginal feed symmetry, blockage, and backlobe radiation effects.

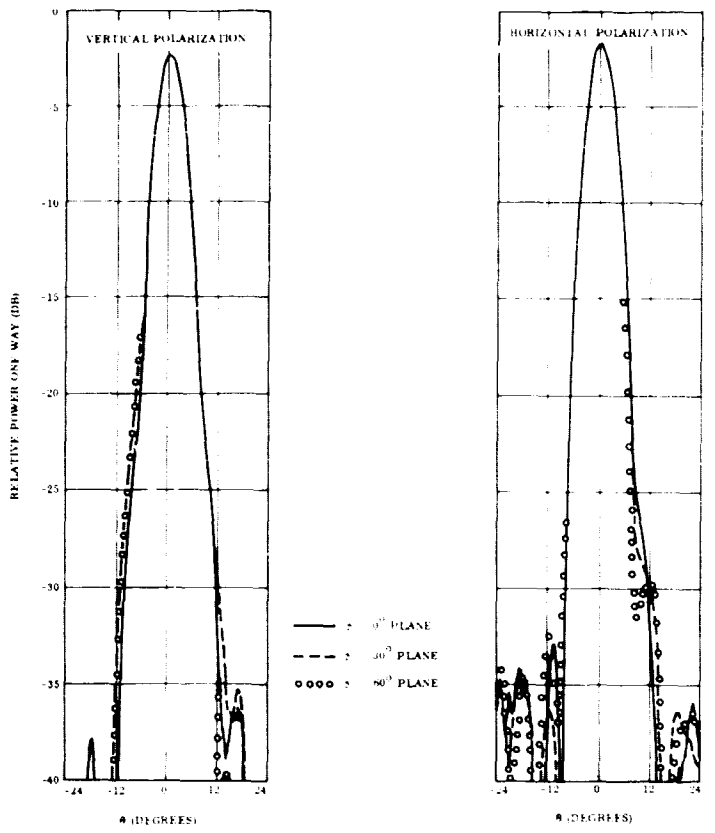

Figure D-3. Pattern Response of a Paraboloid in $\phi = 0^{O}$, 30^{O} and 60^{O} Planes Using a 5-Turn Helix Feed

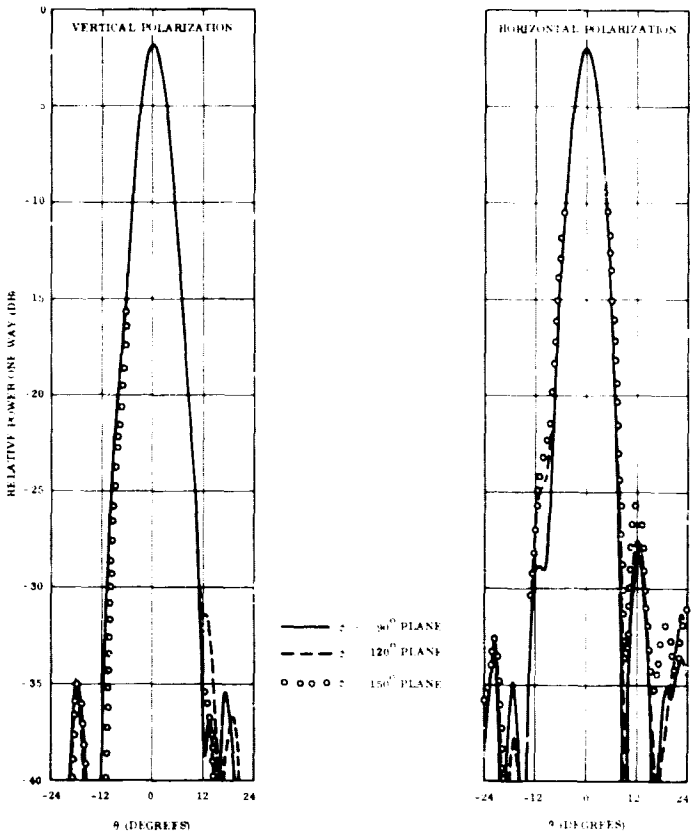

Figure D-4. Pattern Response of a Paraboloid in $\phi = 90^{O}$, 120^{O}, and 150^{O} Planes Using a 5-Turn Helix Feed

D.2 6-TURN HELIX FEED

Corresponding data for the 6-turn helix feed are shown in Figures D-5 through D-8. Again, defocusing did not appear to provide sidelobe suppression. The aperture blockage was about -38 db for this feed which will perturb the main lobe of the paraboloid by -1 db at about the -20 db power level; it can also increase the level of the first sidelobe, located at $\theta = \pm 16.5$ degrees, by 6 db to about -31 db. The measured gain of this feed was 8.3 db for vertical polarization and 9.8 db for horizontal polarization.

Backlobe radiation for vertical polarization had about -38 db relative intensity in the vicinity of the first sidelobe located at $\theta = \pm 16.5$ degrees. Backlobe radiation for horizontal polarization was more intense and contributed heavily to the sidelobe structure located at angles far-removed from broadside. The apparent focal position for this feed was d = 19.3 centimeters. Azimuth pattern cuts demonstrated pattern agreement with prediction down to a level of about -15 db.

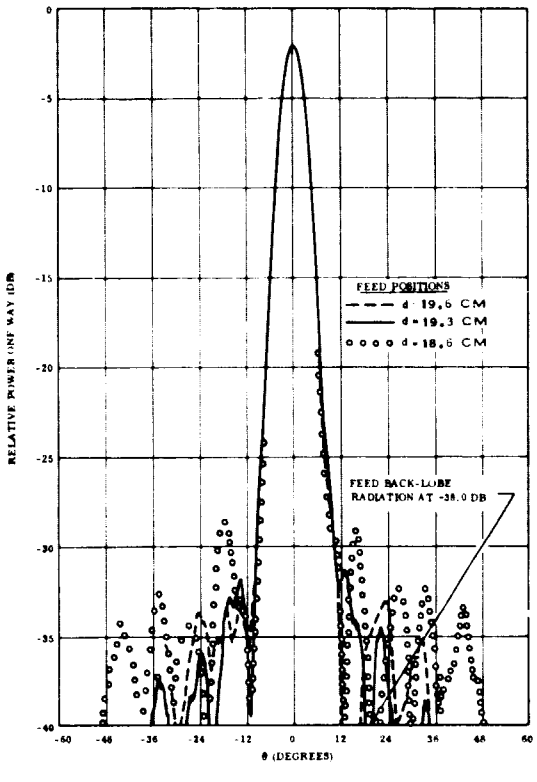

Figure D-5. Paraboloid Patterns in $\phi = 0^{O}$ Plane as Function of 6-Turn Helix Feed Position Using Vertical Polarization

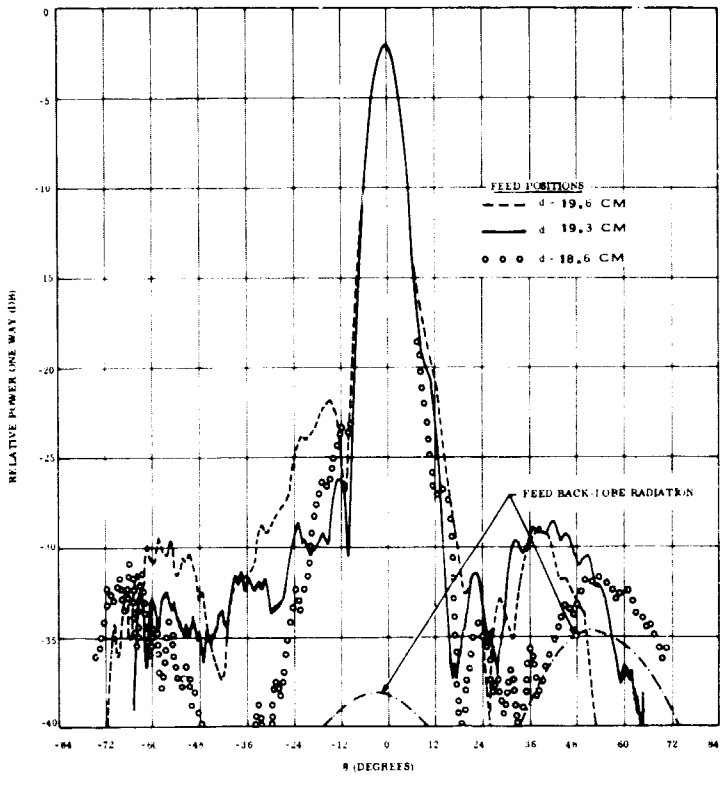

Figure D-6. Paraboloid Patterns in $\phi = 0^{O}$ Plane as a Function of 6-Turn Helix Feed Postion Using Horizontal Polarization

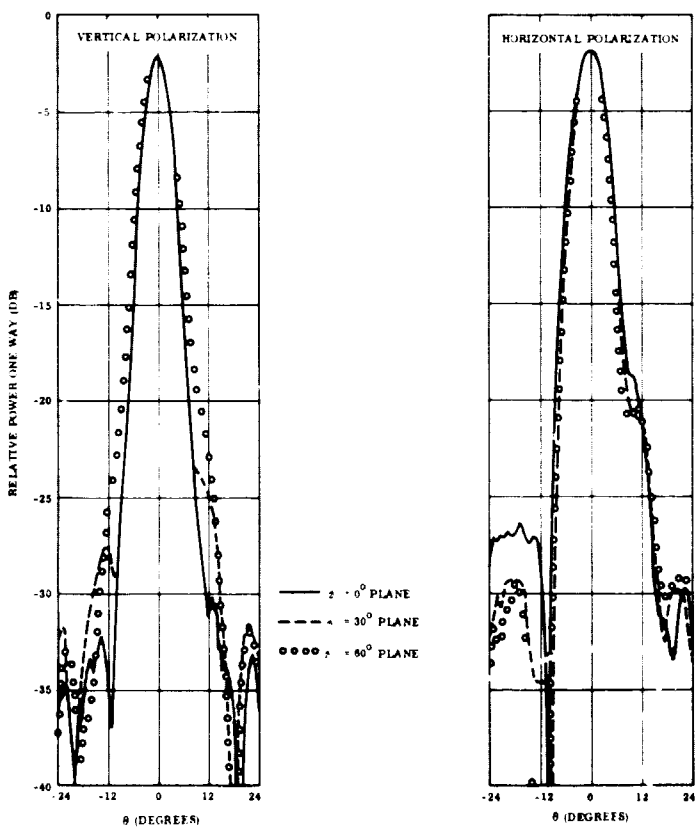

Figure D-7. Pattern Response of a Paraboloid in $\phi = 0^{O}$, 30^{O}, and 60^{O} Planes Using a 6-Turn Helix Feed

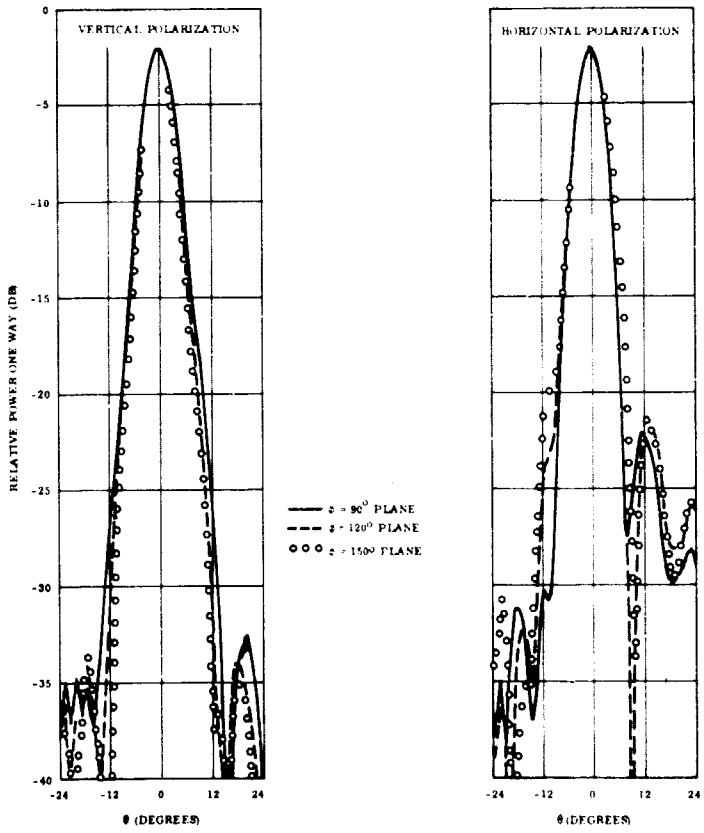

Figure D-8. Pattern Response of a Paraboloid in $\phi = 90^{O}$, 120^{O}, and 150^{O} Planes Using a 6-Turn Helix Feed

APPENDIX E

RING ZONE DESIGN

The radiation fields from a uniformly-excited, continuous ring is given by:

$$E_\theta = A\rho J_o (k\rho \text{ sm } \theta) \sin\phi$$

$$E_\phi = A\rho J_o (k\rho \text{ sm } \theta) \cos\theta \cos\phi \qquad \text{(E-1)}$$

Wherein,

E_θ and E_ϕ are the components of the total radiated electric-field vector using the ring location given in Figure E-1

k is the free space propagation constant

A is the electric-field amplitude

ρ is the radius of the ring

J_o is the Bessel function of o

θ and ϕ are the spherical coordinate angles

The ring zone suppressor produces an azimuthally symmetric, broadside pencil beam pattern whose sidelobes or secondary maxima are determined by the Bessel function $J_o (k\rho \sin\theta)$.

To design the ring for sidelobe suppression, the second sidelobe of the ring pattern is made to spatially coincide with the first sidelobe of the paraboloid pattern to be suppressed. For this condition the, main lobe of the ring will operate in-phase with the paraboloid main lobe. This condition also defines the radius of the ring as

$$\rho = \frac{\chi_{12}}{2\pi \sin\theta'} \lambda \qquad \text{(E-2)}$$

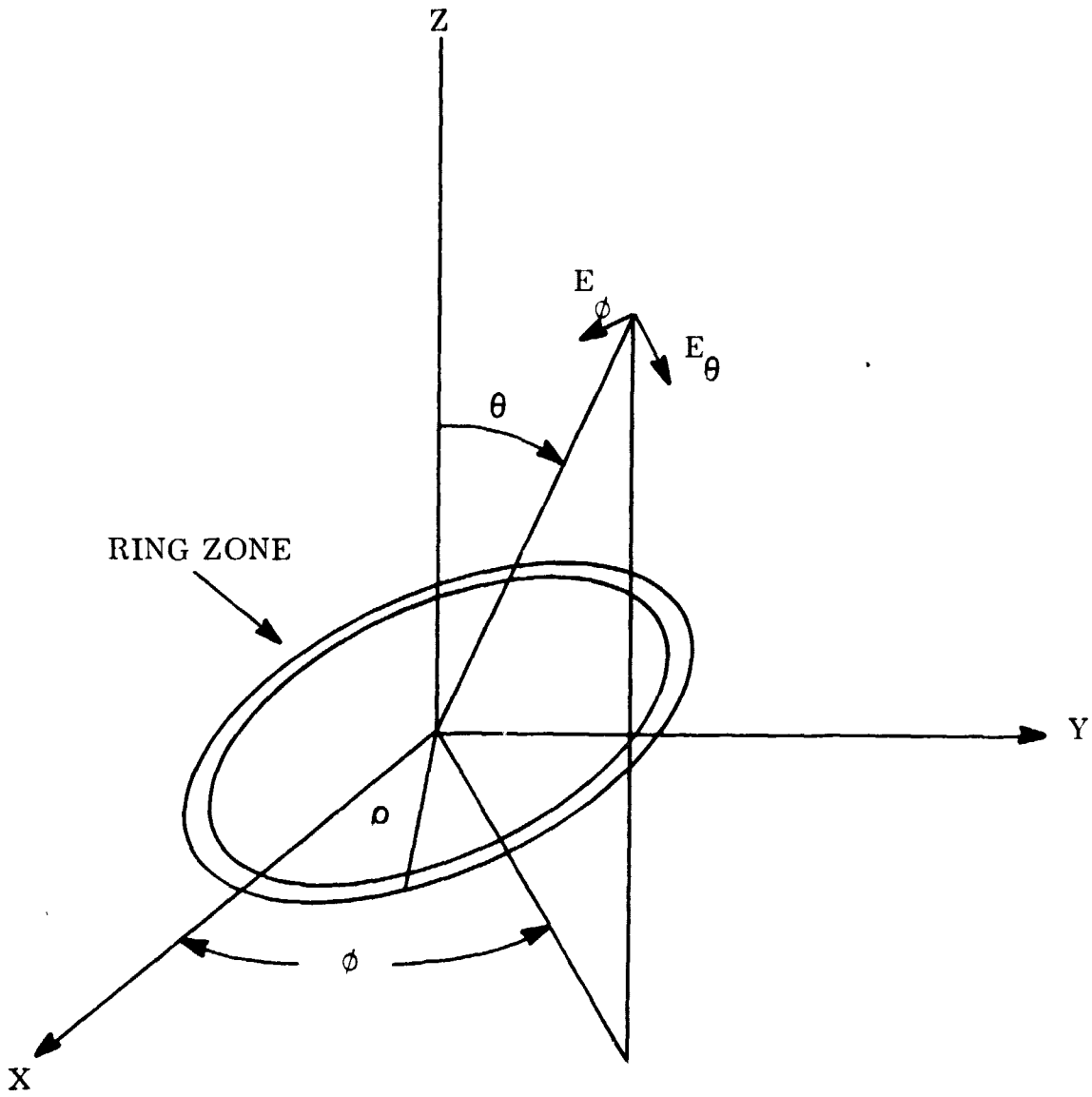

Figure E-1. Ring Zone and Space Geometry

Wherein,

X_{12} is the argument of J_o at which its second, secondary maxima occurs (this argument also corresponds to the second root of the Bessel function J_1), and

θ' is the angle at which the paraboloid first sidelobe is maximum.

The radius ρ is typically greater than the radius of the paraboloid. To illustrate, consider a paraboloid having a radius, $R = 6.12\ \lambda$ and a normalized aperture distribution A(R) given by $A(R) = 0.16 + 0.84\ (1 - R^2)^2$; $|R| \leq 1$. This paraboloid produces a pattern with a

half-power beamwidth of 6 degrees and a first sidelobe of -36.4 db. Assuming that the frequency is 7.5 GHz, the paraboloid first sidelobe occurs at $\theta' = 9.5$ degrees, which, from Equation (E-2), results in $\rho = 6.77\lambda$. The spatial alignment of the next two sidelobes of the ring zone is also of interest and is shown below in Table E-1.

Table E-1. Coincidence of Ring and Paraboloid Sidelobes

Paraboloid Sidelobe Location (degrees)	9.5	13.0	17.5
Ring Sidelobe Location (degrees)	9.5	13.8	18.3

The agreement is good for substantial sidelobe suppression.

To implement this example, a ring containing 20 elements can be used to approximate a continuous ring source. To indicate the pattern symmetry from this approximation, ring patterns are shown for a plane containing two diametrically opposed elements and for a plane which bisects two pairs of diametrically opposed elements (see Figure E-2). As shown, the agreement is very good for $18^{o} \geq \theta \geq -18^{o}$.

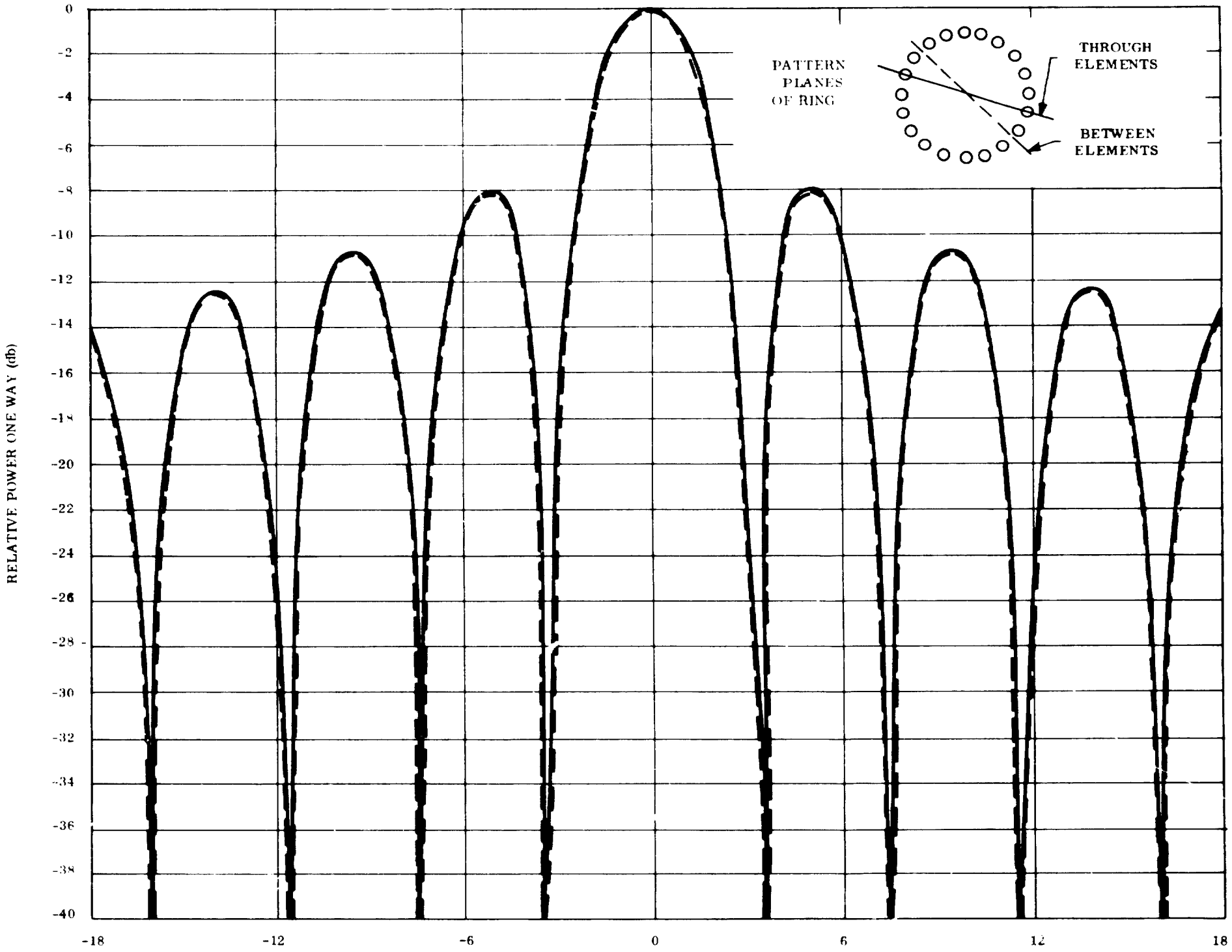

Figure E-2. Pattern Symmetry for Ring Array

APPENDIX F

PARABOLOID CONTOUR MEASUREMENTS

The actual dimension figures of Y and X on the Parabolic Reflector Disc were obtained by using the Bridgeport Mill and a 1-inch Travel Federal Dial Indicator.

The following method was used to measure the curve of the disc to the calculated curve:

a. The disc was securely mounted on the table of the mill and the outside diameter was indicated to find the center of disc. The inside counterbore was also indicated and was found to be concentric to outside within 0.001 inch.

b. The spindle was centered on the disc and a "pinpoint" mark was made on a plug placed in counterbored hole. The indicator was then lined up with the "pinpoint."

c. The dial on the mill table screw, which is graduated in 0.001 inch, was set on 0 and the table was then moved every 0.500 inch. The indicator was set at 0.0081 inch, which is "X" dimension at "Y" 0.500 inch, and this was considered the starting point.

d. The disc was moved 0.500 inch at a time and the height was recorded from the indicator. The indicator had to be reset every 1 inch of vertical travel.

Table F-1 lists the readings found when the disc was set on 0 degrees and Table F-2 when rotated to 90 degrees.

Table F-1. Readings at 0 Degrees

Y (inch)	Calculated Dimension X (inch)	Right Side of Center, Actual Dimension X' (inch)	Difference X_D (Mils)	Left Side of Center, Actual Dimension X' (inch)	Difference X_D (Mils)	
500	0.0081	0.0081	0	0.0081	0	
1.000	0.0324	0.0321	0.7	0.0313	1.1	
1.500	0.0730	0.0735	0.5	0.0722	0.8	
2.000	0.1298	0.1305	0.5	0.1291	0.7	
2.500	0.2029	0.2035	0.7	0.2018	1.1	
3.000	0.2922	0.2935	0.4	0.2912	1.1	
3.500	0.3977	0.3985	1.2	0.3959	1.2	
4.000	0.5194	0.5205	1.1	0.5185	0.9	
4.500	0.6574	0.6582	0.9	0.6557	1.7	
5.000	0.8116	0.8112	0.7	0.8100	1.6	
5.500	0.9821	0.9825	1.1	0.9812	0.9	
6.000	1.1688	0.1703	0.1			
6.500	1.3717	1.1695	2.2			Damaged indicator at
7.000	1.5909	1.5887	2.2			this point and no
7.500	1.8263	1.8242	2.1			further readings were
8.000	2.0779	2.0747	3.2			taken on this axis.
8.500	2.3457	2.3438	2.1			
9.000	2.6298	2.6277	2.1			
9.500	2.9301	2.9279	3.2			

Table F-2. Readings at 90 Degrees

Y (inch)	Calculated Dimension X (inch)	90^{O} Right Side of Center, Actual Dimension X' (inch)	Difference X_D (Mils)	90^{O} Left Side of Center, Actual Dimension X' (inch)	Difference X_D (Mils)
0.500	0.0081	0.0081	0	0.0081	0
1.000	0.0324	0.0321	0.3	0.0309	1.5
1.500	0.0730	0.0735	0.5	0.0715	1.5
2.000	0.1298	0.1305	0.7	0.1280	1.8
2.500	0.2029	0.2035	0.6	0.2009	2.0
3.000	0.2922	0.2935	1.3	0.2900	2.2
3.500	0.3977	0.3985	0.8	0.3947	3.0
4.000	0.5194	0.5205	1.1	0.5162	3.2
4.500	0.6574	0.6582	0.6	0.6540	3.4
5.000	0.8116	0.8112	0.4	0.8081	3.5
5.500	0.9821	0.9825	0.4	0.9789	3.2
6.000	1.1688	0.1703	1.5	0.1653	3.5
6.500	1.3717	1.3730	1.3	0.3679	3.8
7.000	1.5909	1.5918	0.9	0.5874	3.5
7.500	1.8263	1.8270	0.7	0.8234	2.9
8.000	2.0779	2.0792	1.3	0.0742	3.7
8.500	2.3457	2.3480	2.3	0.3440	1.7
9.000	2.6298	2.6312	1.4	0.6292	0.6
9.500	2.9301	2.9325	2.4	0.9302	0.1

The root mean square surface error; X_{RMS}, for the paraboloid is determined by the expression,

$$X_{RMS} = \sqrt{\frac{\sum_{i=1}^{N} (X_{D_i} - \bar{X}_D)^2}{N}}$$

wherein, $\bar{X}_D$ is the average difference in X_D for all readings

X_{D_i} is the difference for the ith reading

N is 64 readings

Using the data in Tables F-1 and F-2 in Equation 3.8-1 yields

$$X_{RMS} = 0.00106 \text{ inch.}$$